Enhancing Output Power of Bifacial Dye-sensitized Solar Cells Using Low Concentrated Light Systems

ティカ, エルナ, プトゥリ

ENHANCING OUTPUT POWER OF BIFACIAL DYE-SENSITIZED SOLAR CELLS USING LOW CONCENTRATED LIGHT SYSTEMS

By

Tika Erna Putri

Department of Electronics

Graduate School of Information Science and Electrical Engineering

Kyushu University

2022

ENHANCING OUTPUT POWER OF BIFACIAL DYE-SENSITIZED SOLAR CELLS USING LOW CONCENTRATED LIGHT SYSTEMS

By

Tika Erna Putri

Department of Electronics

Graduate School of Information Science and Electrical Engineering

Kyushu University

2022

低集光システムを使用した
色素増感太陽電池の出力電力の向上

ティカ エルナ プトゥリ

九州大学大学院

システム情報科学府

電気電子工学専攻

2022 年 9 月

Table of Content

	Page
Cover	i
Table of Content	iv
List of Abbreviations	vi
1. Introduction	1
References	10
2. Dye-Sensitized Solar Cells: Theoretical and Fundamental Theory	15
2.1. Photoelectrochemical Conversion of Solar Energy	16
2.1.1 Photogalvanic Cells	16
2.2. Dye Sensitized Solar Cells (DSSCs)	17
2.2.1 Components of DSSCs	19
2.2.2 Electron Transfer Steps of DSSCs	27
2.2.3 Key Efficiency Parameters of DSSCs	28
2.3. Characterization Technique	30
2.3.1 Doctor Blade Technique	31
2.3.2 Current-Voltage Characteristic	32
2.3.3 Electrochemical Impedance Spectroscopy	36
2.4. Concentrator Photovoltaic (CPV)	38
References	42
3. Dye-Sensitized Solar Cells with Low Concentrated Light System	47
3.1. Experimental Section	49
3.1.1 Cell Fabrication	49
3.1.2 Measurement	50
3.2. Experimental Results and Discussion	51
3.2.1 Low Concentrator	51
3.2.2 Temperature Effect in Different Electrolyte	65
3.2.3 Endurance Test	72
Conclusions	73
References	74

4. Dye-Sensitized Solar Cells with V-Shape Low Concentrated Light System 80
4.1. Experimental Section 82
4.1.1 Cell Fabrication 82
4.1.2 Measurement 82
4.2. Experimental Results and Discussion 84
4.2.1 Effect of Tilt Angle 84
4.2.2 Optical System Parameter 92
4.2.3 Effect of Time 95
4.2.4 Effect of Cell-Mirror Distance 100
Conclusions 103
References 104

5. Low Concentrator Coupled with Flowing Electrolyte System in Bifacial Dye-Sensitized Solar Cells 107
5.1 Experimental Section 109
5.1.1 Cell Fabrication 109
5.1.2 Measurement 110
5.2 Experimental Result and Discussion 111
5.2.1 Flowing Electrolyte Systems 111
5.2.2 Different electrolyte 118
5.2.3 Temperature Reduced FS Systems 119
Conclusions 120
References 121

6 Summary and Future Prospect 125

Acknowledgements 128
List of Publication and Conference 129

List of Abbreviations

A	Area
A_{in}	Entrance aperture
A_{out}	Exit aperture
AC	Alternating current
AN	Acetronitrile
B	Pseudo activation energy
B_P	Boiling point
Cp	Viscosity
C	Capacitance
C_g	Geometrical concentration
C_r	Concentration ratio
CF	Continuously flowing electrolyte system
DC	Direct current
DSSCs	Dye sensitized solar cells
e	Elementary charge
E_A	Activation energy
E_F	Quasi-fermi level
EIS	Electrochemical impedance spectroscopy
f	Frequency
FF	Fill factor
FS	Flowing-stop electrolyte system
FTO	Fluorine doped tin oxide
G	Generation rate
I	Current
I_{max}	Photocurrent
I_L	Light generated current
I_0	Amplitudes of current
I_S	Reverse bias saturation current
IPCE	Incident photon to current conversion efficiency
j	Emission coefficient
J	Current density
J_{SC}	Short circuit current density
k_B	Boltzmann constant

L_p	Hole diffusion length
L_n	Electron diffusion length
MPN	3-methoxypropionitrile
N	Refractive index
n_i	Carrier concentration
$N_{electrons}$	Number of photo-generated electron
$N_{photons}$	Number of incident photon
NC	Normal cell
P_{IN}	Power input
P_{max}	Maximum power output
P_{OUT}	Power output
PN	Propionitrile
Pt	Platinum
q	Magnitude of charge electron
q_i	Charge of ionic specimen
R	Resistance
R_S	Sheet resistance
R_{CT}	Resistance of charge transfer
R_{dC}	Resistance of DC
T	Temperature
T_0	Temperature equilibrium related to glass transition
TiO_2	Titanium dioxide
V	Voltage
V_D	Voltage across the diode
V_{max}	Photo-voltage
V_0	Amplitudes of voltage
V_{OC}	Open circuit voltage
V_T	Thermal voltage
$V(\omega, t)$	Potential in harmonic modulated
X	Distance
Z	Impedance
E	Dielectric constant
λ	Wavelength
σ	Conductivity
μ_i	Mobility
ζ	Over potential

$\boldsymbol{\Phi(\lambda)}$	Photon flux
$\boldsymbol{\omega}$	Angular frequency
$\boldsymbol{\theta}$	Tilt angle
$\boldsymbol{\theta_a}$	Half-acceptance angle
$\boldsymbol{\theta_c}$	Acceptance angle
$\boldsymbol{\theta_i}$	Incident light angle
$\boldsymbol{\eta}$	Power conversion efficiency
$\boldsymbol{\eta_{opt}}$	Optical efficiency angular movement
$\boldsymbol{\eta_{opt,concent}}$	Optical efficiency concentrator system

Chapter 1
Introduction

The history of dye-sensitized solar cells (DSSCs) began in 1839 when Becquerel discovered the phenomenon that a voltage can be produced when two platinum electrodes were immersed in an electrolyte containing a metal halide salt and were exposed to light [1]. After that, during the 1960s, some scientists found that an organic dye is capable of producing electricity at a semiconductor electrode in an electrochemical cell when light irradiates it [2-3]. During the 1970s, the mechanism of photosynthesis was studied to discover the phenomenon of photoexcitation [4]. In a research, chlorophyll pigment was extracted from spinach and used with zinc oxide (ZnO) as semiconductor electrode material in electrochemical cells. Then, in 1972, Tributsch demonstrated the generation of electricity through dye sensitization [5]. Matsumura et al., in 1980, conducted a study in this area, and they inferred that the stability of the dye in the dye-sensitized photocell was challenging [6]. Still, the efficiency of the dye molecules could be improved by fine-tuning the porosity of the semiconductor oxide material.

In 1991, Gratzel and O'Regan advanced in this field by creating a sensitized electrochemical photovoltaic device, a conventional solid-state photovoltaic based on molecular and nano-level components with the semiconductor titanium dioxide (TiO_2) as dye sensitization material [7]. This new conceptual approach was based on the photosynthesis activity in nature, as shown in Fig. 1.1, where the cyclic process of photosynthesis is imitated for harvesting energy using the sun's radiation through a synthetic dye material [2,8]. The concept in DSSCs is similar to that of photosynthesis, where every element implements a different process, thus leading to lower purity demand [9] on the DSSC raw materials, as shown in Fig. 1.2. Consequently, the DSSC is a low-cost alternative photovoltaic technology. This field is advancing rapidly, and DSSCs have become the third generation of photovoltaics. In the last two decades, they have been the

focus of research in light-harvesting technology [9]. Because of their advantages, such as low cost, ease of fabrication, simple device structure, good performance, and eco-friendliness [8-12], DSSCs have a high potential for improvement. In addition, compared to other solar cells in the same generation, DSSCs offer design flexibility regarding shape, color, and transparency.

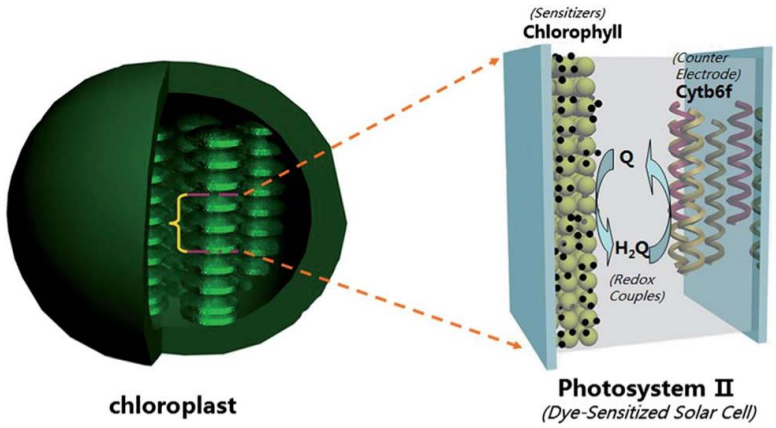

Figure 1.1 Photosynthesis and dye-sensitized solar cells (DSSCs) [8].

Even though DSSCs have several advantages as a light-harvesting technology, their low efficiency, less than 10% [13-18], and low power output are still a major bottleneck compared to other photovoltaic devices in the same generation. Gratzel and O'Regan achieved a solar-to-electricity conversion efficiency (η) of approximately 7% in the first attempt [7]. After rapid progress in DSSCs, in 2008, using an iodine-based redox liquid electrolyte, their efficiency increased to approximately 8% [19]. The efficiency increased to 11.5% when the researchers advanced in solving the corrosive nature of electrolytes, which improved the stability of the devices, photo-voltage, and efficiency [20]. In 2014, DSSCs reached an efficiency of approximately 13% with a coupled zinc porphyrin dye and a cobalt-based redox liquid electrolyte [21-22]. In 2015, the efficiency increased to approximately 14% with DSSCs composed of metal-free organic co-sensitizers and a

cobalt-based redox couple liquid electrolyte [22-23]. However, this performance is still very low compared to that of crystalline silicon, with an efficiency of 26%, and perovskite, with an efficiency of 23%.

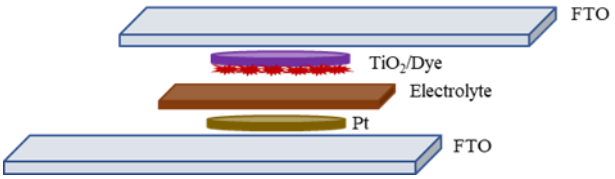

Figure 1.2 Dye-sensitized solar cell structure.

To increase both the efficiency and power output in DSSCs, a bifacial structure has been introduced to optimize the absorption of solar radiation on both sides, front and rear [24-28]. Because it converts the light incident on both sides of the cell, this structure utilizes the sunlight more efficiently and offers the possibility of reducing the cost of solar electricity compared to that of conventional mono facial photovoltaic devices. The bifacial structure utilizes the light reflected by the ground (albedo), which is sent back to the TiO_2 layer, where it can be reabsorbed and converted into electricity. Transparent counter electrodes are the primary requirement in bifacial structures with this strategy. The bifaciality [29] is defined as follows:

$$Bifaciality = \frac{\eta_{rear}}{\eta_{front}} \tag{1.1}$$

with

$$\eta = \frac{P_{OUT}}{P_{IN}} \tag{1.2}$$

where η is energy conversion efficiency, P_{OUT} is power output, and P_{IN} is power input. The magnitude of the bifacility value can measure the success of the bifacial system itself and the materials used. A study on the bifacial DSSC technology reported an energy conversion efficiency of 8.35% using 4-ATP/PANI counter electrodes, an increase of

24.6% compared to DSSCs irradiated from the front only [24]. This result gives hope that bifacial structure can be improved the performance of DSSCs in both power output and efficiency. Nonetheless, the back incident light reflected from the ground is too low compared to the front incident light. To further optimize the DSSC bifacial system, enhancing the incident light from the rear is necessary to achieve incident light harvesting.

Recently, a reflector concentrator has been applied to enhance the incident light from the rear side. Commonly, reflector concentrators with Fresnel lens [30-32] or parabolic mirrors [33-34] have been used to improve the light harvesting of bifacial DSSCs [30-36], especially for the rear side. Chemisana *et al*. classified the concentration ratio of the concentrator into four types: low $(< 10\times)$, medium $(10-100\times)$, high $(100-2000\times)$, and ultrahigh $(> 2000\times)$, depending on light concentration [37]. The power energy efficiency and output power are effectively increased by using a concentrator in the photovoltaic system. That report showed that a photovoltaic (PV) system coupled with a V-through plane concentrator could increase the power energy efficiency and power output by ~18% compared to that without a concentrator [38]. Even though concentrators can increase both power output and power energy efficiency, the application of concentrators in PV systems is still limited because high temperature is a side effect. The high temperature could severely damage DSSCs, especially the liquid electrolyte, which has a low boiling point (under 200 °C) [39-42]. Therefore, a performance evaluation of the DSSC coupled with a V-shape light concentrator system is necessary to determine the magnitude and duration of the increase in power energy efficiency and power output and the stability of its performance.

The liquid electrolyte is preferred for DSSCs owing to its good performance and advantages such as high ionic conductivity, relatively high viscosity, electrochemical

potential window, and room-temperature long-term performance stability [9]. However, the major problem of the liquid electrolyte is that it evaporates easily, is not stable in high temperatures, and is prone to leakage [43]. Many studies have solved the evaporation and high-temperature stability problems in liquid electrolytes. Solid-state and quasi-solid state electrolytes are considered breakthrough technologies to solve the problems of liquid electrolytes [44-45]. They promise long-term stability in DSSC devices [46]. A report showed that a solid-state electrolyte with hole-transporting material (HTM) could avoid leakage while achieving long-term stability [45-46]. Nonetheless, the HTM process is costly owing to the materials it requires, and the production cost of solid-state electrolytes may be high. Poor penetration into the mesoporous TiO_2, low ionic conductivity, low electron transfers from the dye molecules, and faster recombination are also problems of the solid-state electrolyte [47]. The quasi-solid state electrolyte might become a solution to the solid-state electrolyte problems owing to its better penetration and higher electron transfer. However, the efficiencies of quasi-solid state electrolytes in DSSCs are relatively lower than those in liquid electrolytes due to the lower mobility of iodide species through the viscous medium. Given that the performance of liquid electrolytes is still better than that of other states of electrolytes, a cooling system is necessary to use liquid electrolytes but overcome the problem of evaporation and high-temperature stability.

Active cooling systems generally work by flowing water at a speed of approximately 0.1–1 L/min under a block-mounted solar cell system. In contrast, passive cooling systems utilize phase change material (PCM) as a coolant. Various types of cooling systems have been introduced to overcome thermal problems in solar cells, such as PCM-based, thermoelectric-based, air cooling-based, heat pipe-based, and liquid cooling-based. Recently, in a study of Shuai Gu *et al.*, a circulating electrolyte passed

through the DSSCs devices [48]. The result showed that the power energy efficiency could be increased by ~10% under 1-sun illumination (100 mW/cm^2) with various flowing rates. The circulating electrolyte is a promising active cooling system, and it is expected to reduce the temperature and thermal effects of the DSSCs caused by high temperatures. To evaluate the performance of a flowing electrolyte system in a DSSC coupled with a V-shape concentrator system, it is necessary to have a better understanding of how this system works and how it affects the performance of the DSSC coupled with the light concentrator.

At the present time, the performance stability of liquid electrolyte DSSCs is still limited at room temperature. Further, the power conversion efficiency and power output in DSSCs are relatively low even though many improvements in the structure of DSSCs have been made. Further improvements in their performance seem possible using an available system to realize sub phenomena in DSSCs. The current DSSC performance compared with that of other types of photovoltaic devices is shown in Fig. 1.3. From the data, the DSSC still has a low performance, although it has several advantages when compared to other devices. The combination of features suggests that DSSCs might become promising renewable energy devices that can compete with other solar cell devices.

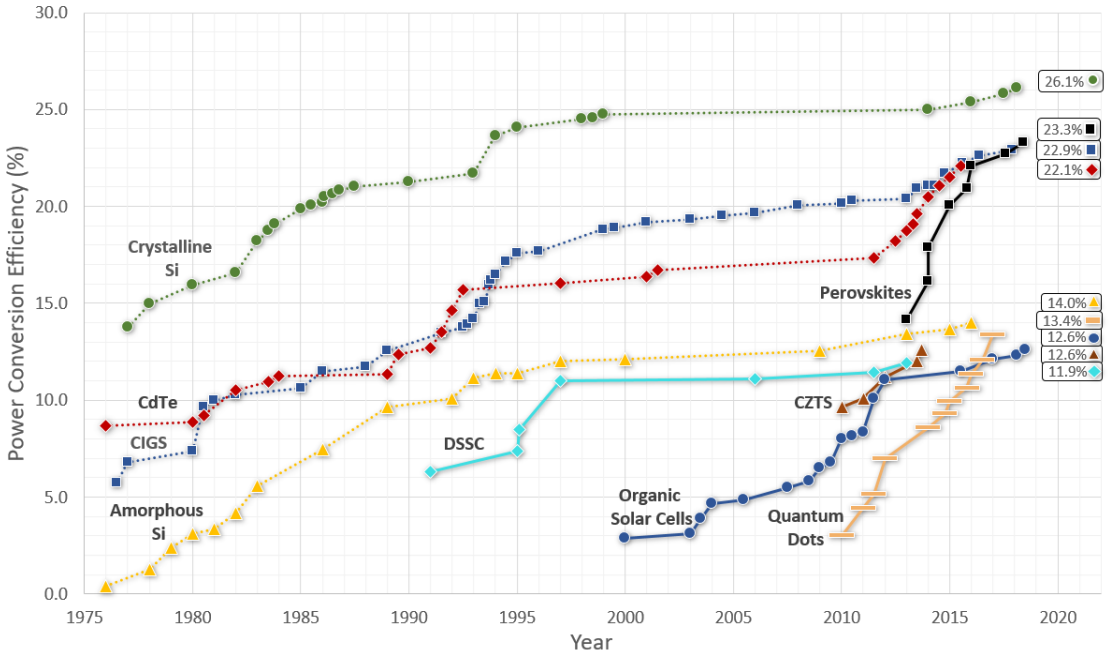

Figure 1.3 Development of the DSSC and other photovoltaic (PV) devices.

In this thesis, the main objective was to enhance the performance and power output of bifacial DSSCs with low-concentrated light. The following research steps were conducted to achieve our objectives:

1. Observation of the performance of DSSCs with a low concentrated light system using a plane mirror as a back reflector and a concave mirror as a back concentrator
2. Evaluation of the performance stability of the DSSC with a V-Shape low concentrated light system.
3. Control of the increase or spike in temperature in DSSCs as side effect of the application of a low concentrator.

This dissertation consists of six (6) chapters. The content of each chapter is briefly described below:

Chapter 1 summarizes the background and objectives and provides an outline of the study.

Chapter 2 addresses the fundaments and theory of DSSCs, including the fabrication method and a characterization technique to observe the performance of DSSCs.

Chapter 3 describes the performance of bifacial DSSCs with low concentrated light. The use of a plane mirror as a back reflector and a concave mirror as a back concentrator to increase the albedo was studied for application in bifacial DSSCs. The investigation focused on increasing the performance measured by variables such as photocurrent, voltage, and power output, and the effect on operational cells of parameters such as time, temperature, and cell degradation.

Chapter 4 discusses the V-Shape system with plane and concave mirrors as the concentrator. The investigation was focused on the enhancement in output power and stabilization of the operational temperature of a bifacial DSSC with a V-Shape concentrator system.

Chapter 5 examines the flowing electrolyte as an active cooling system to support the temperature control of a low concentrator application. The discussion is focused on the effect of the flowing system on the bifacial DSSC performance and operation.

The final chapter, Chapter 6, presents the conclusions. This chapter contains a summary of the experimental results and the prospects for developing bifacial DSSCs with low concentrators in the future.

REFERENCES

[1]. Williams, R. (**1960)** 'Becquerell Photovoltaic Effect in Binary Compounds', *Chem. Phys*., 32, 5, 1505-1514. DOI: https://doi.org/10.1063/1.1730950

[2]. Karthick, S. N., Hemalatha, K. V., Balasingam, S. K., Clinton, F. M., Akshaya, S. and Kim, H-J. (**2020)** *Dye-Sensitized Solar Cells: history, Components, Configuration, and Working Principle. Interfacial Engineering in Functional Materials for Dye-Sensitized Solar Cells, 1st Edition.* Edited by Alagarsamy Pandikumar, Kandasamy Jothivenkatchalam, and Karuppanapillai B. Bhojanaa. John Wiley & Sons, Inc.

[3]. Gerischer, H., Beyerle, M. E., Rebentrost, F., Tributsch, H. (**1968)** 'Sensitization of Charge Injection into Semiconductors with Large Band Gap', *Electrochim. Acta,* 13, 1509-1515. DOI: https://doi.org/10.1016/0013-4686(68)80076-3

[4]. Tributsch, H. and Calvin, M. (**1971)** 'Electrochemistry of Excited Molecules: Photo-Electrochemical reactions of Chlorophylls', *Photochem. and Photobiol,* 14, 95-112. DOI: https://doi.org/10.1111/j.1751-1097.1971.tb06156.x

[5]. Tributsch, H. (**1972**) 'Reaction of Excited Chlorophyll Molecules at Electrodes and in Photosynthesis', *Photochem. and Photobiol*., 16, 261-269. DOI: https://doi.org/10.1111/j.1751-1097.1972.tb06297.x

[6]. Matsumura, M., Matsudaira, S., Tsubomura, H. (**1980)** 'Dye Sensitization and Surface Structures of Semiconductor Electrodes', *Ind. Eng. Chem. Prod. Res. Dev*., 19, 415-421. DOI: https://doi.org/10.1021/i360075a025

[7]. O'Regan, B. and Gratzel, M. (**1991**) 'A Low Cost, High-Efficiency Solar Cell Based on Dye Sensitized Colloidal TiO_2 Films', *Nature*, 353, 737-740. DOI: https://doi.org/10.1038/353737a0

[8]. Yu, Z., Wang, C., Bu, C., Bai, S., Zhou, Z., Tai, Q., Liu, W., Guo, S. and Zao, X-Z. (**2014)** 'Efficient Dye-Sensitized Solar Cells Employing Highly Environmentally-Friendly Ubiquinone 10 Based I_2-free Electrolyte Inspired by Photosynthesis', *J. Matter. Chem. A*, 2, 9007-9010. DOI: https://doi.org/10.1039/C4TA00837E

[9]. Wu, J., Lan, Z., Lin, J., Huang, M., Huang, Y., Fan, L. and Luo, G. (**2015**) 'Electrolytes in Dye-Sensitized Solar Cells', *J. Chem. Rev.*, 115, 2136-2173. DOI: https://doi.org/10.1021/cr400675m

[10]. Yum, J., Baranoff, E., Wenger, S., Nazeeruddin, M. K. and Gratzel, M. (**2011**) 'Panchromatic engineering for dye-sensitized solar cells', *Energy Environ. Sci.*, 4, 842–857. DOI: https://doi.org/10.1039/C0EE00536C

[11]. Chung, I., Lee, B., He, J., Chang, R. P. H. and Kanatzidis, M. G. (**2012**) 'All-solid-state dye-sensitized solar cells with high efficiency', *Nature*, 485. 486–489. DOI: https://doi.org/10.1038/nature11067

[12]. Xue, G., Guo, Y., Yu, T., Guan, J., Zhang, J., Liu, J. and Zuo, Z. (**2012**) 'Degradation Mechanisms Investigation for Long-term Thermal Stability of Dye-Sensitized Solar Cells', *Int. J. Electrochem. Sci.*, **7**, 1496–1511.

[13]. Sharma, K., Sharma, V. and Sharma, S. S. (**2018**) 'Dye-Sensitized Solar Cells: Fundamentals and Current Status', *Nanoscale Res. Lett.,* 13, 381. DOI: https://doi.org/10.1186/s11671-018-2760-6

[14]. Seo, H., Son, MK., Hashimoto, S., Takasaki, T., Itagaki, N., Koga, K. and Shiratani, M. (**2016**) 'Surface Modification of Polymer Counter Electrode for Low-Cost Dye-sensitized Solar Cells', *Electrochim. Acta*, 210, 880-887. DOI: https://doi.org/10.1016/j.electacta.2016.06.020

[15]. Saidi, N. M., Farhana, N. K., Ramesh, S. and Ramesh, K. (**2021**) 'Influence of different concentrations of 4-tert-butyl-pyridine in a gel polymer electrolyte towards improved performance of Dye-Sensitized Solar Cells (DSSC)', *Sol. Energy*, 216, 111-119. DOI: https://doi.org/10.1016/j.solener.2020.12.058

[16]. Omar, A. and Abdullah, H. (**2014**) 'Electron transport analysis in zinc oxide-based dye-sensitized solar cells: A review', *Renewable Sustainable Energy Rev.*, 31, 149-157. DOI: https://doi.org/10.1016/j.rser.2013.11.031

[17]. Seo, H., Nam, SH., Itagaki, N., Koga, K. and Shiratani, M. (**2016**) 'Effect of sulfur-doped TiO_2 on photovoltaic properties of dye-sensitized solar cells', *Electron. Mater. Lett.*, 12, 530–536. DOI: https://doi.org/10.1007/s13391-016-4018-8

[18]. Seo, H., Son, MK., Itagaki, N. and Shiratani, M. (**2016**) 'Polymer counter electrode of poly(3,4-ethylenedioxythiophene): Poly(4-styrenesulfonate) containing TiO_2 nanoparticles for dye-sensitized solar cells', *J. Power Source*, 307, 25-30. DOI: https://doi.org/10.1016/j.jpowsour.2015.12.112

[19]. Bai, Y., Cao, Y., Zhang, J., Wang, M., Li, R., Wang, P., Zakeeruddin, S. M. and Gratzel, M. (**2008**) 'High Performance Dye-Sensitized Solar Cells based on Solvent-Free Electrolytes Produced From Eutetic Melts', *Nat. Mater.*, 7, 626-630. DOI: https://doi.org/10.1038/nmat2224

[20]. Chen, C-Y., Wang, M., Li, J-Y., Pootrakulchote, N., Alibabaei, L., Ngoc-le, C., Decoppet, J-D., Tsai, J-H., Gratzel, C., Wu, C-G., Zakeeruddin, S. M. and Gratzel, M. (**2009**) 'Highly Efficiency Light Harvesting Ruthenium Sensitizer for Thin Film Dye-Sensitized Solar Cells', *J. ACS Nano*, 3, 10, 3103-3109. DOI: https://doi.org/10.1021/nn900756s

[21]. Mathew, S., Yella, A., Gao, P., Baker, R. H., Curchod, B. F. E., Astani, N. A., Tavernelli, I., Rathlisberger, U., Nazeeruddin, Md. K. and Gratzel, M. (**2014**) 'Dye-Sensitized Solar Cells with 13% Efficiency Achived Through the Molecular

Engineering of Porphyrin Sensitizers', *Nat. Chem*., 6, 242-247. DOI: https://doi.org/10.1038/nchem.1861

[22]. Kakiage, K., Aoyama, Y., Yano, T., Oya, K., Fujisawa, J. and Hanaya, M. (**2015**) 'Highly Efficient Dye-Sensitized Solar Cells with Collaborative Sensitization by Silyl-Anchor and Carboxy-Anchor Dyes', *J. Chem. Comm*., 51, 15894-15897. DOI: https://doi.org/10.1039/C5CC06759F

[23]. Hao, Y., Yang, W., Zhang, L., Jiang, R., Mijangos, E., Saygili, Y., Hammarstrom, L., Hagfeldt, A. and Boschloo, G. (**2016**) 'A Small Electron Donor in Cobalt Complex Electrolyte Significantly Improves Efficiency in Dye-Sensitized Solar Cells', *Nat. Commun*., 7:13934. DOI: https://doi.org/10.1038/ncomms13934

[24]. Wu, J., Li, Y., Tang, Q., Yue, G., Lin, J., Huang, M. and Meng, L. (**2014**) 'Bifacial dye-sensitized solar cells: A strategy to enhance overall efficiency based on transparent polyaniline electrode', *Sci. Rep.*, 4, 4028 1–7. DOI: https://doi.org/10.1038/srep04028

[25]. Xu, T., Kong, D., Tang, H., Qin, X., Li, X., Gurung, A., Kou, K., Chen, L., Qiao, Q. and Huang, W. (**2020**) 'Transparent MoS 2 / PEDOT Composite Counter Electrodes for Bifacial Dye-Sensitized Solar Cells', *ACS Omega*, 5, 8687-8696. DOI: https://doi.org/10.1021/acsomega.0c00175

[26]. Miranda-Munoz, J. M., Carretero-Palacios, S., Jimenez-Solano, A., Li, Y.; Lozano, G. and Miguez, H. (**2016**) 'Efficient bifacial dye-sensitized solar cells through disorder by design', *J. Mater. Chem. A*, 4, 1953-1961. DOI: https://doi.org/10.1039/C5TA10091G

[27]. Cai, H., Tang, Q., He, B., Li, R. and Yu, L. (**2014**) 'Bifacial dye-sensitized solar cells with enhance rear efficiency and power output', *Nanoscale*, 6, 15127-15133. DOI: https://doi.org/10.1039/C4NR04911J

[28]. Ito, S., Zakeeruddin, S. M., Comte, P., Liska, P., Kuang, D. and Gratzel, M. (**2008**) 'Bifacial dye-sensitized solar cells based on an ionic liquid electrolyte', *Nat. Photonics*, 2, 693–698. DOI: https://doi.org/10.1038/nphoton.2008.224

[29]. Ooshaksaraei, P., Sopian, K., Zulkifli, R., Alghoul, M. A. and Zaidi, H. (**2013**) 'Characterization of a Bifacial Photovoltaic Panel Integrated with External Diffuse and Semimirror Type reflectors', *Int. J. Photoenergy*, 2013, 465837. DOI: https://doi.org/10.1155/2013/465837

[30]. Wang, G., Shen, F., Wang, F. and Chen, Z. (**2020**) 'Design and experimental study of solar CPV system using CLFR concentrator', *Sustain. Energy Technol. Assess.*, 40, 100751. DOI: https://doi.org/10.1016/j.seta.2020.100751

[31]. Han, X., Tu, L. and Sun, Y. (**2021**) 'A spectrally splitting concentrating PV/T system using combined absorption optical filter and linear Fresnel reflector concentrator', *Sol. Energy*, 223, 168-181. DOI: https://doi.org/10.1016/j.solener.2021.05.039

[32]. Steiner, M., Wiesenfarth, M., Martinez, J. F., Siefer, G. and Dimroth, F. (**2019**) 'Pushing Energy Yield with Concentrating Photovoltaics', *AIP conf. Proc.,* 2149, 060006-1 – 060006-5. DOI: https://doi.org/10.1063/1.5124199

[33]. Selvaraj, P., Baig, H., Mallick, T. K., Siviter, J., Montecucco, A., Li, W., Paul, M., Sweet, T., Gao, M., Knox, A. R. and Sundaram, S. (**2018**) 'Enhancing the efficiency of transparent dye-sensitized solar cells using concentrated light', *Sol. Energy Mater Sol. Cells*, 17, 29-34. DOI: https://doi.org/10.1016/j.solmat.2017.10.006

[34]. Cooper, T., Ambrosetti, G., Pedretti, A. and Steinfeld, A. (**2014**) 'Surpassing the 2D limit: A 600x high-concentration PV collector based on a parabolic trough with tracking secondary optics', *Energy Procedia*, 57, 285–290. DOI: https://doi.org/10.1016/j.egypro.2014.10.033

[35]. Zaghloul, H., Emam, M., Abdelraman, M. A. and Abd Rabbo, M. F. (**2021**) 'Optimization and parametric analysis of multijunction high-concentrator PV cell combined with a straight fins heat sink', *Energy Convers. Manag.,* 243, 114382. DOI: https://doi.org/10.1016/j.enconman.2021.114382

[36]. Shanks, K., Senthilarasu, S. and Mallick, T. K. (**2016**) 'Optics for concentrating photovoltaics: Trends, limit and opportunities for materials and design', *Renew. Sust. Energ. Rev.,* 60, 394-407. DOI: https://doi.org/10.1016/j.rser.2016.01.089

[37]. Chemisana, D. and Mallick, T. K. (**2014**) **'**Building integrated concentrating solar systems. in Solar Energy Sciences and Engineering Applications', 1st Ed.; CRC Press, London, UK, 17, 545-788.

[38]. Ustaoglu, A., Kandili, C., Cakmak, M. and Torlakli, H. (**2020**) 'Experimental and Economical Performance Investigation of V-Trough Concentrator with Different Reflectance Characteristic in Photovoltaic Applications', *J. Clean. Prod.*, 272, 123072. DOI: https://doi.org/10.1016/j.jclepro.2020.123072

[39]. Wang, N. Y., Chiang, S. Y., Chou, T. L., Lee, H. L. and Chiang, K. N. (**2010**) 'Life prediction of high concentration photovoltaic modules subjected to thermal cycling test', *2010 5th International Microsystems Packaging Assembly and Circuits Technology Conference,* 3–6. DOI: 10.1109/IMPACT.2010.5699530.

[40]. Wang, P., Yang, L., Wu, H., Cao, Y., Zhang, J., Xu, N., Chen, S., Decoppet, J. D., Zakeeruddin, S. M. and Gratzel, M. (**2018**) 'Stable and Efficient Organic Dye-Sensitized Solar Cell Based on Ionic Liquid Electrolyte', *Joule,* 2, 2145–2153. DOI: https://doi.org/10.1016/j.joule.2018.07.023

[41]. Raga, S. R. and Fabregat-Santiago. (**2013**) 'Temperature effect in dye-sensitized solar cells', *Phys. Chem. Chem. Phys.,* 15, 2328-2336. DOI: https://doi.org/10.1039/C2CP43220J

[42]. Hirst, L. C. and Daukes, J. E. (**2011**) 'Fundamental Losses in Solar Cells', *Prog. Photovolt: Res. Appl.,* 19, 286-293. DOI: https://doi.org/10.1002/pip.1024

[43]. Nagaraj, P., Sasdharan, A., David, V. and Sambandam, (**2017**) 'Effect of Cross-Linking on the Performances of Starch-Based Biopolymer as Gel Electrolyte for Dye-Sensitized Solar Cell Applications', *Polymers,* 9, 667. DOI: https://doi.org/10.3390/polym9120667

[44]. Raut, P., Kishnani, V., Mondal, K., Gupta, A. and Jana, S. C. (**2022**) 'A review on Gel Polymer Electrolytes for Dye-Sensitized Solar Cells', *Micromachines,* 13. 680. DOI: 10.3390/mi13050680

[45]. Hagfeldt, A., Boschloo, G., Sun, L., Kloo, L. and Pattersson, H. (**2010**) 'Dye-Sensitized Solar Cells', *Chem. Rev.*, 110, 6595-6663. DOI: https://doi.org/10.1021/cr900356p

[46]. Nei de Freitas, J., Nogueira, A. F. and De Paoli, M-A. (**2009**) 'New Insights into Dye-Sensitized Solar Cells with Polymer Electrolytes', *J. Mater. Chem*., 19, 5279-5294. DOI: https://doi.org/10.1039/B900928K

[47]. Iftikhar, H., Sonai, G. G., Hashmi, S. G., Nogueira, A. F., Lund, P. D. **(2019)** 'Progress on Electrolytes Develoment in Dye-Sensitized Solar Cells', *J. MDPI Materials.*, 12, 1998, 1-68. DOI: 10.3390/ma12121998

[48]. Gu, S., Bi, E., Fu, B., Dodbiba, G., Fujita, T., Wilkinson, D. P., Wei, Y., Fang, B. **(2017)** 'A Circulating Electrolyte for High Performance Carbon-Based Dye-Sensitized Solar Cell', *J. ChemComm Comunication.*, 53, 5561-5564. DOI: 10.1039/c7cc02266b

Chapter 2
Dye-Sensitized Solar Cells: Theoretical and Fundamental Study

2.1 Photoelectrochemical Conversion of Solar Energy

The photoelectrochemical solar cell, also called solar cell or photovoltaic cell, is an electrical device that converts the light energy coming from the sun directly into electricity. The phenomenon of the conversion of light into electricity is called photovoltaic effect, which is a physical and chemical phenomenon. The photovoltaic effect is close to the photoelectric effect, a phenomenon where the light is absorbed, causing the excitation of an electron or other charge carrier to a higher-energy state level. Photovoltaic cells are known to be the most efficient routes to solar-energy conversion and storage. The photoelectrochemical phenomenon of photovoltaic cells can be approached by photogalvanic cells using metal electrodes, photovoltaic solar cells based on semiconductor electrodes, and liquid junction photoelectrochemical cells where the semiconductors are immersed in redox electrolytes.

2.1.1 Photogalvanic Cells

The *galvanic effect* is a process of electron generation on potential differences. A photogalvanic cell is a term to describe photo-electrochemical devices. The concept of photogalvanic cells is different from photovoltaic cells. In photovoltaic cells, electricity is generated by electrons excited directly by photons, whereas in photogalvanic cells, an electric current is generated by a molecule excited by a photon through a spontaneous chemical oxidation–reduction (redox) reaction [1-4]. When exposed to sunlight, a particular chemical can carry out an instinctive chemical reaction, which can produce energy from the electron transfer process [3]. The energy produced is then captured before the recombination process occurs. The simple approach is to use two metal electrodes in a dye solution corresponding to the electron acceptor:

$$X^+ + e^- \rightarrow X \quad (reduction)\ (cathode) \tag{2.1}$$

$$Y^+ \rightarrow Y + e^- \qquad (oxidation)\ (anode) \tag{2.2}$$

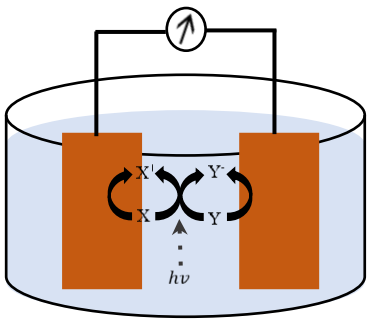

Figure 2.1 Schematic of a photogalvanic cell.

Figure 2.1. shows the schematic principle of photogalvanic cells. The net effect of the mediated reduction would be the driving of the electron through an external load and hence, the overall conversion of light to electricity.

2.2 Dye-sensitized Solar Cells

DSSCs have received significant attention because they have the potential to become low-cost solar cells. In 1991, Gratzel and O'regan made a breakthrough in the field of solar cells by imitating the photosynthesis process in plants and applying it to DSSCs. In the plant, the process of photosynthesis occurs when carotenoids and chlorophyll in green leaves absorb sunlight to convert water and carbon dioxide into carbohydrates and oxygen. In a DSSC, solar energy is absorbed by dye molecules attached to a mesoporous semiconductor and convert it into electricity. Converting solar energy into electricity in a DSSC is quite simple; light is absorbed by the dye molecules causing electrons in the dye to be excited towards the conduction band, and then flow through the semiconductor. The molecules in the dye are then regenerated by an electrolyte containing a redox mediator. The cycle is closed by the reduction of the redox

couple at the counter electrode.

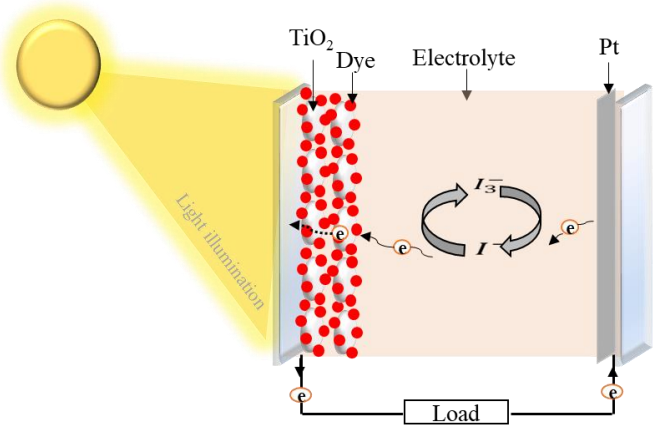

Figure 2.2 Schematic structure of a DSSC.

It is essential to control the energy level and kinetics of the DSSC in order to achieve high efficiency. The kinetics and energy level are related to the processes in the cell. The output current determines the absorption spectra of the dye and the number of photons that can be absorbed and converted into electricity. Meanwhile, the output voltage is determined by the potential difference between the quasi-fermi level (E_F) and the redox mediator. A large surface area of the semiconductor is required to increase the light absorption efficiency so that more dye is absorbed into the semiconductor. A mesoporous semiconductor material consisting of interconnected nanoparticles with a size of approximately 20 nm is generally used to enhance the surface area of the semiconductor. Although the surface area is essential to increase the efficiency of the DSSC because it increases the interface between the dye and the electrolyte, it also increases the possibility of a recombination process. Therefore, controlling the kinetic process and energy level is a challenge in a DSSC. Figure 2.2 shows schematically the basic architecture of a DSSC.

2.2.1 Components of a DSSC

Among the third generation of solar cells, DSSCs have a simple structure formed by a sandwich arrangement of two transparent conducting oxide (TCO) electrodes. The primary structure of a DSSC consists of five components, which are the TCO film-coated glass substrate, photo anode, dye, electrolyte, and counter electrode.

Conducting glass substrate

The TCO-coated glass works as a substrate for the photo anode and counter electrode. Coating of the conductive glass is required for collection of the electrons ejected from the photo anode and passed to the counter electrode through the outer circuit. Commonly, TCO films are made of fluorine-doped tin oxide (FTO) or indium-doped tin oxide (ITO). At room temperature, the TCO film has a very low electrical resistance of less than 15–20 Ω/sq. The conductive substrate should have a maximum transparency to solar radiation, be a highly abundant material, and have low cost [5-9].

Photoanode

In DSSCs, the photoanode plays a significant role as a working electrode with the function of adsorbing dye molecules, transferring electrons, and converting photons into electrical energy [7-11]. Basically, the photoanode consists of a conducting substrate, a semiconductor layer deposed on the conducting substrate, and a sensitizer adsorbed on the semiconductor layer. The performance of a photoanode is strongly dependent on the properties of the semiconductor layer, which should efficiently facilitate light harvesting, electron injection, and electron collection [10,12].

The semiconductor layer is a junction with a large contact area for dye adsorption and allows electrons to transfer through the DSSC. The performance of the DSSC is strongly influenced by the performance of the semiconductor layer, which is determined

by the light harvesting efficiency (LHE) of the dye, the quantum yield of electron injection, and the efficiency collecting the injected electrons [10,13-14]. The ideal semiconductor layer should have a nanostructured mesoscopic morphology to obtain a high specific surface area for dye adsorption, and mesoporous oxides are the most commonly used materials as the semiconductor layer, including TiO_2, ZnO, SnO_2, and Nb_2O_5 [9]. Among them, mesoporous TiO2 is the most applied material in DSSCs owing to its advantages including abundance, nontoxicity, large band gap and suitable band edge levels for charge injection and extraction, long lifespan of the excited electron, resistance to photon corrosion, and low cost [9,11]. The highest reported efficiency based on TiO_2 nanoparticles is 13% [15].

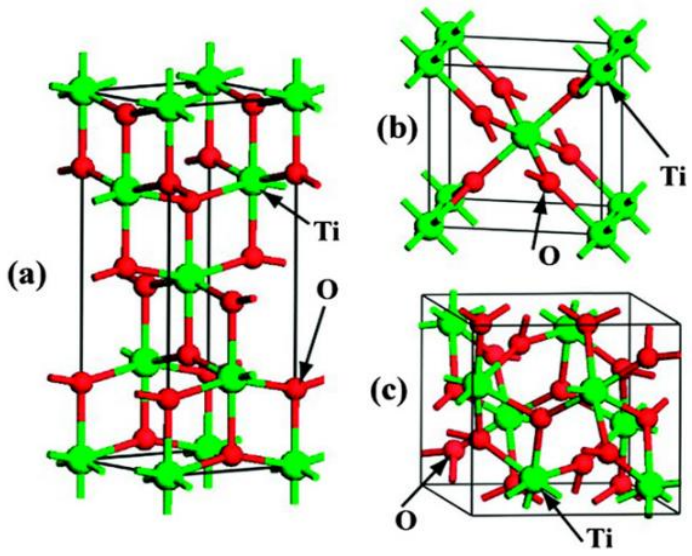

Figure 2.3 TiO_2 crystalline phase a) anatase, b) brookite, and c) rutile [9].

The crystalline TiO_2 is classified into anatase (tetragonal), rutile (tetragonal), and brookite (orthorhombic), as shown in fig 2.3. In DSSCs, anatase is the most commonly used phase owing to its superior charge transport nature [16-17]. The band gap of anatase TiO_2 is 3.2 eV at an absorption edge of 388 nm, and its resistivity is 1015 Ω.cm [6-7,9,18].

Anatase TiO_2 has a high dielectric constant ($\varepsilon = 80$) and provides good electrostatic shielding of the injected electron from the oxidized molecule, preventing the electrons from recombining before the reduction of the dye molecule by the electrolyte. The high refractive index of anatase TiO_2 ($n = 2.5$) results in efficient diffuse scattering of light inside the porous photoanode and hence, significantly enhanced light adsorption [9].

For application in DSSCs, a viscous TiO_2 paste is commonly coated onto a conductive substrate (FTO glass) by screen printing or doctor blade techniques, then annealed at 450–450 °C for 30 min for binder removal. Owing to the annealing, the metal oxide has good adhesion to the FTO glass substrate, interparticle contact, and eventually forms a nanostructured porous electrode. The thickness of the formed porous electrode film is approximately 10–15 μm and the interconnected nanoparticle size ranges from 15 to 30 nm [7].

Dye/sensitizer

The main reason for using dye in DSSC is because the band gap of the TiO_2 semiconductor is too high (~4.2 eV) to absorb visible light and convert it directly into electricity. Dye is required to be entangled in the TiO_2 semiconductor to capture sunlight. The dye is an important part, which plays the centralized role in initiating the mechanism of ejecting electrons on irradiation in DSSCs. The dye/sensitizer acts as a molecular electron pump because it absorbs the incident photons and then generates photoexcited electrons [6,9-10]. A good and efficient sensitizer is adsorbed onto the photoanode semiconductor and has strong and broad absorption of sunlight at all wavelengths below 920 nm, and it also has excellent chemical stability toward light and heat [3,9]. Optimization of the molecular structure of the sensitizer prevents the aggregation on the semiconductor electrode surface.

Electron transport from the sensitizer to the photoanode should be easy to produce a DSSC with good performance. Therefore, the excited state level of the dye should have higher energy than that of the photoanode [6]. The dye absorption spectrum, the amount of dye attached to the semiconductor, the extinction dye coefficient, and the absorption width are important factors affecting the LHE value. The LHE comes from the absorption of the stained semiconductor, according to Eq. 2.3.

$$LHE(\lambda) = 1 - 10^{-A(\lambda)} \tag{2.3}$$

The primary types of sensitizers that have been used during the past decades are metal-based sensitizers and metal-free organic sensitizers. Metal-based sensitizers that have been extensively studied for DSSCs comprise the chromophores of ruthenium complexes. The report shows that ruthenium-based sensitizers can achieve solar-to-electricity conversion efficiencies of approximately 11% [19] under AM1.5 conditions owing to their favorable photoelectrochemical properties, excellent chemical stability, and intense light absorption over a broad visible range. Gratzel et al. developed and modified several efficient Ru-based complex photosensitizers.

The first broadly used Ru-based complex photosensitizer is red dye, better known as N3 (*cis*-bis(isothiocyanato)bis-(4,40-dicarboxylic acid-2,20-bipyridine) Ru (II)) [6,9,19].

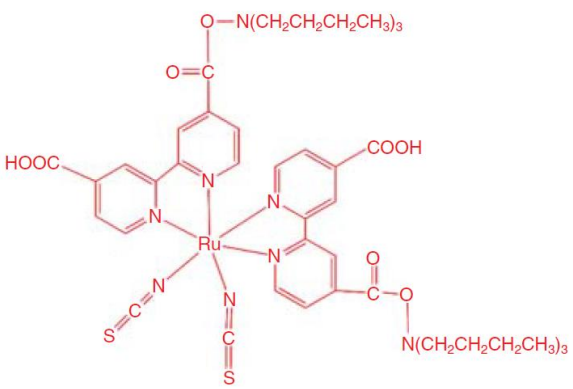

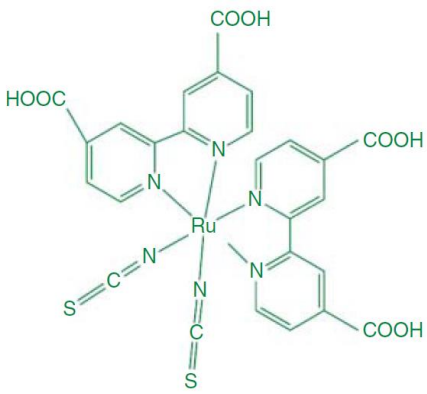

(a) (b)

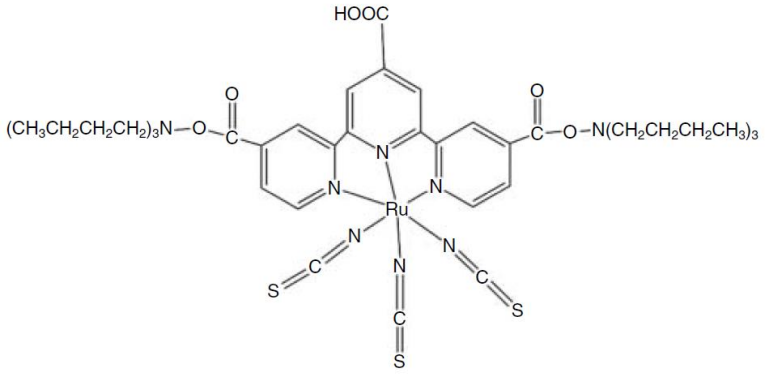

(c)

Figure 2.4 Chemical structures of a) N719, b) N3, and c) black dye used in DSSCs [6,9].

The other two efficient dye sensitizers in the same group are N719 and N749, which is known as black dye. N719 with the formula (*cis*-bis(4,4′-dicarboxy-2,2′-bipyridine) diisothiocyanato-ruthenium(II)) has been considered the reference dye sensitizer in DSSCs owing to its improved power conversion efficiency. Meanwhile, N749 with the formula tris(isothiocyanato)-2,20,200-terpyridyl-4,40,400-tricarballylate Ru(II) is aimed at improving the efficiency of sensitizers in the near-infrared (NIR) region. The ruthenium-based sensitizer shows high energy conversion efficiency especially in the iodide/triiodide-based electrolyte. The structures for these three efficient sensitizers of DSSCs are shown in Fig. 2.4.

Electrolytes

The next important part of a DSSC is the electrolyte. The presence of the redox shuttle in the electrolyte facilitate the transport of charges or ions between the photoanode and counter electrode [3,6-10]. A good electrolyte solvent is one that has low viscosity, high dielectric properties, high boiling point, and negligible vapor pressure. Environmental sustainability, easy processing, and robustness by chemical inertness are also important

from an industrial perspective [3]. Most of all, there are two kinetic requirements for an ideal redox shuttle; it must reduce the dye cation before it recombines with an electron in the photoanode, but not allow the oxidized form of the shuttle to intercept the electron from the photoanode [10]. Those dual criteria of fast dye regeneration and slow interception are a very challenging constraint for identifying effective redox shuttles.

Among the many redox shuttles examined, the iodide/triiodide couple (I^-/I_3^-) has been identified as the best and most commonly used in DSSCs. The I^-/I_3^- redox electrolyte is promising owing to its ability to infiltrate deep inside the semiconductor nanoporous layer, slow recombination loss, and fast regeneration of dye molecules. It is known that the redox shuttle is the one that encourages charge transport between the photoanode and counter electrode. When the dye molecules inject electrons into the semiconductor metal oxide, the tri-iodide in the electrolyte helps in reducing the oxidized dye as quickly as possible to the ground state [6,20]. The iodide, an electron acceptor, moves to the counter electrode and receives its lost electrons and regenerates as tri-iodide. The circuit is completed by the electron migration through the external load. The process of electron transfer is shown in Fig. 2.5.

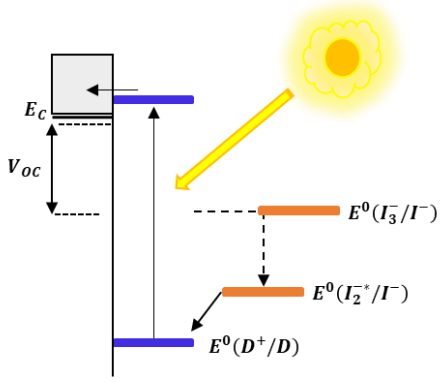

Figure 2.5 Schematic of a DSSC using I^-/I_3^- redox couple.

The report shows that the efficiency obtained by the DSSC is approximately 11% using the I^-/I_3^- redox couple combined with a ruthenium-based sensitizer [21]. The capture of electrons on the surface of the photoanode (usually TiO_2), which is relatively slow, can minimize the recommendation process in the DSSC. For this reason, the efficiency of the DSSC can be increased using an I^-/I_3^- redox couple-based electrolyte. For dye and electrolyte regeneration, the redox potential of the I^-/I_3^- should be considered. Figure 2.5 shows the regeneration process of the I^-/I_3^- redox electrolyte. For some types of the I^-/I_3^- redox couple electrolyte, the dye regeneration process can be expressed as Eq. 2.4:

$$D^+ + I^- \; dye \; regeneration \rightarrow \; D + I_3^-. \tag{2.4}$$

In fact, there are successive reactions at the photoanode semiconductor interface [20,22-24], as shown in Eqs. 2.5 and 2.6:

$$D^+ + I^- \rightarrow [D \ldots I] \, I^- \rightarrow \; D + I_2^{-*} \, I_2^{-*} \rightarrow \; D + I_3^- + I^- \tag{2.5}$$

$$D^+ + I_2^{-*} \rightarrow [I_2 \ldots D] \, I^- \rightarrow \; D + I_3^-. \tag{2.6}$$

The electrolyte regeneration process is complete with the oxidation of I_3^- ions to I^- ions at the counter electrode. The reduction process of I_3^- at the counter electrode may occur sequentially and rapidly [20,24-25], as shown in Eq. 2.7:

$$I_3^- + e^- \rightarrow I^- + I_2^{-*} \, e^- \rightarrow \; 3I^-. \tag{2.7}$$

The application of reaction 2.5 to DSSCs depends on the transport ability of the redox mediator between the photoanode and the counter electrode. The transport ability of this redox mediator is affected by the conductivity and diffusivity of the electrolyte. The conductivity of the electrolyte [20,26] is expressed in Eq. 2.8:

$$\sigma = \sum \mu_i n_i q_i \tag{2.8}$$

with σ is conductivity, μ_i is mobility, n_i is carrier concentration, and q_i is charge of the ionic specimen. The mobility of the specimen ion causes a temperature effect. In homogeneous electrolytes, the temperature dependence of conductivity $(ln\,\sigma \approx 1/T)$ is linear, whereas in heterogeneous electrolytes it is non-linear. This temperature effect can be expressed in the Arrhenius [20,27] and Vogel–Tamman–Fulcher (VTF) equations, [20,28] shown in Eqs. 2.9 and 2.10 below:

$$\sigma = \sigma_0 exp(E_A/k_B T) \tag{2.9}$$

$$\sigma = \sigma_0 exp[-B/k_B(T - T_0)] \tag{2.10}$$

where σ_0 is the conductivity constant, which depends of materials' properties; k_B is the Bolztman constant, E_A is activation energy, B is pseudo activation energy, T is temperature, and T_0 is the temperature equilibrium related to the transition temperature of glass. At present, this redox shuttle is used as electrolyte in any standard cell.

Counter electrode

The counter electrode must also ensure rapid reaction and low overpotential, and therefore, the counter electrode must have good catalytic activity characteristics. The metal material known to have the best catalytic activity is platinum (Pt), and thus Pt is suitable as a counter electrode. Charge transfer resistance (R_{CT}) in DSSCs is generated due to a charge transfer reaction at the counter electrode. To obtain reaction pushing at a certain current density (J), an overpotential (ζ) is required, and under small overpotential conditions, R_{CT} can be expressed by Eq. 2.9:

$$R_{CT} = \zeta/J. \tag{2.11}$$

In ideal conditions, the magnitude of $R_{CT} \leq 1\Omega.cm^2$ to avoid significant losses. One indication of the declining performance of a DSSC is the low fill factor (FF) value, which can occur due to poor counter electrodes.

2.2.2 Electron Transfer Steps in a DSSC

In the process of converting light energy into electricity, the electron transfer process in each part of the DSSC should be known. This electron transfer will affect the performance of the DSSC. The electron transfer process starts from the light illuminating the DSSC. Figure 2.6 shows the electron transfer process in a DSSC.

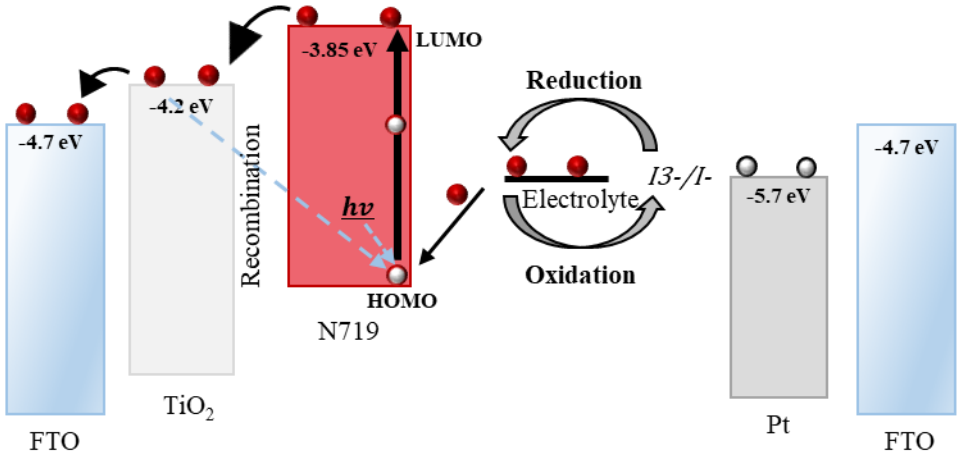

Figure 2.6 Mechanism of electron transfer in a DSSC.

When the light illuminates the DSSC, the dye absorbs incident photons from the light. With the energy from photons, the electron is excited, changing from the ground state to the excited state. The expression for this phenomenon can be written as follows:

$$S + hv \rightarrow S^* \qquad \text{(photoexcitation).} \qquad (2.12)$$

When the electron is at the excited state, the electrons can move or be injected into the semiconductor's conduction band or decay back to the ground state (recombination) [3,9,43]. The formation of the absorption light by the dye can be express as follows:

$$S^* \rightarrow S + hv' \qquad \text{(emission/recombination),} \qquad (2.13)$$

$$S^* \rightarrow S^+ + e^- \qquad \text{(electron injection into } TiO_2 \text{ semiconductor).} \qquad (2.14)$$

The electron that is injected into the conductor band of TiO_2 semiconductor then travels through the FTO glass to pass through the external circuit and reach the counter electrode.

After the electron is injected into the conductor band of TiO2 semiconductor, the oxidized dye will receive the electron from the redox mediator present in the electrolyte and then be reduced rapidly to the ground state, as expressed in Eq. 2.15:

$$3S^+ + 3I^- \rightarrow 2S + I_3^- \qquad \text{(regeneration of dye).} \qquad (2.15)$$

At the same time, the I^- will be oxidized into I_3^- and then diffuse toward the counter electrode. In the last step, I_3^- is reduced back to I^- at the counter electrode. The process of the last step can be expressed as in the following equation:

$$I_3^- + 2e^- \rightarrow 3I^- \qquad \text{(regeneration of } I^-\text{).} \qquad (2.16)$$

If the oxidized dye is reduced rapidly in the absence of the redox mediator to assist the reduction process, then the oxidized dye will interact with the electrons in the TiO_2 layer, resulting in a recombination process without any measurable photocurrent, as follows:

$$S^+ + e^-(TiO_2) \rightarrow S \qquad \text{(recombination).} \qquad (2.17)$$

This recombination process might decrease the performance of DSSCs.

2.2.3 Key Efficiency Parameters of DSSCs

The working ability and working performance of DSSCs are determined by their power conversion efficiency (η) and power output (P_{OUT}). For calculating both efficiency and power output of a DSSC, the short circuit current density (J_{SC}), open circuit voltage (V_{OC}), power input (P_{IN}), and fill factor (FF) should be considered. P_{IN} depends on the light source, generally from a solar simulator with 1 sun illumination or approximately 100 $mW.cm^{-2}$. The sunlight to electric power conversion efficiency (PCE) in a DSSC is given by the following equation:

$$\eta = \frac{P_{OUT}}{P_{IN}} \times 100\% \qquad (2.18)$$

and P_{OUT} can be determined by following expression:

$$P_{OUT} = J_{SC} \times V_{OC} \times FF. \quad (2.19)$$

Meanwhile, J_{SC} is related to the diffusion length of the electron and the surface passivation. The equation for J_{SC} can be approximated as the following equation [41]:

$$J_{SC} = q \times G(L_n + L_p) \quad (2.20)$$

where G is the generation rate, and L_p and L_n are the hole and electron diffusion lengths, respectively. J_{SC} can also be expressed as follows [3,9]:

$$\int IPCE(\lambda) \times e \times \Phi(\lambda) d\lambda \quad (2.21)$$

with

$$IPCE(\lambda) = \frac{N_{electrons}}{N_{photons}}, \quad (2.23)$$

where IPCE is defined as the ratio of the number of photo generated electrons ($N_{electrons}$) flowing in the external circuit to the number of incident photons ($N_{photons}$) with a given wavelength, e is the elementary charge, and $\Phi(\lambda)$ is the photon flux. From the above equation, it can be assumed that J_{SC} depends strongly on the generation rate and diffusion length.

The open circuit voltage (V_{OC}) in a typical photoelectrochemical cell can be described as the difference in energy of the electron at the semiconductor and the counter electrode, or the difference in energy level of the quasi-fermi level of the semiconductor under illumination and the Nernst potential of the electrolyte solution [9,20,24-25]. V_{OC} is measured when no current flows through the cells and for a regenerative photoelectrochemical system, V_{OC} can be expressed with the following equation:

$$V_{OC} = V_T \, ln\left(1 + \frac{J_{SC}}{J_S}\right). \quad (2.23)$$

The next important parameter for observing the performance of a DSSC is the fill factor (*FF*). in principle, *FF* can be described as the ratio of the maximum power output

(P_{max}) from the DSSC to the product of J_{SC} and V_{OC}. In other words, *FF* is a parameter that determines the maximum power of a DSSC [41]. The equation to express *FF* is as follows:

$$FF = \frac{P_{max}}{I_{SC} \times V_{OC}} \tag{2.24}$$

with

$$P_{max} = I_{max} \times V_{max}, \tag{2.25}$$

where I_{max} and V_{max} represent respectively the photocurrent and photo-voltage corresponding to P_{max}. The typical current density and voltage curve, with J_{SC}, V_{OC}, and P_{max}, is shown in Fig. 2.7

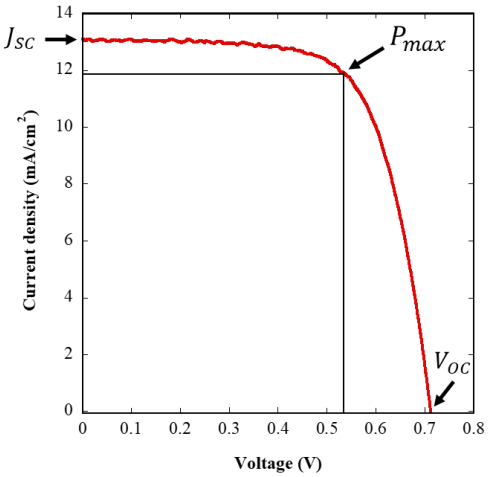

Figure 2.7 Typical current density and voltage curve of a DSSC.

2.3 Characterization Techniques

This section describes the characterization techniques used to identify the phenomena that may occur in a DSSC. The characterization techniques include the coating material technique used to fabricate the photo-anode and counter electrode and the measurement technique used to observe the performance of DSSCs.

2.3.1 Doctor Blade Method

There are several methodologies for synthesis of material coatings, such as spray coating [30-32], dip coating [33,34], doctor blade [29,35], and spin coating [29,36]. Among these methodologies, doctor blade is commonly used in DSSC fabrication owing to its simple procedures and the better performances obtained [29, 37]. Because the deposition method can significantly affect the performance of a DSSC, a brief explanation of the doctor blade method becomes necessary.

Doctor blade coating, also known as 'tape casting' method, is a technique to coat material onto a substrate with a well-defined thickness [29,38-40]. In principle, the doctor blade technique is suitable for coating materials in sol gel form or materials with adequate density. In DSSCs, the TiO_2 photo-anode and Pt counter electrode are coated on the FTO using this method. The process is as follows: TiO_2 and Pt paste are placed on the surface of the FTO with the aid of a blade or rigid spatula. Then, with a constant movement, the TiO_2 and Pt paste are evenly spread on the surface of the FTO substrate. Figure 2.8 shows the doctor blade technique. The TiO_2 and Pt thin films produced from the coating process are then placed on a suitable place with temperature control until evaporation of the solvent and fixation occur, resulting in TiO_2 and Pt coated on the FTO. The thickness of the TiO_2 and Pt thin film can be measured by adjusting the gap between the doctor blade and the FTO substrate.

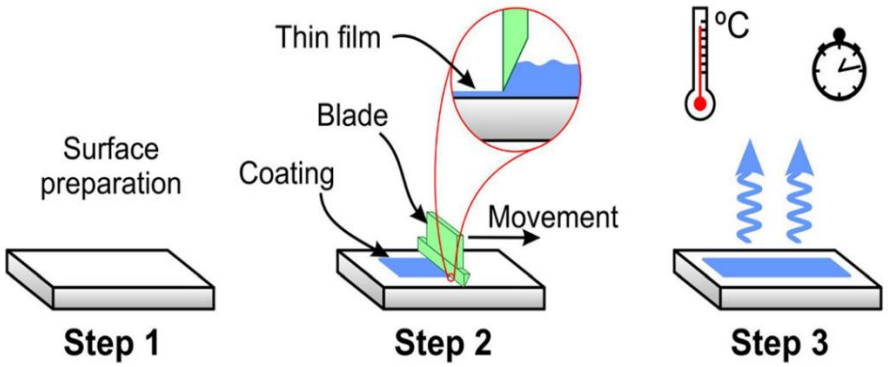

Figure 2.8 Doctor blade method [29].

Several studies report that solar cells using the doctor blade method have better performance compared to other thin film coating methods. In 2018, Ananda et al. reported a comparison between the doctor blade method and the bar coating method for carbon-based counter electrode application. The result shows that DSSCs using the doctor blade method achieve higher performance [37]. In 2019, Ji et. al. observed the performance of an organic solar cell (OSC) using the doctor blade and spin coating methods. An efficiency of ~13% was achieved in the OSC with a ZnO cathode using the doctor blade method.

2.3.2 Current–Voltage Characteristic

Current–voltage ($I-V$) characterization is an important characterization technique for solar cells to determine the energy conversion efficiency. Generally, the $I-V$ characteristics are observed under 1 sun illumination (AM1.5G illumination). In principle, the $I-V$ characteristics are obtained under solar irradiation by changing the external load from zero (short circuit conditions) to infinity load (open circuit conditions).

In theory, the $I-V$ curves of solar cell are considered similar to the $I-V$ curves of a diode in "dark" condition. The $I-V$ curves can be shifted down into the fourth quadrant in the Cartesian diagram with light. When the curves are shifting down

to the fourth quadrant, the power of the diode can be extracted. For this reason, the $I-V$ curve of a solar cell is defined as a superposition of the solar cell diode in the dark with the light-generated current [41,42]. Figure 2.9 (a) shows the effect of light shifting the $I-V$ curve down into the fourth quadrant. The blue curve is the condition when a solar cell is without illumination, where the electrical characteristics of the solar cell are the same as a large diode. When the light illuminates the solar cell, the $I-V$ curve shifts down as the cell begins to generate power, as shown by the red curves. The amount of shift increases as the light intensity increases.

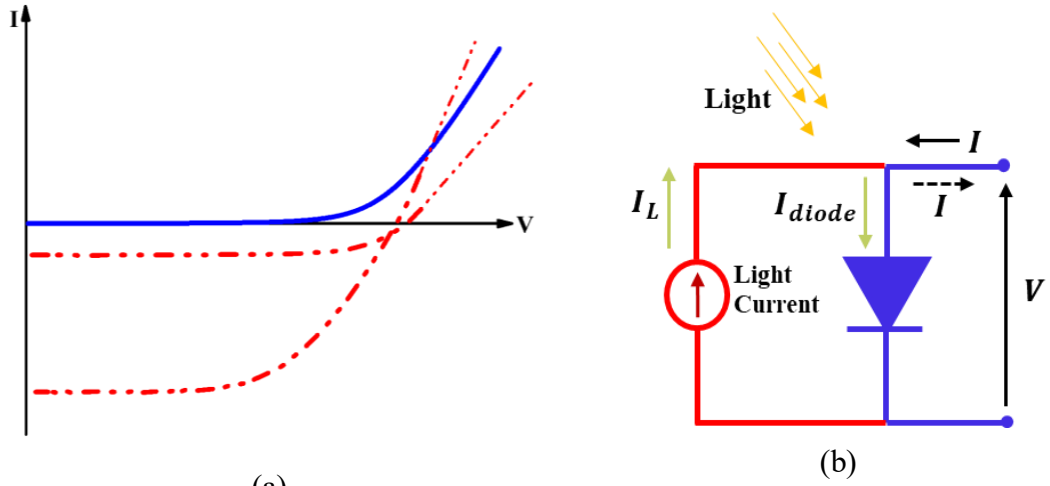

(a) (b)

Figure 2.9 Effect of light shifting the (a) $I-V$ curve down into the fourth quadrant and (b) idealized diode for the $I-V$ characteristics.

The equation used for the $I-V$ characteristics of the idealized diode shown in Fig. 29 (b) under any condition, either forward or applied voltage (reverse bias), according to diode law is the Shockley diode equation:

$$I = I_S\left(e^{\frac{V_D}{jV_T}} - 1\right) \tag{2.26}$$

$$V_T = \frac{kT}{q}, \tag{2.27}$$

where I is the diode current, I_S is the reverse bias saturation current, V_D is the voltage

across the diode, V_T is the thermal voltage, j is the emission coefficient, k is the Boltzmann constant, T is the temperature, and q is the magnitude of charge of an electron. As a solar cell in the dark condition is similar to the diode, then the illumination that a cell adds to the 'dark' currents in the diode generates light generated current (I_L) in the diode law:

$$I = I_S\left(e^{\frac{V_D}{jV_T}} - 1\right) - I_L. \tag{2.28}$$

In a convention, the solar cell curve is flipped into the first quadrant, as shown in Fig. 2.9 (a), and this type of curve is a typical $I - V$ plot in a solar cell.

Because the first quadrant light generated current I_L dominates the saturation current I_S under illumination, Eq. 2.28 becomes

$$I = I_L - I_S\left(e^{\frac{V_D}{jV_T}} - 1\right). \tag{2.29}$$

The (-1) term in Eq. 2.29 can usually be neglected because under illumination, the exponential term is usually $\gg 1$ [41]. Then, the formula can be written as

$$I = I_L - I_S\left(e^{\frac{V_D}{jV_T}}\right). \tag{2.30}$$

Substituting Eq. 2.27 into Eq. 2.30, the formula becomes

$$I = I_L - I_S\left(e^{\frac{V_D}{\frac{jkT}{q}}}\right), \tag{2.31}$$

$$I = I_L - I_S\left(e^{\frac{qV_D}{jkT}}\right). \tag{2.32}$$

Rearranging Eq. 2.32, V_D can be described as

$$I_L - I = I_S\left(e^{\frac{qV_D}{jkT}}\right) \tag{2.33}$$

$$\frac{I_L - I}{I_S} = e^{\frac{qV_D}{jkT}} \tag{2.34}$$

$$ln\left(\frac{I_L - I}{I_S}\right) = \frac{qV_D}{jkT} \tag{2.35}$$

$$V_D = \frac{jkT}{q} ln\left(\frac{I_L - I}{I_S}\right). \tag{2.36}$$

The other important parameter determined from the $I-V$ curves that are used to characterize solar cells is the short circuit current (I_{SC}). I_{SC} is the maximum current through the DSSC when the voltage across the cell is zero [9,41]. The I_{SC} is shown in Fig. 2.8 (a). For an ideal solar cell, I_{SC} and I_L are identical because I_{SC} is derived from the generation and collection of light generation carriers and moderate resistive loss mechanism at ideal solar cells. There are several dependency factors on I_{SC}, such as the area of the solar cell, number of photons caused by light intensity, spectrum of the incident light, optical properties, and minority-carrier collection probability [41]. Generally, I_{SC} is expressed as J_{SC} to remove the dependence of the solar cell area. Therefore, the relationship between I_{SC} and J_{SC} can be expressed as the following equation:

$$I_{SC} = J_{SC}A. \tag{2.37}$$

The open circuit voltage (V_{OC}) is the maximum voltage of a solar cell when the current is zero. In principle, the open circuit voltage is an amount of forward bias on the solar cell caused by the bias of solar cell junction with the light-generated current. V_{OC} is shown on the $I-V$ curves in Fig. 2.9 (a). The equation for V_{OC} is derived from Shockley equation under light illumination:

$$I = I_L - I_S\left(e^{\frac{V_D}{jV_T}} - 1\right) \tag{2.38}$$

$$\frac{I_L - I}{I_S} + 1 = e^{\frac{V_D}{jV_T}} \tag{2.39}$$

$$ln\left(\frac{I_L - I}{I_S} + 1\right) = \frac{qV_D}{jkT} \tag{2.40}$$

Because V_{OC} is the condition when the current through the solar cell is at zero point, the equation for V_{OC} is found to be

$$V_{OC} = \frac{jkT}{q} ln \left(\frac{I_L}{I_S} + 1\right). \quad (2.41)$$

From the equation, it can be simply assumed that V_{OC} might increase linearly with temperature. However, it is difficult to explain the effect of temperature briefly because the increasing temperature changes the intrinsic carrier concentration that results in increasing I_S.

2.3.3 Electrochemical Impedance Spectroscopy

Electrochemical impedance spectroscopy (EIS) is a technique used to investigate the kinetics of electrochemical and photoelectrochemical processes, including the clarification of relevant ionic and electronic processes that occur at different interfaces in various electrochemical devices. EIS is carried out by applying harmonic modulated small-amplitude AC potential $V(\omega, t)$ with certain frequency range $(f = \frac{\omega}{2\pi})$ to an electronical system to measure the current $I(\omega, t)$ of the system, where ω is the angular frequency. The impedance $Z(\omega)$ of the system can be expressed as

$$Z(\omega) = \frac{V(\omega, t)}{I(\omega, t)}. \quad (2.42)$$

When $\omega \to 0$ at $V(\omega, t)$, it is said that the system is driven by DC current and the impedance coincides with the DC resistance (R_{dC}). Thus, Eq. 2.42 can also be written as

$$Z(0) = \frac{V(0, t)}{I(0, t)} = R_{dC} \quad (2.43)$$

in the example of impedance with 0 phase difference.

In complex form, the AC voltage and current can be expressed as $V(\omega, t) = V_0 e^{i\omega t}$ and $I(\omega, t) = I_0 e^{f(\omega t - \theta)}$, respectively, where f is linear frequency, $i = \sqrt{-1}$,

and V_0 and I_0 are the amplitudes of voltage and current signal. Thus, Eq. 2.42 can be written as

$$Z(i\omega) = \frac{V(\omega,t)}{I(\omega,t)} = Z(\omega) = \frac{V_0}{I_0}e^{i\theta} = Z_0 e^{i\theta}. \quad (2.44)$$

Then, by applying Euler's relationship and replacing Z_0 with $|Z|$, Eq. 2.44 can be written as

$$Z(i\omega) = |Z|(\cos\theta + i\sin\theta). \quad (2.45)$$

The general expression for impedance is

$$Z(\omega) = Z_{Re} + iZ_{Im} = Z' + iZ'' \quad (2.46)$$

where $Z_{Re} = Z' = |Z|\cos\theta$ and $Z_{Im} = Z'' = |Z|\sin\theta$ are the real and imaginary part of the impedance, respectively.

EIS data are displayed in the form of a Nyquist and Bode plot. Z" is plotted against Z' for different ω in the Nyquist plot. In the Bode plot, $\log|Z|$ and θ are plotted against $\log f$, where $\theta = \tan^{-1}(Z''/Z')$.

By applying a sinusoidal voltage, $V(\omega,t) = V_0 \sin\omega t$. With the resistance R, the current flowing through the resistor can be described as $I(\omega,t) = \frac{V(\omega,t)}{R} = \frac{V_0}{R}\sin\omega t$. Thus, the impedance of a resistor can be written as

$$Z_R(\omega) = \frac{V(\omega,t)}{I(\omega,t)} = R \quad (2.47)$$

where $V(\omega,t)$ and $I(\omega,t)$ are in phase. At $V(\omega,t)$, capacitance C has a resultant current $I(\omega,t) = C\frac{dV(\omega,t)}{dt} = C\omega V_0 \cos\omega t = C\omega V_0 \sin(\omega t + \frac{\pi}{2})$, where $q = CV$ and $\frac{dq}{dt} = I_t$. As $I_0 = \omega C V_0$, the current trough capacitor becomes $I_t = I_0 \sin(\omega t + \frac{\pi}{2})$. The impedance of the capacitor can be written as

$$Z(\omega) = \frac{V(\omega,t)}{I(\omega,t)} = \frac{1}{\omega C} \quad (2.48)$$

where $\frac{1}{\omega C}$ or $\frac{1}{j\omega C}$ is termed the reactance of a capacitor and $I(\omega, t)$ leads $V(\omega, t)$ by a phase difference of $\frac{\pi}{2}$ [44].

2.4 Concentrator Photovoltaic

An imaging optical system has three main components, namely, the object, the optics, and the image it forms. The light started from the object, captured by the optical system, is then concentrated onto a point in the image. In non-imaging optical systems, a light source and receiver are used instead of an object and image, respectively [45].

The idea of concentrator photovoltaic (CPV) systems is to use a refractive or reflective non-imaging optical component to concentrate and direct sunlight onto a highly reduced area on a solar cell to produce increased energy conversion [46]. Two mediums with refractive indexes n_1 and n_2, respectively, separated by an optical system is shown in figure 2.10. The system concentration ratio can be defined as

$$C_r = \eta_{opt,concent} \times C_g \tag{2.49}$$

where $\eta_{opt,concent}$ denotes the optical efficiency of the concentrator system given by

$$\eta_{opt,concent} = \frac{P_{out}}{P_{in}} \tag{2.50}$$

where P_{out} is the light power exiting the concentrator, P_{in} is the light power entering the concentrator, and C_g is the geometrical concentration defined by the ratio of entrance and exit surface, which is given by

$$C_g = \frac{A_{in}}{A_{out}} = \frac{n_2 \sin\theta_{out}}{n_1 \sin\theta_{in}} \tag{2.51}$$

where A_{in} is the entrance aperture area and A_{out} the exit aperture.

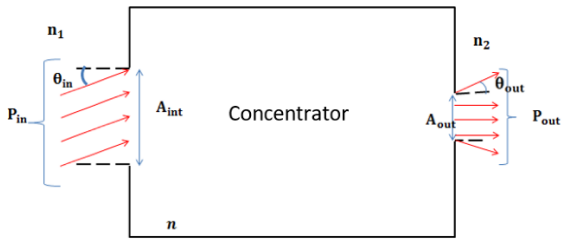

Figure 2.10 General view of an optical system [45].

The compound parabolic concentrator (CPC) was introduced as a way to send the maximum concentrate radiation light trough the exit aperture area or the receiver. Figure 2.11 shows the form of a 2D CPC and the path of an edge ray inside. In Fig. 2.11 (a), the ray enters the CPC at an angle θ to the vertical direction and is reflected toward the receiver's edge. The ray is reflected to the receiver as in the case of the ray entering with angle $\theta_1 < \theta$ presented in fig 2.11 (b). In contrast, the ray ends up going backwards and exits trough the entrance aperture when entering the CPC with angle $\theta_2 > \theta$, as shown in Figure 2.11 (c). The ratio between the number of rays that enter the receiver and the number of rays that enter the PCP is called the acceptance, which is defined as

$$Acceptance = \frac{Number\ rays\ enter\ the\ reciever}{Number\ rays\ enter\ the\ CPC}. \qquad (2.52)$$

Therefore, for $\theta_1 < \theta$ and $\theta_1 > -\theta$ the acceptance is 1 (all the rays entering the receiver) and for $\theta_2 > \theta$ and $\theta_2 < -\theta$ the acceptance is 0 (all the rays entering the CPC are rejected). Angle θ is called the half acceptance angle because the CPC accepts all the radiation within the angle 2θ contained between $-\theta$ and $+\theta$[45].

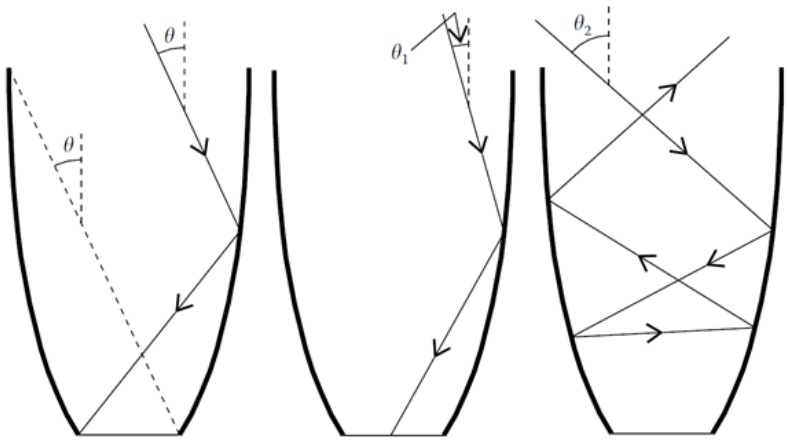

Figure 2.11 Trajectories of three types of rays inside a CPC. (a) A ray entering the CPC at an angle to the vertical of half-acceptance angle θ. This ray is reflected to the edge of the receiver. (b) A ray entering the CPC at an angle to the vertical smaller than θ is accepted (hits the receiver). (c) A ray entering the CPC at an angle larger than θ is rejected by retroreflection (ends up exiting through the entrance aperture) [45].

Besides the acceptance angle of the optic systems above, there is the acceptance angle of a concentrator module. The acceptance angle of a module is a quantity that characterizes the angular tolerance of a module to misalignment between its normal and the perpendicular incident solar rays. It is generally defined as the maximum full angle through which the module can be rotated while continuing to produce 80% of its normal direct irradiation (DNI) normalized maximum power, as shown in Fig. 2.12 [46].

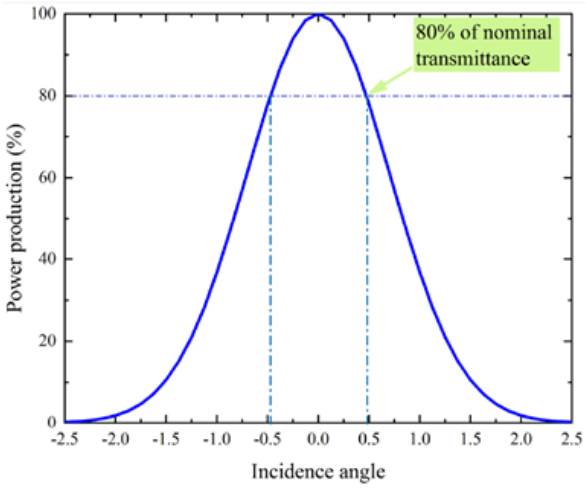

Figure 2.12 Hypothetical power production of a module [46].

The I_{SC} of a photovoltaic module in a concentrating system, at constant temperature, depends only on the irradiance on the module, which is determined solely by the optical efficiency of the concentrator. The comparison between the I_{SC} as function of the transverse angle of the incident light and the I_{SC} of a reference module can be used to determine the optical efficiency of the system toward the angular movement of the module. The optical efficiency can be expressed as

$$\eta_{opt}(\theta_T) = \frac{1}{C_g} \frac{I_{SC}^{conc}(\theta_T)}{I_{SC}^{reference}(\theta_T)} \tag{2.53}$$

where θ_T is the transverse incident light angle and C_g is the geometrical concentration defined by the ratio of entrance and exit surface [47].

REFERENCES

[1]. Robinson, J. K., McMurry, J. E., and Fay, R. C. (**2020**) '*Chemistry (8th Edition)'*, United Stated of America: Pearson Education, ISBN: 978-0-134-85623-0 (student edition).

[2]. Zumdahl, S. S., Zumdahl, S. A. (**2007**) '*Chemistry (7th Edition)'*, Boston New York: Houhjton Mifflin Company, ISBN: 978-0-618-52844-8 (student edition).

[3]. Kalyanasundaram, K. (**2010**) '*Fundamental Science: Dye-Sensitized Solar Cells (1st Edition)'*, Lausanne, Switzerland: EPFL Press, ISSBN: 978-2-940222-36-0.

[4]. Clark, W. D. K., Eckert, J. A. (**1975**) 'Photogalvanic Cells', *Journal of Solar Energy*, Vol. 17: 147-15. DOI: https://doi.org/10.1016/0038-092X(75)90052-3

[5]. Yang, Z., Gao, S., Li, T., Liu, F. Q., Ren, Y., Xu, T. (**2012**) 'Enhanced Electron Extraction from Template-Free 3D Nanoparticulate Transparent Conducting Oxide (TCO) Electrodes for Dye-Sensitized Solar Cells', *Journal of ACS Appl. Mater. Interfaces,* 4, 8, 4419–4427. DOI: https://doi.org/10.1021/am301090a

[6]. Karthick, S. N., Hemalatha, K. V., Balasingam, S. K., Clinton, F. M., Akshaya, S., Kim, H. J. (**2020**) 'Dye-Sensitized Solar Cells: History, Components, Configuration, and Working Principle, in Pandikumar, A., Jothivenkatachalam, K., Bhojanaa, K. B. (eds), *Interfacial Engineering in Functional Materials for Dye-Sensitized Solar Cells (1st Edition)*, United State of America: John Wiley & Sons Inc, pp 1-16, ISBN: 9781119557333. DOI: https://doi.org/10.1002/9781119557401.ch1

[7]. Pandikumar, A., Jothivenkatachalam, K., Bhojanaa, K. B. (**2020**) '*Interfacial Engineering in Functional Materials for Dye-Sensitized Solar Cells (1st Edition)'*, United State of America: John Wiley & Sons Inc, ISBN: 9781119557333. DOI: 10.1002/9781119557401

[8]. Lau, K. K. S. and Soroush, M. (**2019**) Overview of Dye-Sensitized Solar Cells, in Soroush, M. and Lau, K. K.S. (eds), *'Dye- Sensitized Solar Cells: Mathematical Modeling, and Materials Design and Optimization'*, Elsevier: Joe Hayton, PP:1-49, ISBN: 978-0-12-814541-8, DOI: 10.1016/B978-0-12-814541-8.00001-X

[9]. Lin, L. Y. and Ho, K. C. (**2018**) 'Dye-Sensitized Solar Cells', in Guenther, B. D. and Steel, D. G. (eds), *Encyclopedia of Modern Optics (2nd Edition)*, Vol. 5, 270-281. DOI: 10.1016/B978-0-12-803581-8.09545-X

[10]. Hu, Y. H. and Wei, W. (**2018**) 'Dye-Sensitized Materials', in Dincer, I. (ed), *Comprehensive Energy Systems*, vol. 2, 150-181, DOI: 10.1016/B978-0-12-809597-3.00216-9

[11]. Akila, Y., Muthukumarasamy, N. and Velauthapillai, D. (**2019**) 'TiO_2-Based Dye-Sensitized Solar Cells', in Thomas, S., Sakho, E. H. M., Kalarikkal, N., Oluwafemi,

S. O. and Wu, J. (eds), *Nanomaterial for Solar Cell Applications*, Elsevier Inc., 127-144. DOI: 10.1016/B978-0-12-813337-8.00005-9

[12]. Gratzel M. (**2004**) Conversion of Sunlight to Electric Power by Nanocrytalline Dye-Sensitized Solar Cells, *J. Photochem. Photobiol. A: Chem.,* 164, 3-14. DOI: https://doi.org/10.1016/j.jphotochem.2004.02.023

[13]. Adachi, M., Murata, Y., Okada, I. and Yoshikawa, S. (**2003**) 'Formation of Titania Nanotubes and Application for Dye-Sensitized Solar Cells', *J. Electrochem. Soc.,* Vol. 150, Issue 8, G488-G493. DOI: 10.1149/1.1589763

[14]. Bisquert, J. and Vikhrenko, V. S. (2014) 'Interpretation of the Time Constants Measured by Kinetic Techniques in Nanostructured Semiconductor Electrodes and Dye-Sensitized Solar Cells', *J. Phys. Chem. B*, 108, 2313-2322. DOI: 10.1021/jp035395y

[15]. Mathew, S., Yella, A., Gao, P., Baker, R. H., Churchod, B. F. E., Ashari-astani, N., Tavernelli, I., Rothlisberger, U., Nazeeruddin, Md, K. and Gratzel, M. (**2014**) 'Dye-Sensitized Solar Cells with 13% Efficiency Achieved Through the Molecular Engineering of Porphyrin Sensitizers', *Nat. Chem.*, Vol. 6, 242-247. DOI: 10.1038/NCHEM.186

[16]. Rauf, M.A., Hisaindee, S. and Meetani, M. A. (**2011**) 'An Overview on Photocatalytic Degradation of Azo Dyes in presence of TiO_2 Doped with Selective Transition Metals', *Desalination*, 276, 13-27. DOI: 10.1016/j.desal.2011.03.071

[17]. Park, H., park, Y., Kim, W. and Choi, W. (**2013**) 'Surface Modification of TiO_2 Photocatalyst for Environmental Applications, *J. Photochem. Photobiol. C: Photochem. Rev*., 15, 1-20. DOI: 10.1016/j.jphotochemrev.2012.10.001

[18]. Ardakani, H. K. (**1994**) 'Electrical and optical properties of in situ "hydrogen-reduced" titanium dioxide thin films deposited by pulsed excimer laser ablation', *Thin Solid Films,* 248, 2, 234-239. DOI: 10.1016/0040-6090(94)90017-5

[19]. Nazeeruddin, M. K., Kay, A., Rodicio, I., Baker, R. H., Muller, E., Liska, P., Vlachopoulos, N. and Gratzel, M. (**1993**) 'Conversion of light to Electricity by *cis*-X_2Bis(2,2'-Bipyridyl-4,4'-Dicarboxylate)Ruthenium(II) Charge-transfer Sensitizers (X=Cl^-, Br^-, I^-, CN^-, and SCN^-) on Nanocrystalline TiO_2 Electrodes', *J. Am. Chem. Soc.* Vol. 115, No. 14, 6382-6390. DOI: 10.1021/ja00067a063

[20]. Wu, J., Lan, Z., Lin, J., Huang, M., Huang, Y., Fan, L. and Luo, G. (**2015**) 'Electrolytes in Dye-Sensitized Solar Cells', *J. Chem. Rev.,* 115, 5, 2136-2173. DOI: 10.1021/cr400675m

[21]. Chiba, Y., Islam, A., Watanabe, Y., Komiya, R., Koide, N. and Han, L. (**2006**) 'Dye-Sensitized Solar Cells with Conversion Efficiency of 11.1%', *Jpn. J. Appl. Phys.,* Vol. 45, No. 25, pp. L638-L640. DOI: https://doi.org/10.1143/JJAP.45.L638

[22]. Privalov, T., Boschloo, G., Hagfeldt, A., Svensson, P. and Kloo, L. (**2009**) 'A Study of the Interactions between I^-/I_3^- Redox Mediators and organometallic Sesnitizing Dyes in Solar Cells', *J. Phys. Chem. C,* 113, 783-790. DOI: 10.1021/jp81020c

[23]. Rowley, J. G., Farnum, B. H., Ardo, S. and Meyer, G. J. (**2010**) 'Iodide Chemistry in Dye-Sensitized Solar Cells: making and Breaking I-I Bonds for Solar Energy Conversion', *J. Phys. Chem. Lett.,* 1, 3132-3140. DOI: 10.1021/jz101311d

[24]. Boschloo, G. and Hagefeldt, A. (**2009**) 'Characteristic of the Iodide/Triiodide Redox Mediator in Dye-Sensitized Solar Cells', *J. Acc. Chem. Res.,* Vo. 42, No. 11, pp. 1819-1826. DOI: 10.1021/ar900138m

[25]. Ferber, J., Stangl, R. and Luther, J. (**1998**) 'An Electrical Model of the Dye-Sensitized Solar Cell', *Journal of Solar Energy Materials and Solar Cells,* Vol. 53, pp. 29-54, DOI: 10.1016/S0927-0248(98)00005-1

[26]. Ratner, M. A. and Shriver, D. F. (**1988**) 'Ion Transport in Solvent-Free Polymers', *J. Chem. Rev*., 88, 1, 109-124. DOI: 10.1021/cr00083a006

[27]. Arrhenius, S. A. Z. (**1889**) 'On the Reaction Rate of the Inversion of Non-Refined Sugar Upon Souring', *Z. Phys. Chem., 4, 226–248*

[28]. Fulcher, G. S. (**1925**) 'Analysis of Recent Measurements of the Viscosity of Glasses, Journal of the American Ceramic Society', Vol. 8, Issue 6, pp. 339-355. DOI: 10.1111/j.1151-2916.1925.tb16731

[29]. Frederichi, D., Scaliante, M. H. N. O., Bergamasco, R. (**2021**) 'Structured Photocatalytic Systems: Photocatalytic Coating in Low-Cost Structures for Treatment of Water Contaminated with Micropollutants – A Short Review', Environ Sci. Pollut. Res', 28: 23610-23633. DOI: 0.1007/s11356-020-10022-9

[30]. Gardon, M., Guilemany, J. M. (**2014**) 'Milestones in Functional Titanium Dioxide Thermal Spray Coatings: A review', *J. Therm. Spray Technol.*, 23, 577-595. DOI: 0.1007/s11666-014-0066-5

[31]. Li, F., Lan, X., Wang, L., Kong, X., Xu, P., tai, Y., liu, G., Shi, J. (**2020**) 'An Efficient Photocatalyst Coating Strategy for Intimately Coupled Photocatalysis and Biodegradation (ICPB): Powder Spray Method', *Chem. Eng. J.*, 383, 123092. DOI: 10.1016/j.cej.2019.123092

[32]. Zhai, M., Liu, Y., Huang, j., Hou, W., Wu, S., Zhang, B., Li, H. (**2020**) 'Fabrication of TiO2-SrCO3 Composite Coatings by Suspension Plasma Spraying: microstructure

and Enhanced visible light Photocatalytic Performances', *J. Therm. Spray Technol*., 29, 1172-1182. DOI: 10.1007/s11666-020-01022-9

[33]. Marien, C. B. D., Le Pivert, M., Azais, A., M'Bra, I. C., Drogui, P., Dirany, A., Robert, D. (**2019**) 'Kinetic and mechanism of Paraquat's Degradation: UV-C photosys vs UV-C Photocatalysis with TiO2/SiC Foams', *J. Hazard. Mater.,* 370: 164-171. DOI: 10.1016/j.jhazmat.2018.06.009

[34]. Hakki, H. K., Allahyari, S., Rahemi, N., Tasbihi, M. (**2019**) 'Surface Properties, Adherence, and Photocatalytic Activity of Sol-Gel Dip-Coated TiO2-Zno Films on Glass Plates', *C. R. Chim.,* 22: 393-405. DOI: 10.1016/j.crci.2019.05.007

[35]. Sirirerkratana, K., Kemacheevakul, p., Chuangchote, S. (**2019**) 'Color Removal From Wastewater by Photocatalytic Process Using Titanium Dioxide-Coated Glass, Ceramic tile, and Stainless Steel Sheets', *J. Clean. Prod.,* 215: 123-130. DOI: 10.1016/j.jclepro.2019.01.037

[36]. Tahir, M. B., Hajra, S., Khalid, N. R., Rizwan, M. and Watto, G. N. (**2018**) 'Development of Sol Gel Derived Nanocrystalline TiO2 Thin Films via Indigenous Spin Coating Method', *J. Inorg. Organoment Polym.*, 28: 1-8. DOI: 10.1007/s10904-017-0690-x

[37]. Ananda, W., Mutiari, A. and Widiatmoko, P. (2017) 'Development Method of Making Dye-Sensitized Solar Cell (DSSC) using Carbon as Counter Electrode', *Conference Paper of The 15th International Conference Quality in Research (QIR),* ISSN: 1411-1284.

[38]. Berni, A., Mennig, M. and Schmidt, H. (**2004**) *Sol-Gel Technologies for Glass Producers and Users: Doctor Blade, 1st Edition,* Germany: Kluwer Academic Publisher, ISBN: 978-1-4419-5455-8

[39]. Francis, L. F. and Roberts, C. C. (**2016**) Dispersion and Solution Processes, in Francis, L. F. *'Material Processing'*, Elsevier Inc. pp. 415-512. DOI: 10.1016/B978-0-12-385132-1.00006-9

[40]. Cherrington, R. and Liang, J. (**2016**) Materials and Deposition Processes for Multifuctionality, in Goodship, V., Middleton, B. and Cherrington, R. (eds), *Design and Manufacture of Plastic Components for Multifunctionality*, Elsevier Inc., pp. 19-51. DOI: 10.1016/B978-0-323-34061-8.00002-8

[41]. Honsberg, C. and Bowden, S. (2019) Photovoltaics Education Website: I-V Curve, *www.pveducation.org* (Accessed: 22 Mei 2022)

[42]. Lindholm, F. A., Fossum, J. G. and Burgess, E. L. (**1979**) 'Application of the Superposition Principle to Solar-Cell Analysis', *IEEE Trans. Electron Devices*, 26, 3: 165-171. DOI: 10.1109/T-ED.1979.19400

[43]. Katumo, N., Mugo, S. W., Ngaruiya, J. M., Ngumbi, P. K. and John, B. M. (**2015**) Graphene Supported Platinum Counter Electrode for Dye Sensitized Solar Cells, *Int. J. Innov. Res. Technol. Sci. Eng.*, 4, 12, 2319-8753. DOI: 10.15680/IJIRSET.2015.0412106

[44]. Rahman, Md. M.; Nath, C. N. and Lee, J. (**2015**) 'Electrochemical Impedance Spectroscopic Analysis of Sensitization-Based Sola Cells', *Isr. J. Chem*., 55, 99-1001. DOI: 10.1002/ijch.201500007

[45]. Chaves, J. (**2008)** 'Introduction to Nonimaging Optics', Florida, USA: CRC Press, ISBN-13: 978-1-4200-5429-3.

[46]. Himer, S. E., Ayane, S. E., Yahyaoui, S. E., Salvestrini, J-P. and Ahaitouf, A. (**2020**) 'Photovoltaic Concentration: Research and Development', *Energies*, 13 (21), 5721. DOI: https://doi.org/10.3390/en13215721

[47]. Nilson, J. (**2005**) 'Optical Design and Characterization of Solar Cocentrators for Photovoltaics', Lund Institute of Thechnology, Lund, Sweden: Devision of Architecture and Building Design, ISBN: 91-85147-15-X.

Chapter 3

Dye-Sensitized Solar Cells with Low Concentrated Light System

The abundance of solar energy shows the significant role of solar cell technology in solving the global energy crisis and environmental problems caused by the depletion of fossil fuel reserves. Among the available solar cells, DSSCs are attractive owing to their simple fabrication process, low cost, performance stability, and eco-friendliness [1–4]. Despite these advantages, the low power output and efficiency of less than 10% [5–10] still are a major bottleneck in DSSC development.

To increase the efficiency and power output, a bifacial structure has been utilized by exploiting the solar radiation absorptions on the front and rear surface of solar cell [11–15]. Furthermore, in the bifacial system, a back reflector could also be used to enhance the reflectivity for increasing light-harvesting at the rear side of solar cells [16–17]. A reflector concentrator, such as a Fresnel lens [18-20] or a parabolic mirror [21,22], is commonly used to improve light harvesting of solar cells [18-25]. Solar concentrators are categorized into low ($< 10\times$), medium ($10\times - 100\times$), high ($100\times - 2000\times$), or ultrahigh ($> 2000\times$) depending on light concentration [26]. A concentrating photovoltaic system is effective to increase solar cell output power and efficiency. Despite the benefit, the application of concentrators in solar cells is still limited owing to side effects such as high-temperature operation. High temperatures could be fatal for a solar cell, especially for DSSCs because of the damage to the liquid electrolyte [27-29].

Liquid electrolytes are the most widely used transport medium for DSSCs. The liquid electrolyte should be chemically and physically stable, a good solvent for redox couple components and various additives, and less viscous to minimize charge carrier transport resistance. Moreover, the electrolyte should not cause significant dissociation of the adsorbed dye, electrode, and sealing materials [30-34]. The solvent is a fundamental component in liquid electrolytes. Among organic solvents, acetonitrile has the best

performance despite its toxicity and has a boiling point of 82 °C [35-36]. Other nitrile-based organic solvents such as propionitrile [37] and 3-methoxypropionitrile [38] offer better thermal stability (97 and 164 °C boiling points, respectively) and are less toxic [30]. Although the thermal stability and performance of nitrile-based solvent electrolytes have already been investigated [39-42], the nitrile-based electrolyte performance and thermal stability under concentrated light has yet to be explored.

Here, we evaluated the performance characteristics of bifacial DSSCs coupled with a reflector and a low light concentrator. A plane mirror and concave aluminum-coated mirror were adopted as back reflector and concentrator, respectively. The investigation was focused on the increase in performance of a DSSC when coupled with a back reflector and concentrator, effective mirror distance, cell degradation by operational time, and rise in temperature.

3.1 Experimental Section

3.1.1 Cell Fabrication

Bifacial DSSCs were fabricated using doctor blade methods. Two FTO glass substrates (Sigma Aldrich 2.3 mm, ~13 Ω/sq) were cut to a size of 1.5 × 2 cm^2 and cleaned using acetone, ethanol, and purified water for 20 min. TiO_2 (Solaronix Ti-Nanoxide T/SP) was printed on the FTO glass using the doctor blade method and sintered at 450 °C for 30 min in an electric furnace. After the substrate was cold, a dye solution (N719 Solaronix) was soaked on FTO/TiO_2 for 20–24 h. A hole was made on the other FTO glass for iodine injection. Platinum paste (Dyesol PT-1) was printed on the FTO glass using the doctor blade method and sintered at 450 °C for 30 min in an electric furnace.

Two sealants (Solaronix Meltonix 1170-60) were cut to a size of 1.4 × 1.4 cm^2, and the hole was made on one of them with a size of 1.25 × 1.25 cm^2. Afterward, the

FTO/Pt/sealant with hole and the FTO/TiO_2/Dye were overlapped into an FTO/Pt/Sealant/Dye/TiO_2/FTO sandwich structure. Subsequently, the cell was put on a hotplate and pressed until the sealant melted. After that, iodide electrolyte (AN-50, Solaronix) was injected into the cell through the hole in the FTO/Pt side and it was closed using the second sealant. The structure of the DSSC is shown in Fig. 3.1.

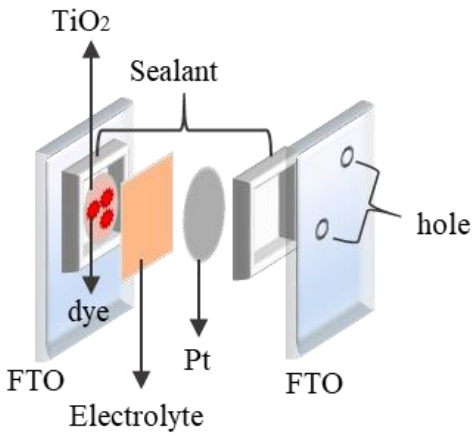

Figure 3.1 DSSC assembly

3.1.2 Measurement

The performance of the bifacial DSSC was measured with a source meter (Keithley 2400) under illumination from a Xenon lamp equipped with an air mass (AM) 1.5 filter. Plane aluminum-coated mirrors (Edmund Optics, 43-469) were used as the low concentrator. Conventional measurements without mirrors were conducted to obtain the characteristics of the bifacial DSSC under front light illumination at 8 cm below the light source. The effect of the measurement time and mirror distance were investigated with the plane mirror concentrator as a parameter mirror distance x (0, 1, 2, 3, …, 10) cm between the mirrors and the solar cells, as shown in Fig. 3.2. The surface temperature of each side of the bifacial DSSC was measured with a thermocouple. The area power density of light incident on the DSSC was deduced using a power and energy meter (NOVA P/N 7Z01500 OPHIR Japan ltd.).

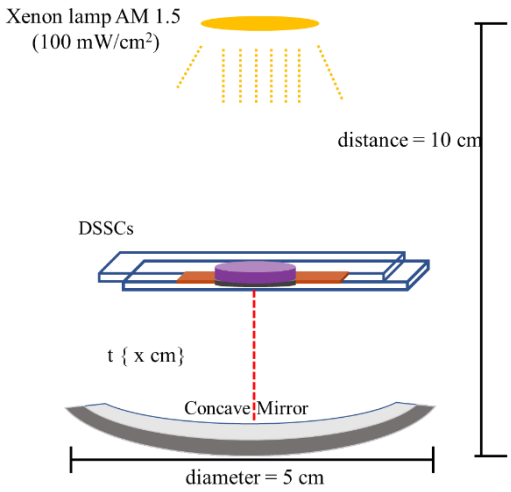

Figure 3.2 Experimental setup.

3.2 Experimental Results and Discussion

3.2.1 Low Concentrator

This section will discuss the DSSC using a plane mirror as the back reflector and a concave mirror as the low concentrator. To determine the performance of the DSSC, the effect of distances and operational time were observed. Furthermore, the effect of temperature in DDSCs with different electrolytes has also been investigated.

A. Photocurrent–Voltage Analysis

Optical parameter

The acceptance angle of a solar cell module can be expressed as the maximum full angle through which the module can be rotated while continuing to produce 80% of its DNI normalized maximum power. The plane back reflector and back concentrator acceptance angles for different incident light angles with a distance of 2 cm from cell to mirror are shown in figure 3.3. The power production at 0° incident angle was smaller than that at some other angles. This may occur because part of the light is reflected or

absorbed by the DSSC before it is reflected by the mirror. The half-acceptance angles for the plane and concave mirrors are 44° and 24° from the vertical direction, respectively.

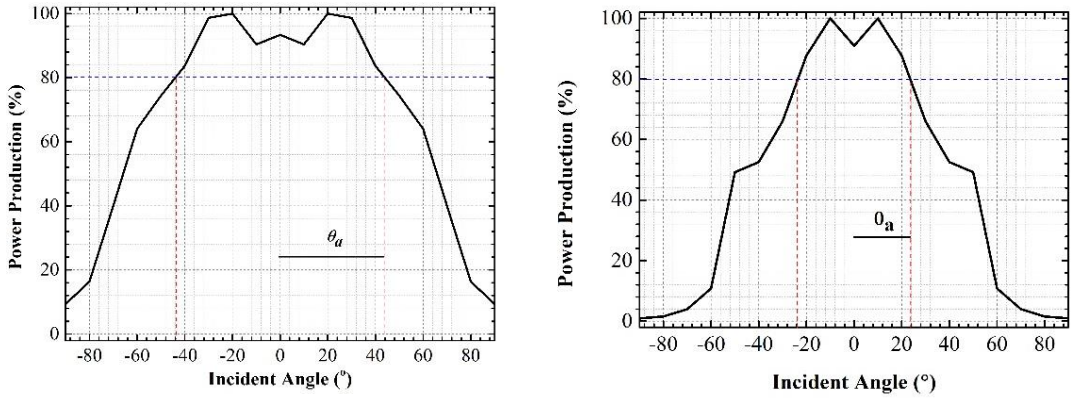

(a) (b)

Figure 3.3 Normalized power production at different light incident angles for the (a) plane and (b) concave mirror with 2 cm cell-to-mirror distance

The optical efficiency was used to measure the angular dependence of the optical system toward the incident light angle. It can be expressed as

$$\eta_{opt}(\theta_T) = \frac{1}{C_g} \frac{I_{SC}^{conc}(\theta_T)}{I_{SC}^{reference}(\theta_T)} \tag{3.1}$$

where θ_T is transverse incident light angle and C_g is the geometrical concentration defined by the ratio of entrance and exit surfaces [43]. The optical efficiency of the plane and concave mirrors with 2 cm cell-to-mirror distance is shown in Fig. 3.4. The plane mirror has optical efficiency of ~ 0.18 as the plane mirror itself is only a reflector, and a large amount of reflected light does not hit the DSSC cell. The concave mirror has maximum optical efficiency of 0.18. The reason for this low optical efficiency may be that the aperture of the cell as receiver is smaller than the aperture of the mirror concentration point at 2 cm distance from the mirror. This causes that a significant amount of reflected light does not hit the cell (receiver). Other possibility to explain the low optical efficiency is that the limited DSSC light conversion leads to heat accumulation in

the cell. In contrast with the plane mirror, the concave mirror concentrates the reflected light, but as the incident angle increases, the concentration point of the reflected light moves from the original point and the optical efficiency decreases to near 0.

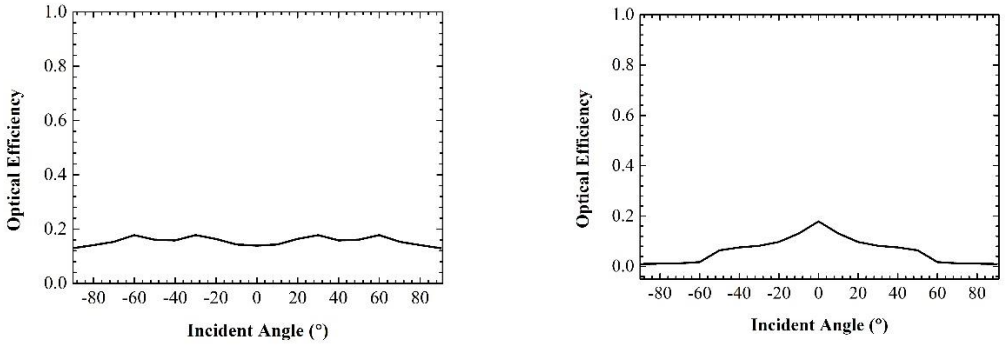

(a) (b)

Figure 3.4 Optical efficiency at different light incident angles for the (a) plane and (b) concave mirrors with 2 cm cell-to-mirror distance.

Effect of distance

A different plane mirror (back reflector) and concave mirror (back concentrator) distance was applied to determine the effective mirror distance of rear-side illumination regarding the performance and operation of the DSSC. The cell-to-mirror distance observed in this study ranged from 1 to 10 cm. Photovoltaic–voltage curves with a variation of the plane mirror back reflector distance are shown in fig 3.5 (a). P_{OUT} was increased when comparing the conditions with plane mirror concentrator applied and with no mirror. The measurement results summarized in Table 3.1 reveal that the performance of the DSSC increases according to J_{SC}, whereas that with the other parameters tends to be the same. As the illumination from the front side remains the same (constant source–DSSC distance), the increase in J_{SC} was caused by the rear side illumination. The highest result was obtained at 2 cm mirror distance with J_{SC} of 11.50 $mA.cm^{-2}$ and P_{OUT} of 5.62 $mW.cm^{-2}$. At this distance, the rear side illumination is assumed to be in the

maximum condition. We assumed that at a distance less than 2 cm, the light mirror reflection was reduced by the shadowing/shading effect on the mirror by the cell itself. In contrast, an increasing distance will reduce the self-shading from the cell but also the amount of reflected light arriving at the rear-side cell. At 10 cm distance, the values of J_{SC} and P_{OUT} decrease to 10.02 $mA.cm^{-2}$ and 4.90 $mW.cm^{-2}$, respectively. It is assumed that with increasing mirror distance, the scatter of the light reflected by the plane mirror becomes wider, which decreases the possibility of the reflected light to reach the dye.

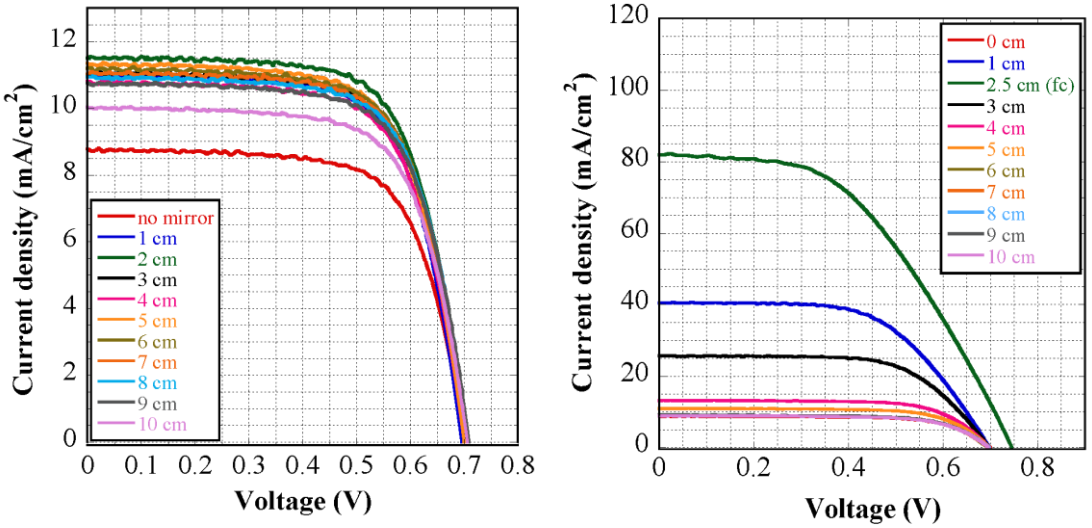

(a) (b)

Figure 3.5 *J–V* curves of DSSCs coupled with (a) a plane mirror back reflector and (b) a concave mirror back concentrator at different cell–mirror distances

A concave mirror with a diameter of 5 cm was used as a back concentrator. The light focused by the concentrator reaching the TiO_2/dye from the rear side of the DSSC can increase the illumination significantly and lead to a rise in J_{SC}. As shown in Fig. 3.5 (b), the highest J_{SC} was produced at a distance of 2.5 cm (focal point), where it achieved ~82 $mA.cm^{-2}$, nine times more than that under the no mirror condition. The light

reflected by the concave mirror is shown in Fig. 3.4. The light varies as the cell distance from the focal point of the concave mirror leads to a lower J_{SC}. Furthermore, at distances of more than 6 cm, the effect of the concave mirror back concentrator becomes negligible.

Table 3.1 Photovoltaic parameter of DSSCs coupled with plane mirror back reflector

x (cm)	V_{OC} (V)	J_{SC} $(mA.cm^{-2})$	FF	P_{OUT} $(mW.cm^{-2})$
No mirror	0.70	8.78	0.69	4.25
1	0.70	11.02	0.69	5.26
2	0.70	11.50	0.69	5.62
3	0.70	11.01	0.69	5.34
4	0.70	10.80	0.68	5.16
5	0.70	11.35	0.68	5.41
6	0.70	11.19	0.69	5.42
7	0.71	11.02	0.69	5.35
8	0.71	10.92	0.69	5.32
9	0.71	10.75	0.69	5.24
10	0.71	10.02	0.69	4.90

Table 3.2 Photovoltaic parameter of DSSCs coupled with concave mirror back concentrator

x (cm)	V_{OC} (V)	J_{SC} $(mA.cm^{-2})$	FF	P_{OUT} $(mW.cm^{-2})$
No mirror	0.70	8.78	0.69	4.25
1	0.70	40.40	0.59	16.54
2.5	0.75	81.90	0.47	29.01
3	0.70	25.65	0.64	11.42
4	0.70	13.12	0.69	6.34
5	0.70	10.92	0.69	5.29
6	0.69	9.01	0.70	4.35
7	0.70	8.98	0.69	4.32
8	0.70	8.99	0.69	4.32
9	0.70	9.07	0.69	4.35
10	0.70	8.84	0.69	4.27

The geometrical ratio (C_g) changes with the increase in distance as the mirror output aperture increases, as shown in Fig. 3.6 (a). As the aperture of the module solar cell remains the same, a substantial amount of light from the concave concentrator will fall on the outside of the module, as shown in Fig. 3.6 (b)

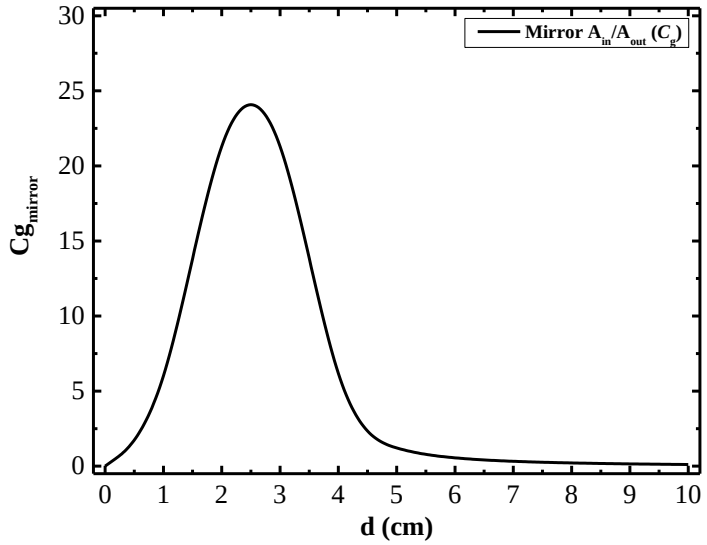

(a)

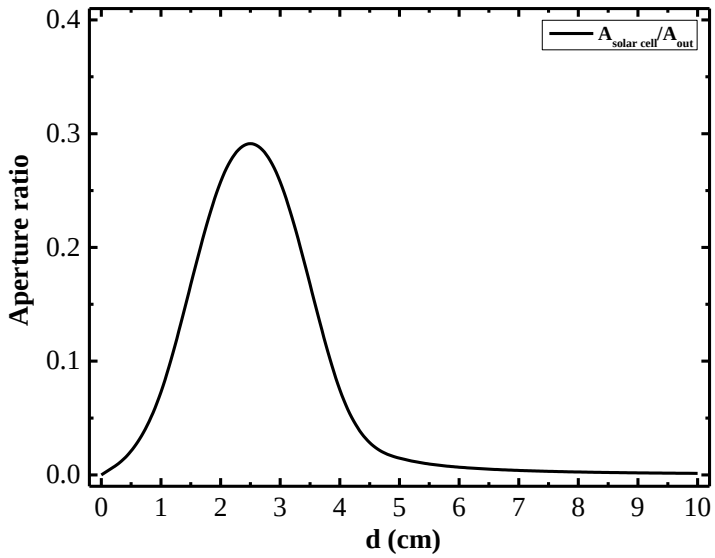

(b)

Figure 3.6 (a) Calculated concave mirror Cg at different points of distance from the mirror, and (b) solar cell and output mirror aperture ratio.

Even though a significant amount of light energy falls outside the solar cell, the optical efficiency can be used to observe the solar cell enhancement. The optical efficiency concentrator system can be expressed as

$$\eta_{opt,concent} = \frac{P_{out}}{P_{in}} \qquad 3.2$$

where P_{out} is the light power exiting the concentrator and P_{in} is the light power entering the concentrator [44]. The I_{SC} depends only on the adsorbed P_{out}, and the enhancement in I_{SC} determines the energy ratio that can be adsorbed by the DSSC [45]. This can be expressed as follows:

$$Current\ enhancement = \frac{J_{SC}^{conc}}{J_{SC}^{without\ mirror}}. \qquad 3.2$$

The plane and concave mirror optical efficiency and current enhancement are shown in fig 3.7. Even if the optical efficiency of the reflector plane mirror is less than 1, the J_{SC} of the DSSC becomes enhanced with an effective DSSC-to-mirror distance between 1 and 10 cm. In contrast, the concave mirror optical efficiency is in line with the J_{SC} enhancement with an effective DSSC-to-mirror distance between 1 and 4 cm.

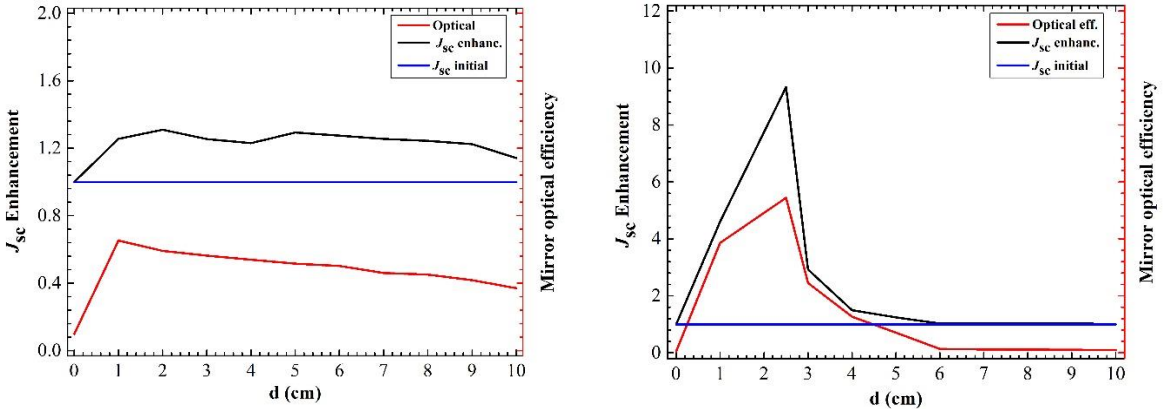

(a) (b)

Figure 3.7 J_{SC} enhancement, J_{SC} initial value, and mirror optical efficiency of (a) plane and (b) concave mirrors

Effect of operational time

The effect of time was examined to determine the adequate time for the DSSC to operate under concentrated light. At this point, the performance of the DSSC was observed every 30 min under a plane and concave mirror. The mirror distance was adjusted at 2 cm for the plane mirror and at 2.5 cm for the concave mirror as the highest rear illumination effect was obtained at these distances. The photocurrent–voltage curve for the DSSC with a plane mirror is shown in Fig. 3.8. The *J–V* curve showed an steady value during the measurement. In contrast, the performance of the DSSC coupled with a concave mirror completely dropped before 30 min of operation. The temperature increased sharply leading to electrolyte evaporation. The spike in temperature caused by the concave mirror concentrator decreased the performance of the DSSC, as shown by the sharp decrease in the *J–V* curves in Fig. 3.8 (b). The electrolyte completely evaporated, in the DSSC sample exhibited in Fig. 3.9 because the temperature reached more than 150 °C, whereas the acetonitrile electrolyte boiling point is approximately 82 °C.

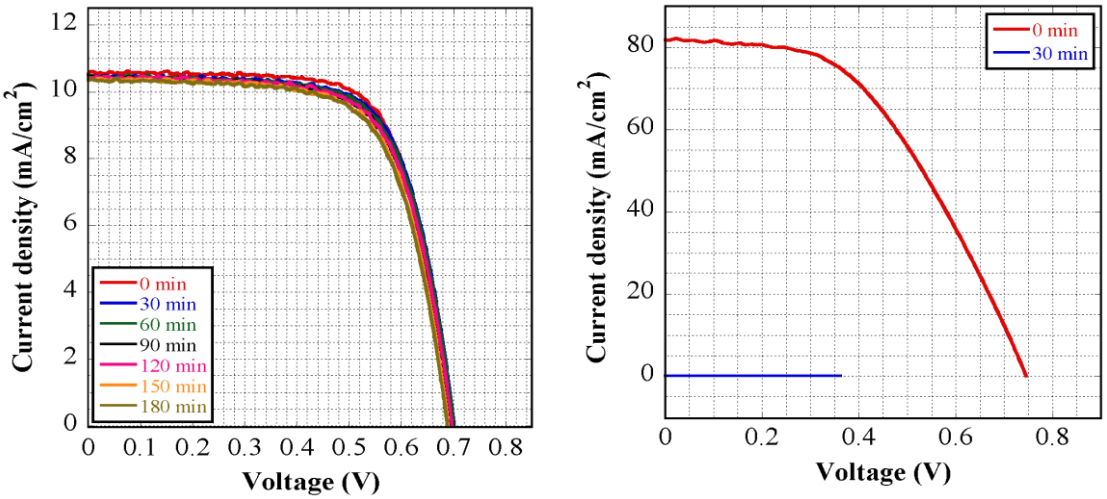

(a) (b)

Figure 3.8 *J–V* curves of DSSCs coupled with (a) a plane mirror for 180 min and (b) a concave mirror for 30 min operational time.

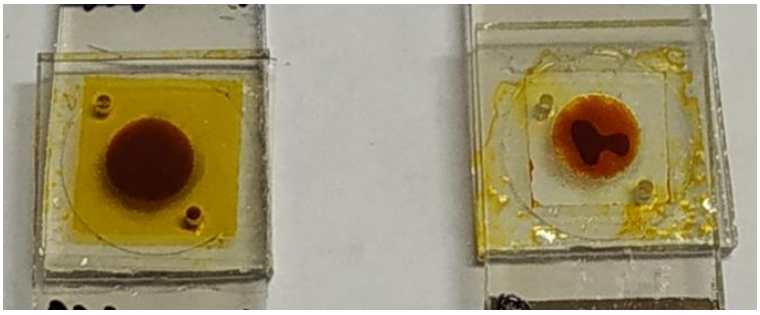

(a) (b)

Figure 3.9 DSSC sample coupled with a concave mirror (a) before and (b) after 30 min operational time.

B. Electrochemical Impedance Spectroscopy

Effect of distance

The charge transfer information, electron diffusion in the electrolyte/dye/TiO_2 interfaces, ion diffusion in the electrolyte, recombination process in the TiO_2/electrolyte interface, and redox regeneration at the Pt counter electrode/electrolyte interfaces can be explained based on the EIS [46-48] analysis. Figure 3.10 shows the equivalent circuit of the impedances in the DSSC and the frequency range used during the EIS measurement. The range frequency in the EIS analysis consists of ultra-high, high, middle, and low frequencies. The ultra-high and high frequency were used for detecting the electrode surface resistance and charge transportation at the counter electrode, the middle frequency (Z_2) for charge transfer at FTO/TiO_2/dye/electrolyte interfaces, and the low frequency (Z_1) for charge transport at the electrolyte [6,49-52].

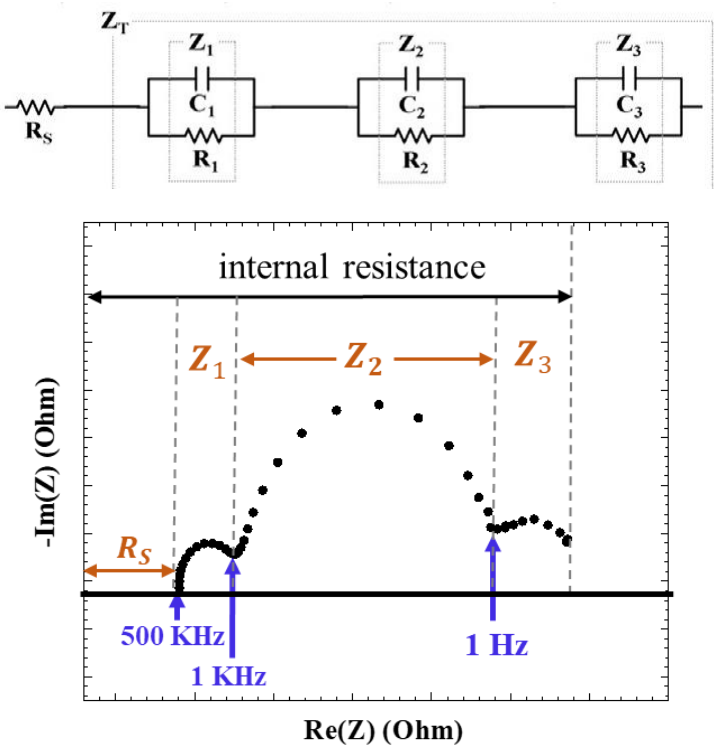

Figure 3.10 Equivalent circuit for electrochemical impedance spectroscopy (EIS) in DSSCs.

The EIS of a DSSC coupled with plane mirror back reflector is shown in Fig. 3.11 (a), and Table 3.3 presents information of Z_1 and Z_2. The second semicircle (Z_2) changed with different cell–plane mirror distances. In contrast, the change in Z_1 and Z_3 was not significant. Z_2 is related to the charge transfer at the interfaces of the TiO_2/dye photoanode. The decrease in R_{CT2} caused by the applied plane mirror indicated the increase of light adsorption in the dye, which leads to fast excitation electrons in the dye and TiO_2 photoanode.

Figure 3.11 (b) shows the Nyquist plot in a DSSC coupled with a concave mirror back concentrator. The second semicircle (Z_2) is similar to that of the plane mirror, and it also changes with an increase in current density. Z_1 and Z_2 show an increase in the semicircle. A summary of the EIS analysis is presented in Table 3.4. When the concave

mirror concentrator is applied to the DSSC, the resistance shows small values. These small values indicate that fast electron transport occurs in both the FTO/TiO_2/dye/electrolyte and electrolyte/Pt/FTO interfaces. Although Pt has a high reflectivity [11,53], the light absorption from the rear side is still sufficiently large to produce a small resistance. The small Z_2 semicircle at 2.5 cm cell-mirror distance or in the focus point indicates that the fast injection electrons from dye to TiO_2 and the recombination process are reduced. The resistance of R_{CT1} and R_{CT2} increased with increasing cell–mirror distance.

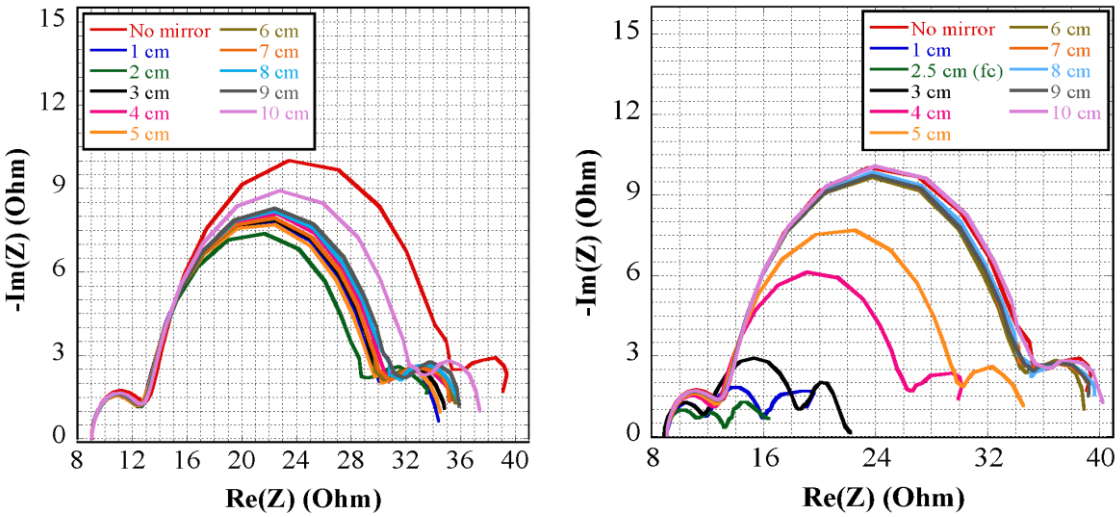

Figure 3.11 Nyquist plots of DSSCs coupled with (a) a plane mirror reflector and (b) a concave mirror concentrator.

Table 3.3 EIS parameter of DSSCs coupled with plane mirror back reflector

x (cm)	Rs (Ω)	Z1 R_{CT1} (Ω) C_1 (μF)	Z2 R_{CT2} (Ω) C_2 (μF)
No mirror	9.07	4.60 2.22	22.27 149
1	9.02	4.16 2.46	17.55 189
2	9.02	4.12 2.48	16.39 202
3	9.01	4.21 2.43	17.46 190
4	9.03	4.13 2.48	17.81 186
5	9.03	4.06 2.52	17.16 193
6	9.03	4.11 2.49	17.55 189
7	9.02	4.22 2.42	17.66 188
8	9.03	4.17 2.46	18.33 181
9	9.02	4.19 2.44	18.70 177
10	9.03	4.35 2.35	19.62 169

Table 3.4 EIS parameter of DSSCs coupled with concave mirror concentrator

x (cm)	Rs (Ω)	Z1 R_{CT1} (Ω) C_1 (μF)	Z2 R_{CT2} (Ω) C_2 (μF)
No mirror	9.07	4.60 2.22	22.27 149
1	9.13	2.98 2.34	4.36 163
Focus (2.5)	9.05	2.74 1.73	3.42 208
3	8.90	3.18 2.19	7.09 216
4	9.10	3.94 1.77	13.65 165
5	9.11	4.21 2.43	17.18 193
6	9.07	4.52 2.26	21.56 154
7	9.08	4.52 2.27	21.63 153
8	9.09	4.43 2.31	21.57 154
9	9.07	4.52 2.26	21.82 152
10	9.07	4.58 2.23	22.24 149

Effect of operational time

Figure 3.12 shows the Nyquist plot from EIS measurements of a DSSC coupled with a plane mirror concentrator. Three semicircles appear as Z_1, Z_2, and Z_3 were observed. The Z_1 and Z_2 semicircles increase with increasing time. The EIS data are listed in Table 3.6. The slight increases in R_{CT1} after 120 min of operation indicate that

the electron transfer process at the Pt/electrolyte interface has slightly decreased.

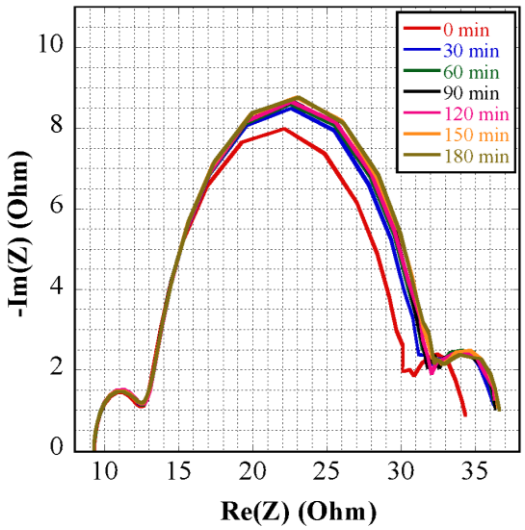

Figure 3.12 Nyquist plot of the effect of time on a DSSC coupled with a plane mirror concentrator.

A slight increase also occurred in R_{CT2} with increasing time. Generally, R_{CT2} is a resistance in dye/TiO_2 that indicates the process of the charge transfer electron and recombination. Even though plane mirror concentrators support light harvesting, a recombination process can still occur in DSSCs. The slight increase in R_{CT2} with increasing time might be caused by the slight increase in the recombination process that occurs despite the slight decreasing performance in the counter electrode.

Table 3.5 EIS parameter of operational time DSSCs coupled with plane mirror reflector

t (min)	Rs (Ω)	Z1 R_{CT1} (Ω) C_1 (μF)	Z2 R_{CT2} (Ω) C_2 (μF)
0	9.30	3.72 1.87	17.78 187
30	9.30	3.97 1.75	18.53 179
60	9.29	3.86 1.80	19.04 174
90	9.27	3.88 1.79	18.98 175
120	9.28	4.01 2.55	19.22 173
150	9.27	4.04 1.72	19.35 171
180	9.27	4.07 2.51	19.66 169

3.2.2 Temperature Effect in Different Electrolytes

Performance of DSSCs with nitrile-based liquid electrolytes

This section presents a comparation and evaluation of the performance of acetonitrile, propionitrile, and 3-metoxy propionitrile, as the commonly used organic solvent-based liquid electrolytes in DSSCs under low concentrated light. The results can be used as reference to select a suitable electrolyte for concentrated light application in DSSCs.

The performance of a bifacial DSSC device is determined by its photovoltage (V_{OC}), photocurrent density (J_{SC}), and fill factor (FF). Figure 3.13 (a) shows the $J-V$ analysis of DSSCs with three different types of electrolytes. The used DSSC electrolytes were iodide redox with acetonitrile (AN-50), propionitrile (PN-50), and 3-

methoxypropionitrile (Z-100 or MPN-100)-based solvents, as listed in Table 3.6. AN-50 produced the highest J_{SC} = 9.14 mA·cm^{-2}, followed by Z-100 (7.26 mA·cm^{-2}), and PN-50 (6.59 mA·cm^{-2}). V_{OC} in Table 3.7 slightly increases because of the increase in illumination power, which may cause a rapid decrease in the number of electrons in the dye, leading to an increase in dye potential. In contrast, the decrease in FF, especially in AN-50, may be caused by slow electron regeneration in the dye, leading to an increase in recombination. The highest maximum power output (P_{OUT}) was produced using AN-50.

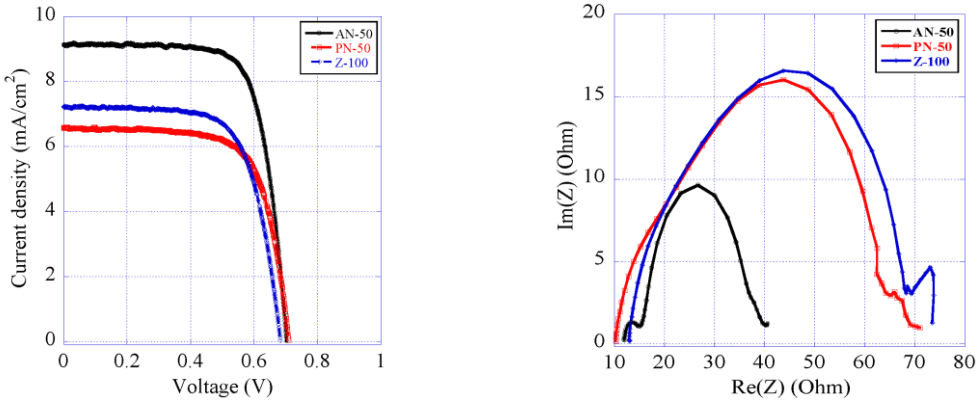

(a) **(b)**

Figure 3.13 Comparison of AN-50, PN-50, and Z-100. (a) $J-V$ and (b) EIS of DSSCs under the no mirror condition.

EIS was used to evaluate the variation in impedance on different component interfaces in a DSSC. The Nyquist plot of EIS generally shows three semicircles with different processes, based on the characteristics of each electrolyte used [49,54-55]. The first semicircle (R_{CT1}) represents the charge transfer resistance at the Pt counter electrode and electrolyte interfaces. The second semicircle (R_{CT2}) corresponds to the charge transfer resistance in the TiO_2/dye/electrolyte and electron recombination mechanism in TiO_2. The third semicircle (R_{CT3}) represents I^-/I_3^- diffusion in the electrolyte. The EIS in Fig. 3.13 (b) shows the AN-50 charge transfer resistance of two semicircles consisting of R_{CT1} and

R_{CT2}. Meanwhile, the R_{CT1} and R_{CT2} of PN-50 and Z-100 only show a single semicircle followed by R_{CT3}. The AN-50 second-semicircle (R_{CT2}), lower than R_{CT1} and R_{CT2} of PN-50 and Z-100, indicates that the charge transfer at the Pt electrode or TiO_2/dye and electrolyte interface of AN-50 was faster than that of PN-50 and Z-100, as is also shown in Fig. 3.14. It is shown that acetonitrile (AN) as a solvent has better ion diffusion, which is attributed to its low viscosity (0.33 cp) compared to the others [56].

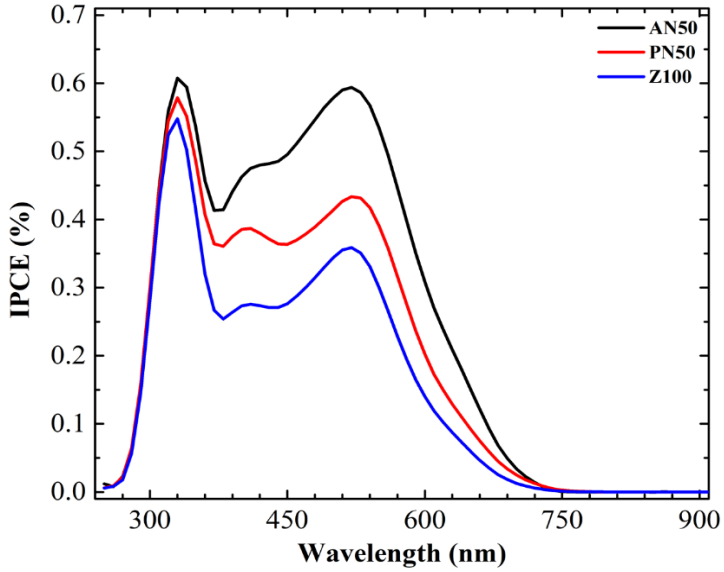

Figure 3.14 Incident-photon-to-current efficiency (IPCE) of AN-50, PN-50, and Z-100. AN-50 has the highest IPCE spectrum, which indicates highest charge carrier compared to PN-50 and Z-100.

Table 3.6. Physical parameters of solvents for electrolyte in DSSCs [57]

Electrolyte Name	AN-50	PN-50	Z-100 (MPN-100)
Solvent	Acetonitrile	Propionitrile	3-methoxypropionitrile
Formula	CH_3CN	CH_3CH_2CN	$CH_3O(CH_2)_3CN$
Product Type	Iodide Based Redox Electrolyte	Iodide Based Redox Electrolyte	Iodide Based Redox Electrolyte
Redox	Iodide/Tri-Iodide	Iodide/Tri-Iodide	Iodide/Tri-Iodide
Redox Concentration	50 mM	50 mM	100 mM
Additives	*Ionic liquid, lithium salt, pyridine derivative*	*Ionic liquid, lithium salt, pyridine derivative*	*Ionic liquid, alkyl benzimidazole, thiocyanate.*
Donor number	14.1	16.1	16.1
Boiling Point (Bp)/ °C	82	97	164
Viscosity/cp	0.33(30°C)	0.39(30°C)	2.5
Dielectric Constance (ε)	36	27(20°C)	6

Nitrile-based electrolyte under concentrated light

The low concentrated mirror was applied with 1.5 and 2 cm cell-to-mirror distance. The distances were selected to observe the influence of temperature on the electrolyte performance of the DSSCs. The parameters P_{OUT}, V_{OC}, and J_{SC} for all electrolytes listed in Table 3.7 significantly increased, and the FF of the cell decreased compared to the condition without mirror. The light intensity produced by the low concentrated concave mirror simultaneously increased the excited electron in the dye and led to the increase in the J_{SC} of all cells. The P_{OUT} and PCE were also improved in the 1.5 cm mirror distance. However, the decrease in cell $J-V$ squareness (FF) despite the increase in J_{SC} , $P_{OUT,}$ and PCE indicated an increase in loss in the cell. These losses may cause an increased recombination in the electrolyte by the jump of J_{SC}. In the 2 cm distance, the loss was

significant, leading to a reduced overall PCE in all the cell samples.

Table 3.7. Photovoltaic and photoelectric parameter electrolyte at different illumination distance

x (cm)	P_{IN} (mW/cm^2)	Electrolyte	V_{OC} (V)	J_{SC} (mA/cm^2)	FF	P_{OUT} (mW/cm^2)	η (%)
No-mirror	105	AN-50	0.70	9.14	0.73	4.73	4.46
		PN-50	0.71	6.59	0.70	3.27	3.08
		Z-100	0.68	7.26	0.69	3.41	3.21
1.5	240	AN-50	0.78	65.33	0.44	22.56	9.04
		PN-50	0.78	43.72	0.50	17.12	7.13
		Z-100	0.79	34.03	0.54	14.60	6.08
2	307	AN-50	0.76	74.21	0.44	24.53	7.99
		PN-50	0.76	52.10	0.50	19.72	6.42
		Z-100	0.76	49.98	0.51	19.50	6.35

The R_{CT} in the electrolyte was inversely proportional to J_{SC} as $R_{CT} = \zeta / J_{SC}$ [27], where ζ is the overpotential required to drive the current. The decrease in R_{CT} in Fig. 3.15 and Table 3.8 indicates the charge transfer to the electrolyte by the Pt electrode, and the dye regeneration to cover the electron loss in the dye by cycle I^-/I_3^- diffusion in the electrolyte increased, followed by a rise in the number of electrons excited in TiO_2/dye (J_{SC}).

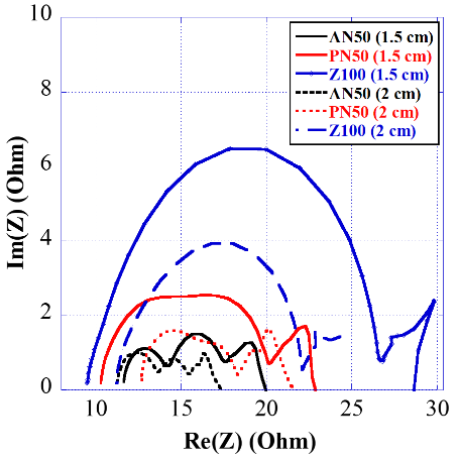

Figure 3.15 EIS of DSSCs with AN-50, PN-50, and Z-100 electrolytes influenced by a concave mirror concentrator at 1.5 and 2 cm distances.

Table 3.8. The EIS of DSSCs in 2 measurement condition

Electrolyte	No Mirror			1.5 cm mirror distance			2 cm mirror distance		
	Rs (Ω)	Z1 R_{CT1} (Ω) C (μF)	Z2 R_{CT2} (Ω) C (mF)	Rs (Ω)	Z1 R_{CT1} (Ω) C (μF)	Z2 R_{CT2} (Ω) C (mF)	Rs (Ω)	Z1 R_{CT1} (Ω) C (μF)	Z2 R_{CT2} (Ω) C (mF)
AN-50	11.79	3.71 2.76	26.73 396	11.57	2.83 2.46	3.68 284	9.55	2.77 2.51	3.97 391
PN-50	10.05	60.19 37.52	7.25 14	10.01	10.84 14.03	2.12 74	10.92	11.63 19.24	4.37 24
Z-100	12.73	58.89 17.8	4.3 116	9.62	17.49 5.91	2.98 52	10.48	10.17 14.96	3.18 107

The effect of temperature caused by the low concentrated concave mirror to the 3 h cell performance is shown in Fig. 3.16. Each graph shows a sudden drop in P_{OUT} and J_{SC} after the first measurement. These drops may be caused by the accumulation of electrons, because the excited electron has higher speed compared with the electron regeneration in the dye. The temperature at 1.5 cm mirror distance shows the different increases in temperature of the three electrolytes. Z-100 was the slowest in temperature

rise compared to AN-50 and PN-50. Figure 3.16 (a) shows the overall performance of the cell that remained stable, indicating that the electrolyte could work normally under 90 °C cell body temperature. In the 2 cm distance mirror in Fig. 3.16 (b), the performance of AN-50 and PN-50 started to degrade, indicating that an increase in temperature above 90 °C affected AN-50 (Bp: 82 °C) and PN-50 (Bp: 97 °C), which have low solvent boiling points. Even tough Z-100 has the lowest performance, it showed a stable performance suitable for application in low concentrated light in DSSCs.

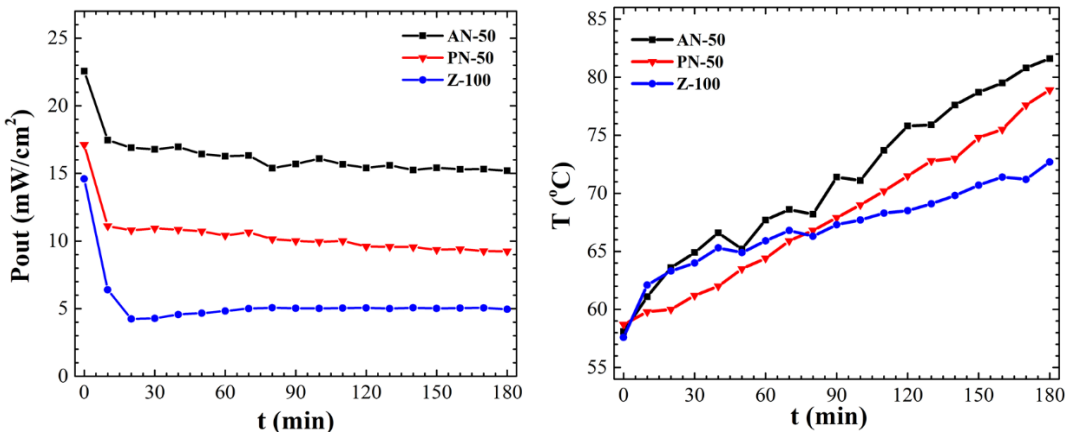

(a)

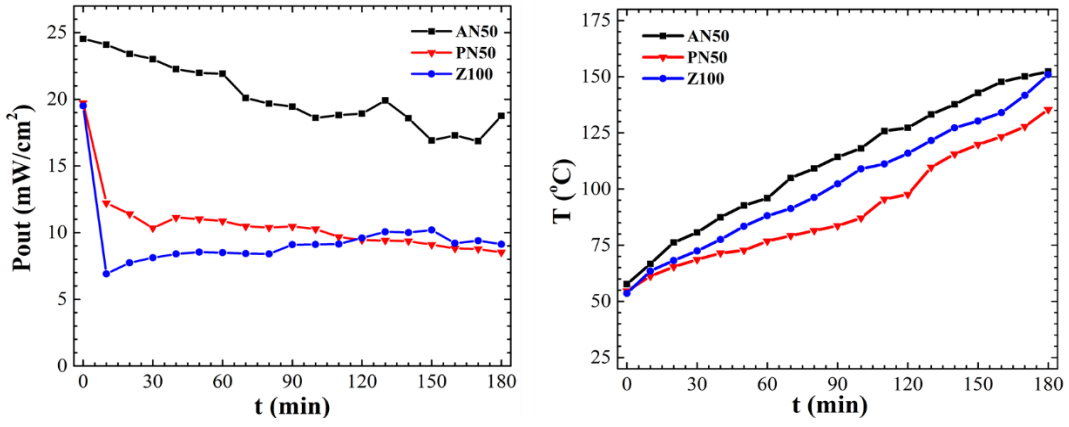

(b)

Figure 3.16 P_{OUT} and temperature fluctuation at a) 1.5 cm and b) 2 cm cell-to-mirror distances during a 3 h measurement.

3.2.3 Endurance Test

To further investigate the effect of temperature on the endurance of the cell, the same cell with the mirror at 2 cm distance was measured for 4 days during a 3 h measurement test each day, as shown in Fig. 3.17. Overall, the DSSC' P_{OUT} of all cells were stable without degradation, even after being subjected to a temperature stress (130–155 °C) during the 3 h measurement in the first day. The An-50 and PN-50 cells showed gradual performance degradation, and the performance of AN-50 was stopped at day four. The degradation shows the possibility of a decrease in iodide redox in the electrolyte owing to electrolyte evaporation under high temperatures. Z-100 was stable until day three of measurement and started to degrade by day four.

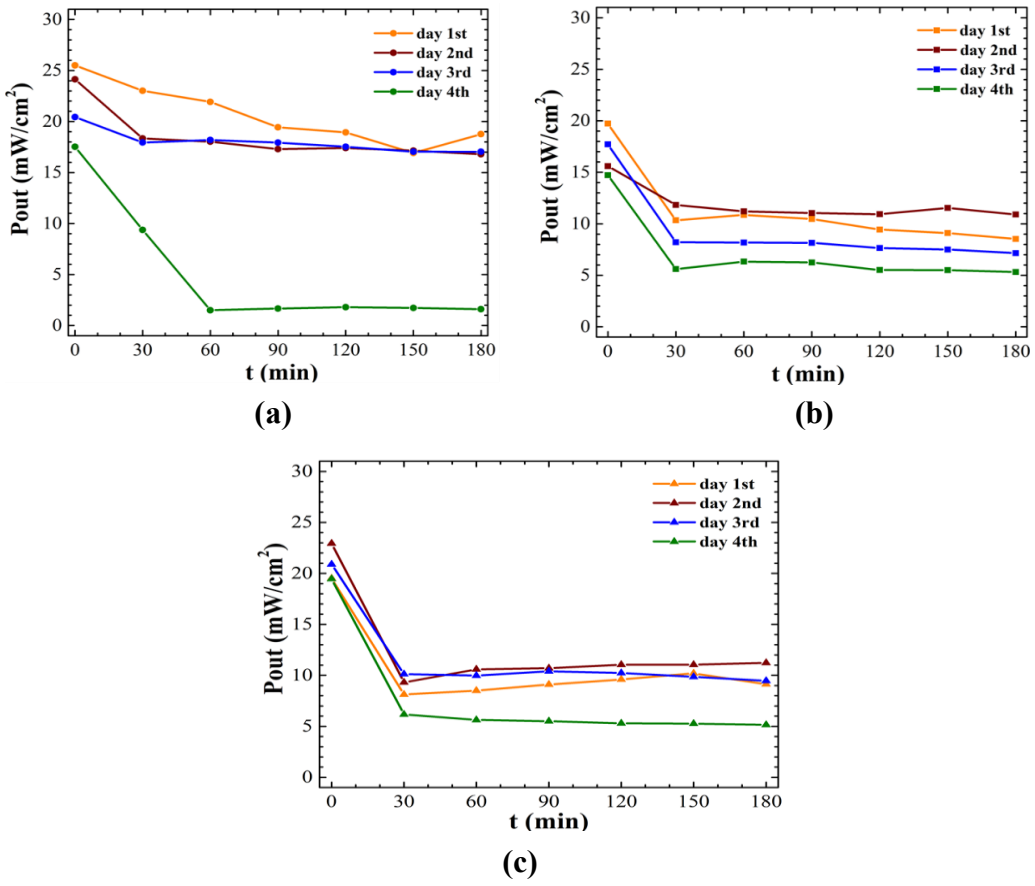

Figure 3.17 Endurance test with 2 cm distance for a) AN-50, (b) PN-50, and c) Z-100 for 4 days and 3 h measurement.

3.3 Conclusions

The performance of bifacial DSSCs was investigated under a back reflector and back concentrator. The plane mirror as back reflector successfully increased the J_{SC} to 11.50 $mA.cm^{-2}$ and P_{OUT} to 5.62 $mW.cm^{-2}$ at 2 cm mirror distance. Even better, the concave mirror as back concentrator successfully increased the J_{SC} to ~82 $mA.cm^{-2}$ and P_{OUT} to 29.01 $mW.cm^{-2}$ at 2.5 cm mirror distance (focal point). The EIS of DSSCs with back reflector and concentrator shows the changes in Z_2 as an attribute of the increasing J_{SC}. The DSSCs with plane mirror reflector has stable performance during 180 min of operational time. In contrast, the electrolyte of the DSSC with concave mirror concentrator evaporated before 30 min of operation. The result shows the potential of the back reflector and concentrator to enhance the performance of DSSCs.

DSSC electrolytes containing three different nitrile-based solvents were investigated under a low concentrated concave mirror. The performance of all the cells increased 4–8 times under the influence of the low concentrated light. The DSSC shows stable performance with a concave mirror at 1.5 cm distance during a 3 h measurement with temperature under 90 °C. AN-50 shows the best performance and response to the concentrated light of the concave mirror at 2 cm distance, with the highest J_{SC} (74.21 mA.cm^{-2}), P_{OUT} (24.53 mW/cm^2), and η (7.99%) compared to those of PN-50 and Z-100. The increase in J_{SC} by a concentrated light leads to a decrease in FF, which may be caused by the increase in cell loss trough recombination. The performance of cells with AN-50 and PN-50 start to degrade at 3 h measurement duration with 2 cm mirror distance, which may be caused by the temperature increase above the boiling points of the electrolyte solvents. Meanwhile, Z-100 shows performance stability during 4 days measurement, even with the lowest J_{SC} (49.98 mA.cm^{-2}), P_{OUT} (19.50 mW/cm^2), and η

6.35% in the first day. These results show the advantages of the investigated electrolytes for low concentrated light application in DSSCs.

REFERENCES

[1]. Regan, B. O. and Gratzel, M. (**1991**) 'A low-cost, high-efficiency solar cell based on dye-sensitized colloidal TiO_2 films', *Nature*, 353, 737–740.

[2]. Yum, J., Baranoff, E., Wenger, S., Nazeeruddin, M. K. and Gratzel, M. (**2011**) 'Panchromatic engineering for dye-sensitized solar cells', *Energy Environ. Sci.,* 4, 842–857.

[3]. Chung, I., Lee, B., He, J., Chang, R. P. H. and Kanatzidis, M. G. (**2012**) 'All-solid-state dye-sensitized solar cells with high efficiency', *Nature,* 485, 486–489.

[4]. Xue, G., Guo, Y., Yu, T., Guan, J., Zhang, J., Liu, J. and Zuo, Z. (**2012**) 'Degradation Mechanisms Investigation for Long-term Thermal Stability of Dye-Sensitized Solar Cells', *Int. J. Electrochem. Sci.,* **7**, 1496–1511.

[5]. Sharma, K., Sharma, V. and Sharma, S. S. (**2018**) 'Dye-Sensitized Solar Cells: Fundamentals and Current Status'. *Nanoscale Res. Lett.,* 13, 381.

[6]. Seo, H., Son, MK., Hashimoto, S., Takasaki, T., Itagaki, N., Koga, K. and Shiratani, M. (**2016**) 'Surface Modification of Polymer Counter Electrode for Low-Cost Dye-sensitized Solar Cells', *Electrochim. Acta*, 210, 880-887.

[7]. Saidi, N. M., Farhana, N. K., Ramesh, S. and Ramesh, K. (**2021**) 'Influence of different concentrations of 4-tert-butyl-pyridine in a gel polymer electrolyte towards improved performance of Dye-Sensitized Solar Cells (DSSC)', *Sol. Energy,* 216, 111-119.

[8]. Omar, A. and Abdullah, H. (**2014**) 'Electron transport analysis in zinc oxide-based dye-sensitized solar cells: A review', *Renewable Sustainable Energy Rev.,* 31, 149-157.

[9]. Seo, H., Nam, SH., Itagaki, N., Koga, K. and Shiratani, M. **(2016**) 'Effect of sulfur-doped TiO_2 on photovoltaic properties of dye-sensitized solar cells', *Electron. Mater. Lett.,* 12, 530–536.

[10]. Seo, H., Son, MK., Itagaki, N. and Shiratani, M. (**2016**) 'Polymer counter electrode of poly(3,4-ethylenedioxythiophene): Poly(4-styrenesulfonate) containing TiO_2 nanoparticles for dye-sensitized solar cells', *J. Power Source,* 307, 25-30.

[11]. Wu, J., Li, Y., Tang, Q., Yue, G., Lin, J., Huang, M. and Meng, L. (**2014**) 'Bifacial dye-sensitized solar cells: A strategy to enhance overall efficiency based on transparent polyaniline electrode, *Sci. Rep.,* 4 (4028) 1–7.

[12]. Xu, T., Kong, D., Tang, H., Qin, X., Li, X., Gurung, A., Kou, K., Chen, L., Qiao, Q. and Huang, W. (**2020**) 'Transparent MoS 2 / PEDOT Composite Counter Electrodes for Bifacial Dye-Sensitized Solar Cells', *ACS Omega* 5, 8687-8696.

[13]. Miranda-Munoz, J. M., Carretero-Palacios, S., Jimenez-Solano, A., Li, Y., Lozano, G. and Miguez, H. (**2016**) 'Efficient bifacial dye-sensitized solar cells through disorder by design*', J. Mater. Chem. A,* 4, 1953-1961.

[14]. Cai, H., Tang, Q., He, B., Li, R. and Yu, L. (**2014**) 'Bifacial dye-sensitized solar cells with enhance rear efficiency and power output', *Nanoscale*, 6, 15127-15133.

[15]. Ito, S., Zakeeruddin, S. M., Comte, P., Liska, P., Kuang, D. and Gratzel, M. (**2008)** **'**Bifacial dye-sensitized solar cells based on an ionic liquid electrolyte', *Nat. Photonics*, 2, 693–698.

[16]. Lo, C. K., Lim, Y. S. and Rahman, F. A. (**2015**) 'New integrated simulation tool for the optimum design of bifacial solar panel with reflectors on a specific site', *Renew. Energy,* 81, 293–307.

[17]. Ooshaksaraei, P., Sopian, K., Zulkifli, R., Alghoul, M. A. and Zaidi, S. H. (**2013**) 'Characterization of a bifacial photovoltaic panel integrated with external diffuse and semimirror type reflectors', *Int. J. Photoenergy,* 2013, 465837.

[18]. Wang, G., Shen, F., Wang, F. and Chen, Z. (**2020**) Design and experimental study of solar CPV system using CLFR concentrator, *Sustain. Energy Technol. Assess.,* 40, 100751.

[19]. Han, X., Tu, L. and Sun, Y. (**2021**) A spectrally splitting concentrating PV/T system using combined absorption optical filter and linear Fresnel reflector concentrator. *Sol. Energy,* 223, 168-181.

[20]. Steiner, M., Wiesenfarth, M., Martinez, J. F., Siefer, G. and Dimroth, F. (**2019**) Pushing Energy Yield with Concentrating Photovoltaics, *AIP conf. Proc.,* 2149, 060006-1 – 060006-5.

[21]. Selvaraj, P., Baig, H., Mallick, T. K., Siviter, J., Montecucco, A., Li, W., Paul, M., Sweet, T., Gao, M., Knox, A. R. and Sundaram, S. (**2018**) 'Enhancing the efficiency of transparent dye-sensitized solar cells using concentrated light', *Sol. Energy Mater Sol. Cells,* 175, 29-34.

[22]. Cooper, T., Ambrosetti, G., Pedretti, A. and Steinfeld, A. (**2014**) 'Surpassing the 2D limit: A 600x high-concentration PV collector based on a parabolic trough with tracking secondary optics', *Energy Procedia,* 57, 285–290.

[23]. Zaghloul, H., Emam, M., Abdelraman, M. A. and Abd Rabbo, M. F. (**2021**) 'Optimization and parametric analysis of multijunction high-concentrator PV cell combined with a straight fins heat sink', *Energy Convers. Manag.,* 243, 114382.

[24]. Pilawjian, G. (**2012**) 'Analysis of Photovoltaic Concentrating Solar Energy Systems', *J. Syst. Softw.,* 2, 110-112.

[25]. Shanks, K., Senthilarasu, S. and Mallick, T. K. (**2016**) 'Optics for concentrating photovoltaics: Trends, limit and opportunities for materials and design', *Renew. Sust. Energ. Rev.*, 60, 394-407.

[26]. Chemisana, D. and Mallick, T. K. (**2014**) 'Building integrated concentrating solar systems', in Solar Energy Sciences and Engineering Applications, 1st Ed.; CRC Press, London, UK, 17, 545-788.

[27]. Wang, N. Y., Chiang, S. Y., Chou, T. L., Lee, H. L. and Chiang, K. N. (**2010**) Life prediction of high concentration photovoltaic modules subjected to thermal cycling test. *2010 5th International Microsystems Packaging Assembly and Circuits Technology Conference.* 3–6.

[28]. Wang, P., Yang, L., Wu, H., Cao, Y., Zhang, J., Xu, N., Chen, S., Decoppet, J. D., Zakeeruddin, S. M. and Gratzel, M. (**2018)** Stable and Efficient Organic Dye-Sensitized Solar Cell Based on Ionic Liquid Electrolyte. *Joule*, 2, 2145–2153.

[29]. Raga, S. R. and Fabregat-Santiago (**2013**) 'Temperature effect in dye-sensitized solar cells', *Phys. Chem. Chem. Phys.,* 15, 2328-2336.

[30]. Ustaoglu, A., Kandilli, C., Cakmak, M. and Torlaklı, H. (**2020**) 'Experimental and Economical performance investigation of V-trough concentrator with different reflectance characteristic in photovoltaic applications', *J. Clean. Prod.*, 272, 123072.

[31]. Yusof, S. M. M. and Yahya, W. Z. N. (**2016**) 'Binary Ionic Electrolyte for Dye Sensitized Solar Cells', *Procedia Eng*., 148, 100-105.

[32]. Fang, Y., Ma, P., Cheng, H., Tan, G., Wu, J., Zheng, J., Zhou, X., Fang, S., Dai, Y. and Lin, Y. (**2019**) Synthesis of Low-Viscosity Ionic Liquids for Application in Dye-Sensitized Solar Cells, *Chem.: Asian J*., 14, 4201-4206.

[33]. Asghar, M. I., Miettunen, K., Halme, J., Vahermaa, P., Toivola, M., Aitola, K. and Lund, P. (**2010**) 'Review of Stability for Advanced Dye Solar Cells', *Energy Environ. Sci.*, 3, 418-426.

[34]. Iftikhar, H., Sonai, G. G., Hashmi, S. H., Nogueira, A. F., Lund, P. D. (**2019**) 'Progress on Electrolytes Development in Dye-Sensitized Solar Cells', *Materials*, 12, 12, 1998.

[35]. Langmar, O., Ganivet, C. R., Scharl, T., Torre, G., Torres, T., Costa, D. C., Guldi, D. M. (**2018**) 'Modifying the Semiconductor/Electrolyte Interface in CuO p-Type Dye-Sensitized Solar Cells: Optimization of Iodide/Triiodide-Based Electrolytes', *ACS Appl. Energy Mater.,* 1, 6388−6400.

[36]. Fang, H., Ma, J., Wilhelm, M. J., DeLacy, B. G. and Dai, H. L. (**2021**) 'Influence of Solvent on Dye-Sensitized Solar Cell Efficiency: What is so Special About Acetonitrile?', *Part. Part. Syst. Charact.,* 38, 2000220.

[37]. Venkatesan, S., Hidayati, N., Liu, I. and Lee, Y. L. (**2016**) 'Highly efficient gel-state dye-sensitized solar cells prepared using propionitrile and poly(vinylidene fluoride-co-hexafluoropropylene)', *J. Power Sources*, 336, 385-390.

[38]. Harikisun, R. and Desilvestro, H. (**2011**) 'Long-term Stability of Dye Solar Cells', *Solar Energy,* 85, 1179–1188.

[39]. Mohanty, S. P. and Bhargava, P. (**2015**) 'Impact of Electrolytes Based on Different Solvents on the Long Term Stability of Dye Sensitized Solar Cells', *Electrochimica Acta,* 168, 111–115.

[40]. Venkatesan, S., Su, S. V., Kao, S. C., Teng, H. and Lee, Y. L. (**2015**) 'Stability improvement of gel-state dye-sensitized solar cells by utilization the co-solvent effect of propionitrile/acetonitrile and 3- methoxypropionitrile/acetonitrile with poly(acrylonitrile-co-vinylacetate)', *J. Power Sources*, 274, 506-511.

[41]. Radhakrishnan, S., Munukutla, L. V., Htun, A. and Kannan, A. M. (**2011**,) **'**The Dye Sensitized Solar Cell Stability and Performance Study Using Different Electrolytes', *MRS Online Proceedings Library,* 841, 1322.

[42]. Sarwar, S., Lee, M., Park, S., Dao, T. T., Ullah, A., Hong, S. and Han, C. H. (**2020**) 'Transformation of A Liquid Electrolyte to A Gel Inside Dye Sensitized Solar Cells for Better Stability and Performance', *Thin Solid Films*, 704, 138024.

[43]. Nilson, J. (**2005**) 'Optical Design and Characterization of Solar Cocentrators for Photovoltaics', Lund Institute of Thechnology, Lund, Sweden: Devision of Architecture and Building Design, ISBN: 91-85147-15-X.

[44]. Chaves, J. (**2008)** 'Introduction to Nonimaging Optics', Florida, USA: CRC Press, ISBN-13: 978-1-4200-5429-3.

[45]. Paul, D. I. (**2015**)' Theoretical and Experimental Optical Evaluation and Comparison of Symmetric 2D CPC and V-Trough Collector for Photovoltaic Applications', Int. J. Photoenergy, 2015, 693463. DOI: http://dx.doi.org/10.1155/2015/693463.

[46]. J. Bisquert and F. Fabreagat-Santiago (**2010**) 'Impedance spectroscopy: a general introduction and application to dye-sensitized solar cells', in K. Kalyanasundaram

(ed) *Dye-Sensitized Solar Cells* First Edition. p. 457. CRC; Taylor & Francis, Boca Raton, Fla, USA.

[47]. Sarker, S., Ahammad, A. J. S., Seo, H. W. and Kim, D. M. (**2014**) 'Electrochemical Impedance Spectra of Dye-Sensitized Solar Cells: Fundamentals and Spreadsheet Calculation', *International Journal of Photoenergy,* Article ID 851705.

[48]. Santiago, F. F., Bisquert, J., Palomares, E., Otero, L., Kuang, D., Zakeeruddin, M. and Gratzel, M. (**2007**) 'Correlation Between Photovoltaic performance and Impedance Spectroscopy of Dye-Sensitized Solar cells based on Ionic Liquids', *J. Phys. Chem. C.*, 111, 6550-6560.

[49]. Chawarambwa, F. L., Putri, T. E., Attri, P., Kamataki, K., Itagaki, N., Koga, K. and Shiratani, M. (**2021**) 'Highly Efficienct and Transparent Counter Electrode for Application in Bifacial Solar Cells', *Journal of Chemical Physic Letters,* 768, 138369.

[50]. Wang, Q., Moser, J. E. and Gratzel, M. (**2005**) 'Electrochemical Impedance Spectroscopy Analysis of Dye-Sensitized Solar Cells', *J. Phys. Chem. B.,* 109, 14945-14953.

[51]. Seo, H., Son, M. K., Kim, J. K., Choi, J., Choi, S., Kim, S.K. and Kim, H. J. (**2012**) 'Analysis of Current Loss from a Series-parallel Combination of Dye-Sensitized Sloar Cells Using Electrochemical Impedance Spectroscopy', *Photonic and nanostructures – Fundamentals and Application,* 10, 568-574.

[52]. Chawarambwa, F. L., Putri, T. E., Attri, P., Kamataki, K., Itagaki, N., Koga, K. and Shiratani, M. (**2021**) 'Effect of Concentrated Light on the Performance and Stability of a Quasi-Solid Electrolyte in Dye-Sensitized Solar Cells', *Chem. Phys. Lett.*, 781, 138986.

[53]. Tai, Q., Chen, B., Guo, F., Xu, S., Hu, H., Sebo, B. and Zhao, X. Z. (**2011**) 'In-Situ Prepared Transparent Polyaniline Electrode and Its Application in Bifacial Dye-Sensitized Solar Cells', *Journal of ACS Nano*. Vol. 5, No. 5, 3795-3799.

[54]. Buraidah, M. H., Shah, S., Teo, L. P., Chowdury, F. I., Careem, M. A., Albison, I., Mellader, B. E. and Arof, A.K. (**2017**) 'High efficiecnt dye sensitized solar cells using phthaloylchitosan based gel polymer electrolytes', Electrochim. Acta 245, 846-853.

[55]. Chowdhury, F. I., Buraidah, M. H., Arof, A. K., Mellander, B. E., and Noor, I. M. (**2020**) 'Impact of tetrabutylammonium, iodide and triiodide ions conductivity in polyacrylonitrile based electrolyte on DSSC performance', *Sol. Energy*, 196, 379-388.

[56]. Hauch, A., and Georg, A. (**2001**) 'Diffusion in the electrolyte and charge transfer reaction at the platinum electrode in dye-sensitized solar cells', Electrochim. Acta 46, 3457-3466.

[57]. Wu, J., Lan, Z., Lin, J., Huang, M., Huang, Y., Fan, L. and Luo, G. (**2015**) 'Electrolyte in Dye-Sensitized Solar Cells', *J. Chem. Rev.,* 115, 2136-2173.

Chapter 4

Dye-Sensitized Solar Cells with a V-Shape Low Concentrated Light System

The abundance of solar energy shows the significant role of solar cell technology in solving the global energy crisis and environmental problems caused by the depletion of fossil fuel reserves. Solar energy harvesting tools include the solar cell and solar concentrator. Among the available solar cells, DSSCs are attractive due to their simple fabrication process, low cost, performance stability, and eco-friendliness [1–4]. Despite these advantages, the low power output and efficiency of less than 10% [5–10] still are a major constraint for DSSC development. A bifacial structure and concentrated illumination could be applied to increase the power output and efficiency of this type of solar cells.

The bifacial structure exploits the solar radiation absorption on the front and rear surfaces of solar cells [11–15]. In general, a back reflector is used to increase reflectivity and increase light-harvesting at the rear side of solar cells in a bifacial system [16–17]. Meanwhile, a concentrating photovoltaic system is effective to increase the solar cell output power. For instance, a concentrating photovoltaic (PV) system with a V-trough plane concentrator obtained 17.8% higher power than the PV system under standard solar radiation (1-sun) with a temperature of ~70 °C [18]. However, the application of concentrators in solar cells is still limited owing to the high-temperature operation. Especially, there is a lack of studies of DSSCs with concentrators, probably because of the high-temperature damage of the liquid electrolyte [19-21].

This section presents an evaluation of the performance of a DSSC with low light V-shape concentrator plane and concave aluminum-coated mirrors. The experiment was carried out to determine the effectiveness of the V-shape low concentrated light system in improving the performance of the DSSC. The focus of this experiment is the enhancement in output power of bifacial DSSCs because the output power is one of the essential

characteristics from a practical viewpoint. The effect of temperature was observed to know how much it influences the DSSC's performance.

4.1 Experimental Method

4.1.1 Cell Fabrication

The bifacial DSSC was fabricated using the doctor blade method. Two FTO glass substrates (Sigma Aldrich 2.3 mm, ~13 Ω/sq) were cut to a size of 1.5 × 2 cm^2 and cleaned using acetone, ethanol, and purified water for 20 min. TiO_2 (Solaronix Ti-Nanoxide T/SP) was printed on the FTO glass using the doctor blade method and sintered at 450 °C for 30 min in an electric furnace. After the substrate was cold, a dye solution (N719 Solaronix) was soaked on the FTO/TiO_2 for 20–24 h. A hole was made on the other FTO glass for iodine injection. Platinum paste (Dyesol PT-1) was printed on the FTO glass using the doctor blade method and sintered at 450 °C for 30 min in an electric furnace.

Two sealants (Solaronix Meltonix 1170-60) were cut to 1.4 × 1.4 cm^2, and the hole was made on one of them with a size of 1.25 × 1.25 cm^2. Afterwards, the FTO/Pt/sealant with the hole and the FTO/TiO_2/dye were overlapped into an FTO/Pt/Sealant/Dye/TiO_2/FTO sandwich structure. Subsequently, the cell was put on a hotplate and pressed until the sealant melted. After that, iodide electrolyte (AN-50, Solaronix) was injected into the cell through the hole on the FTO/Pt side and closed using the second sealant.

4.1.2 Measurement

The performance of the bifacial DSSCs was measured with a source meter (Keithley 2400) under illumination from a Xenon lamp equipped with an air mass (AM) 1.5 filter. Plane and concave aluminum-coated mirrors (Edmund Optics, 43-469) were used as a low concentrator as shown in Fig. 4.1. Conventional measurements without

mirrors were conducted to obtain the characteristics of the bifacial DSSC under the front light illumination at a position 8 cm below the light source.

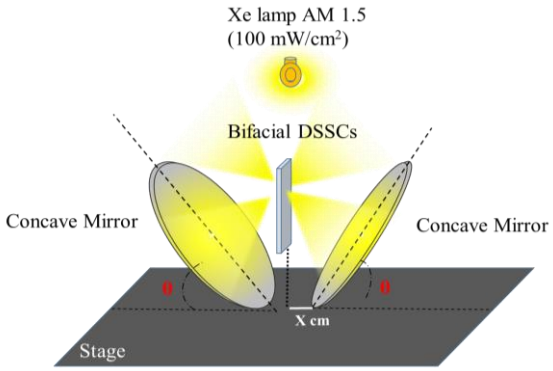

Figure 4.1 DSSC with V-Shape low concentrated light system.

The effects of the measurement time, tilt angle, and mirror distance were investigated with the V-shape concentrator with the parameters of mirror tilt angle (15°, 30°, 40°, 45°, 60°, 75°) and mirror distance x (0, 1, 2, 3, 4) cm between the mirrors and the solar cells, as shown in Fig. 4.2. The surface temperature of each side of the bifacial DSSC was measured with a thermocouple.

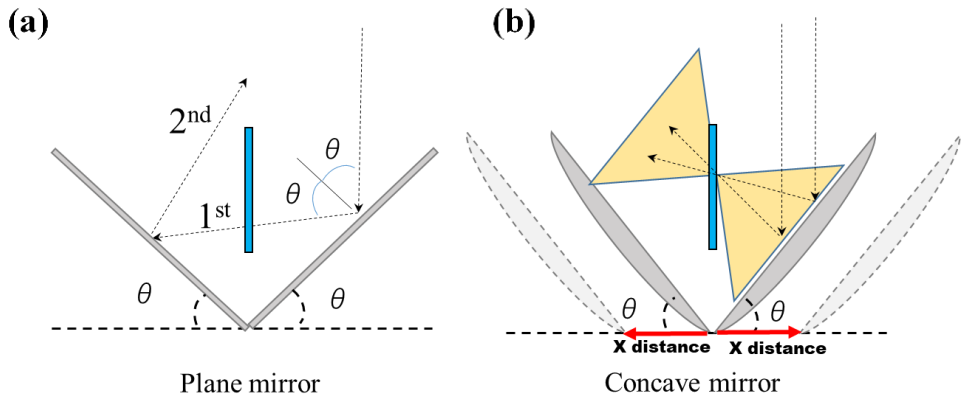

Figure 4.2 Schematic of tilt angle θ variation, distance variation, and reflected light direction in a (a) plane mirror and (b) concave mirror.

The optical properties of the V-shape mirror system were measured at maximum

P_{out} of the mirror tilt angle. The light source (Ohm pure beam lediantor, 400 lumens) was rotated in different angles with the vertical condition as initial point, as shown in Fig. 4.3.

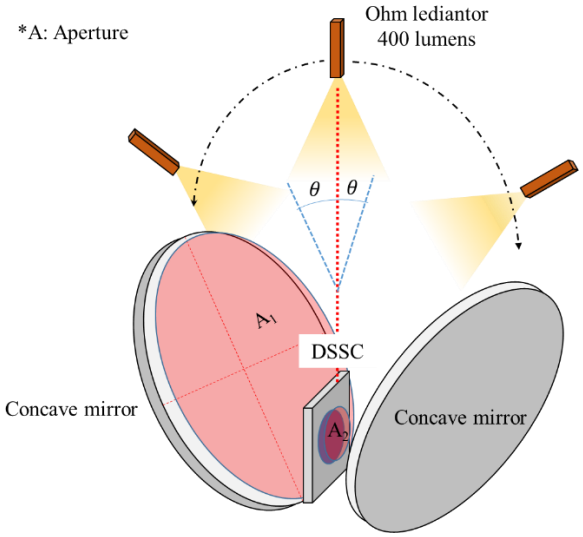

Figure 4.3 Optical parameter measurement setup.

The area power density of the light incident on the DSSC was deduced using a power and energy meter (NOVA P/N 7Z01500 OPHIR Japan ltd.) with an individual one-side mirror, as both sides have a similar mirror condition.

4.2 Experimental Results and Discussion

4.2.1 Effect of Tilt Angle

The effect of tilt angle was examined to observe the best performance of the DSSC based on the V-shape tilt angle of the plane and concave mirror concentrator. In this part, several variations in the tilt angle are applied to find the best angle to support the increased performance of DSSCs. The power density (mW/cm^2) depends on the mirror tilt angle. At some tilt angles, the light passes through the solar cell in multipath ways, significantly enhancing the output power and the apparent efficiency. J-V curve measurements and

EIS of the bifacial DSSC under the V-shape plane and concave mirror concentrator were carried out to understand the effect of spread and concentrated light irradiation.

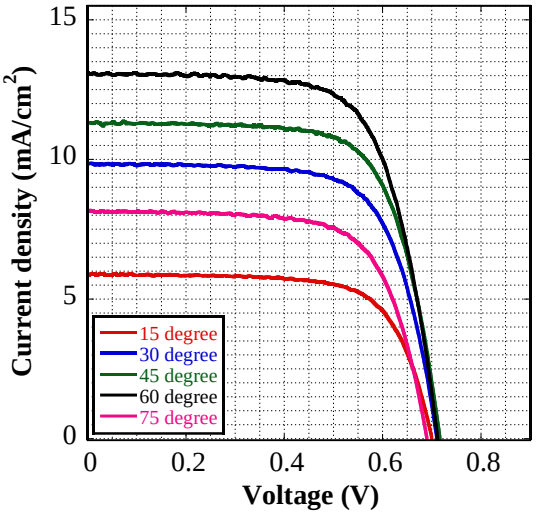

Figure 4.4 $J-V$ curves showing the effect of various tilt angles on the plane mirror V-shape concentrator

The *J-V* curves of bifacial DSSCs with V-shape plane mirror concentrator and various tilt angles are presented in Fig. 4.4, and a summary of the results is presented in Table 4.1. The PCE depends on the P_{in} and P_{out} ratio. As the P_{in} value depends on the mirror tilt angle and the DSSC is highly responsive to low illumination, the PCE was not suitable as a parameter for increasing the cell performance in concentrated light DSSCs. The parameters for increasing the performance of DSSCs with a plane and concave mirror concentrator depend on P_{out}. P_{out} increases with increasing tilt angle. The maximum P_{out} with the plane mirrors is 6.42 $mW.cm^{-2}$ at 60°. The increase in P_{out} in the plane mirror may be caused by repeated reflection in the V-Shape structure.

Table 4.1 *J-V* performance of bifacial DSSCs with plane mirror concentrator

Tilt angle (°)	V_{OC} (V)	J_{SC} (mA.cm^{-2})	FF	P_{in} (mW/cm^2)	P_{out} (mW/cm^2)	η (%)
15	0.70	5.87	0.70	18.21	2.89	15.87
30	0.70	9.84	0.70	76.63	4.83	6.31
45	0.71	11.31	0.70	102.51	5.62	5.50
60	0.71	13.10	0.70	98.03	6.51	6.64
75	0.69	8.14	0.69	6.27	3.87	61.72

The increase in J_{SC} is caused by the increasing light absorbance in the dye, which leads to an enhancement in electron excitation and electron injection in the dye/TiO_2 interfaces. At a low angle, the amount of reflected light that experienced multiple reflection was low, which led to low P_{in} and J_{SC}. In contrast, at a high angle, the amount of light falling into the mirror was reduced because P_{in} was also lowered.

Figure 4.5 shows the Nyquist plot from the EIS measurement at various tilt angles in a bifacial DSSC with a V-shape plane mirror concentrator. The Nyquist plot shows information regarding the charge transfer process in bifacial DSSCs. Each process of charge transfer in a bifacial DSSC is represented by the semicircles Z_1, Z_2, and Z_3. Z_1 shows the surface resistance of the electrode and charge transportation at the counter electrode, which are detected in the ultra-high to high frequency range. Z_2 shows charge transfer at the FTO/TiO_2/dye/electrolyte interfaces, which is detected in the middle frequency, and Z_3 shows the charge transport and redox couple in the electrolyte, which are detected in the low frequency range [6,22-28]. The equivalent circuit for electrochemical impedance spectroscopy in a bifacial DSSC is shown in Fig. 3.6.

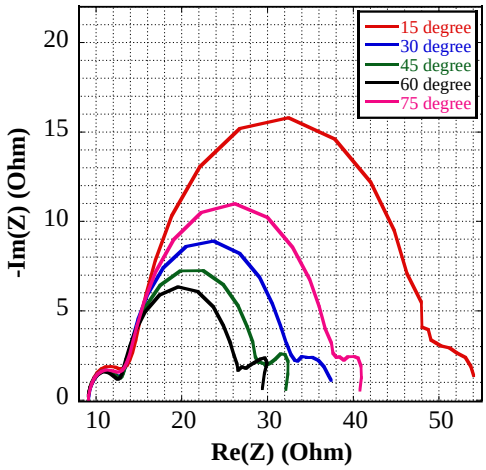

Figure 4.5 Nyquist plot of various tilt angles in a bifacial DSSC V-shape system with plane mirror concentrator.

The Z_2 semicircle decreased with increasing tilt angle. The decrease in the Z_2 semicircle indicated that the charge transfer in dye/TiO_2 interfaces increased along with the increasing incident light form both sides of the bifacial DSSC. The high Z_2 value at 15° and 75° tilt angles caused by the P_{in} at 15° and 75° is lower than other tilt angles, attaining 18.21 $mW.cm^{-2}$ and 6.27 $mW.cm^{-2}$, respectively. Despite the angles that prevent light from hitting the DSSCs, the effective tilt angle for a bifacial DSSC with a V-shape system using a plane mirror concentrator is 60°. At 60°, the dye can absorb more light than other tilt angles resulting in more electrons excited and injected into TiO_2.

The charge transfer process in dye/TiO_2 also can be affected by the ability of the counter electrode in the process of transferring electrons to the electrolyte to regenerate the electrons in the dye [6]. The resistance in the Z_1 semicircle shows the lowest value at 60°, indicating that a fast charge transfer process occurred. As the Pt counter electrode has good catalytic activity, it facilitates the transfer of electrons towards the electrolytes. A summary of the results is presented in Table 4.2.

Table 4.2 EIS parameter of effect of tilt angles bifacial DSSCs under V-Shape with plane mirror concentrator

Tilt Angles (°)	**Rs** (Ω)	**Z1** R_{CT1} (Ω) C (µF)	**Z2** R_{CT2} (Ω) C (µF)
15	9.07	5.32 2.83	34.2 143
30	9.10	4.51 2.27	20.25 164
45	9.05	4.43 2.31	16.21 205
60	9.06	4.19 2.44	14.06 160
75	9.09	4.46 2.29	24.51 135

Various tilt angles were also applied to the V-Shape system using a concave mirror concentrator with 30°, 40°, 45°, and 60°. The summarized results are shown in table 4.3. The highest result was obtained with tilt angles at 40°, with P_{out} of 24.31 $mW.cm^{-2}$. The J_{SC} reached 62 $mA.cm^{-2}$ at a tilt angle 40°, and at this point the DSSC was in the focus area of the concave mirror. At the focal point, the light is concentrated to provide a large amount of photon energy to the dye, which is absorbed and excites electrons. This large number of excited electrons leads to an increase in J_{SC}. V_{OC} increased to 0.74 V, possibly because of the increased light concentration [29-30].

Table 4.3 I-V performance of bifacial DSSCs with concave mirror concentrator

Tilt angle (°)	V_{OC} (V)	J_{SC} $(mA.cm^{-2})$	FF	P_{in} $(mW.cm^{-2})$	P_{out} $(mW.cm^{-2})$	η (%)
30	0.68	14.36	0.64	171.68	6.23	3.63
40	0.74	62.0	0.53	522.49	24.31	4.65
45	0.68	9.56	0.65	80.61	4.21	5.22
60	0.57	1.62	0.63	5.13	0.60	11.70

The increases in J_{SC} and power output (P_{out}) at the 40° tilt angle were followed by decreases in the fill factor (FF), as presented in Table 4.3, which suggested a reduction in cell performance. The reduction in FF was mainly caused by a decreasing performance in the counter electrode [31]. The platinum counter electrode is considered to have the best performance in DSSCs [32-33]. The decreasing performance of the bifacial DSSC is not due to poor catalytic performance of the Pt counter electrode, but it is mainly because the high speed of the excited electrons and electron injection in the dye/TiO_2 interfaces are not matched by the electron transfer rate at Pt/electrolyte.

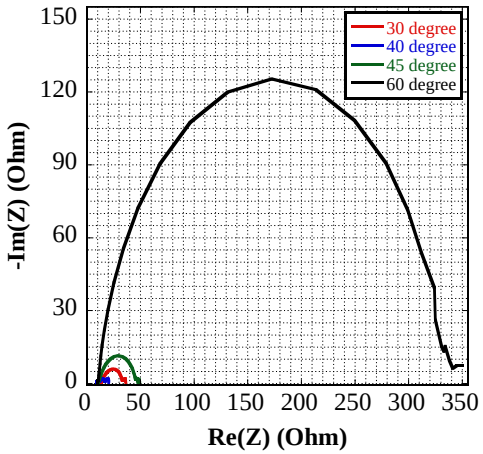

Figure 4.6 Nyquist plots of bifacial DSSCs with various tilt angles.

Figure 4.6 shows a Nyquist plot of the EIS of a bifacial DSSC with a V-shaped system using a concave mirror concentrator. The smallest second circle was at an angle of 40° and the largest one was at a 60° angle. The increase in J_{SC} led to the reduced impedance, as explained by the equation $R_{CT} = \zeta / J_{SC}$.

Overall, the tilt angle dependence of P_{out} in a bifacial DSSC under a V-Shape concentrated light system using plane and concave mirror concentrators is shown in Fig. 4.7. A summary of the results of a comparison of the performance of bifacial DSSCs between a plane mirror and a concave mirror concentrator at optimum tilt angles is presented in Table 4.4.

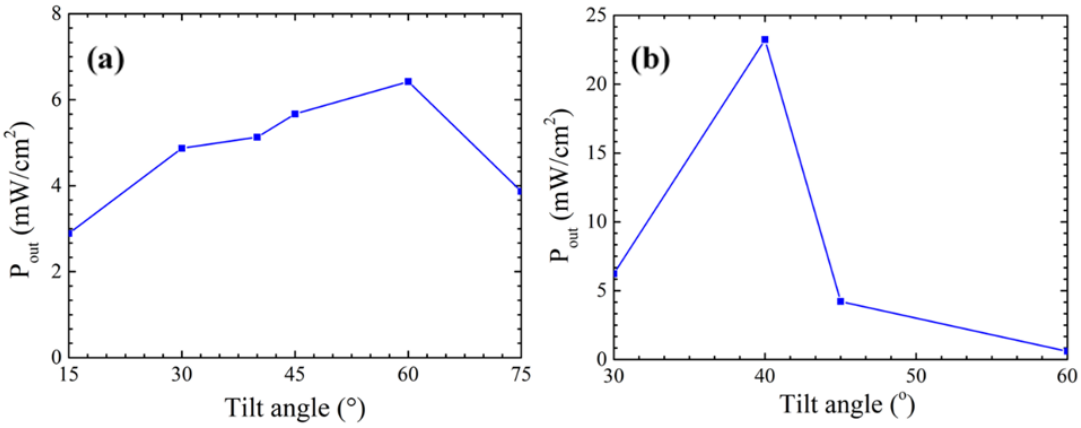

Figure 4.7 Tilt angle dependence of P_{out} in bifacial DSSCs with (a) a plane mirror and (b) a concave mirror V-Shape concentrator system.

Table 4.4 Comparison of bifacial DSSCs without mirror performance with plane mirror and concave mirror V-shape concentrator at the optimum performance.

Tilt angle (°)	V_{OC} (V)	J_{SC} (mA.cm^{-2})	FF	P_{in} (mW/cm^2)	P_{out} (mW/cm^2)	η (%)
-	0.70	8.78	0.69	106.49	4.25	3.99
60 (plane)	0.71	13.10	0.69	98.03	6.42	6.60
40 (concave)	0.74	62.0	0.53	522.49	24.31	4.65

The maximum P_{out} with the plane mirrors is 6.42 mW/cm^2 at 60°, whereas with concave mirrors it is 24.31 mW/cm^2 at 40°. As indicated in Table 4.4, the individual plane mirror did not increase the power input (P_{in}, 98.03 mW/cm^2) from the source (106.49 mW/cm^2). The concave mirrors have a concentrated light power density of P_{in} = 522 mW/cm^2, increasing P_{out} to 24.3 mW/cm^2. The increase in current density J_{SC} with the concave mirrors was larger than that with the plane mirrors, primarily because the light intensity is higher with the former than with the latter. Figure 4.8 shows an I–V and EIS performance comparison of bifacial DSSCs using plane and concave mirror concentrators. The rises in J_{SC} and power output (P_{out}) with the concave mirror concentrator are followed by a decrease in FF, as shown in Table 4.4. As an attribute of the increasing J_{SC}, the increase in transport and redox reaction rate is revealed by the decreasing diffusion resistance (R_{CT2}), as shown in Fig. 4.8 (b).

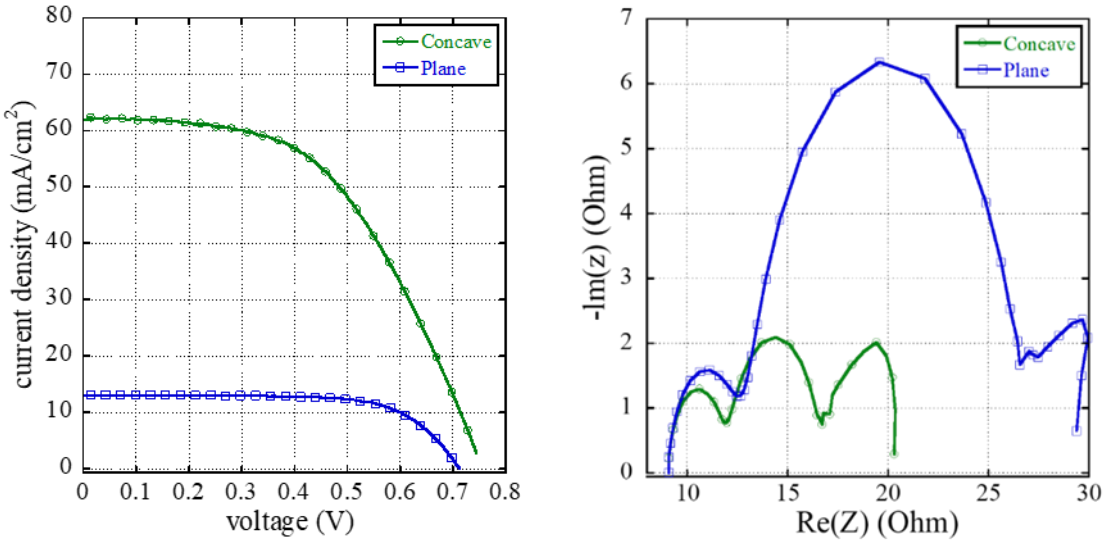

(a) **(b)**

Figure 4.8 (a) I–V graph and (b) Nyquist plot of bifacial DSSCs with a plane mirror at $\theta = 60^0$ and a concave mirror at $\theta = 40^0$

4.2.2 Optical System

Acceptance angle

The acceptance angle of the V-shape system was measured with different incident light (source) angles (θ_i). Figure 4.9 shows the normalized power production with different incident light source angles θ_c for V-shape systems with 0 distance and 60° mirror tilt angle. The half-acceptance angle θ_a of the V-shape plane system was 10°. In our V-shape system with a bifacial DSSC, the incident light angle from the Pt and TiO_2 side results in different power production. In the V-shape plane mirror, the incident light angle comes from the Pt side, which has higher power production than the TiO_2 side. It is indicated that the number of lights reflected by the concentrator is higher than the number of direct lights (the incident light comes from the TiO_2 side).

The power production resulted from the accumulation of direct light and reflected light by the V concentrator. In the case of light from the TiO_2 side, the dominant

power comes from direct light to TiO_2 (front side of the DSSC) and reflected light to TiO_2 and Pt (front and rear), otherwise it is reversed. As the power efficiency at the front side DSSC higher than the rear side. The result in Fig. 1 indicated that the number of lights reflected by the concentrator is higher than the number of direct lights as the power produced by incident light in $-\theta$ angle (Pt-side) higher than $+\theta$ angle (TiO_2 side).

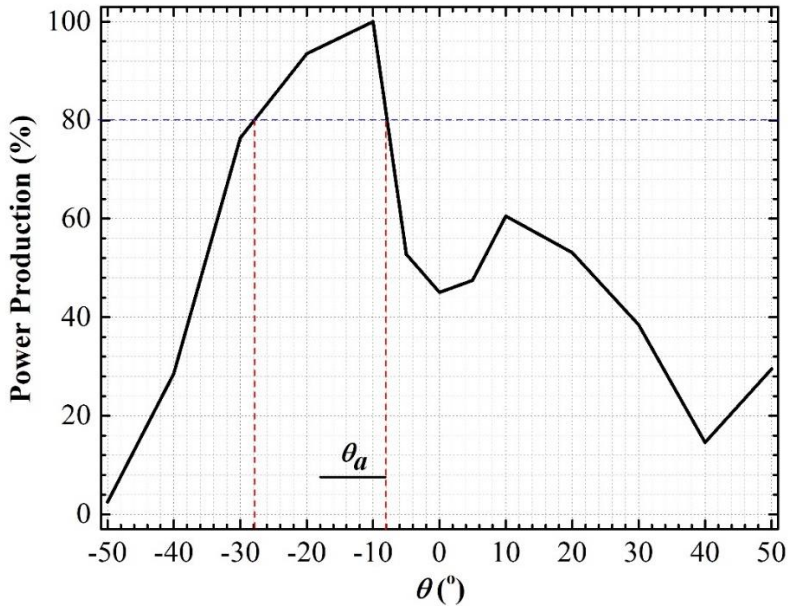

Figure 4.9 Power production in different incident light angle of V-shape plane mirror.

The normalized power production with different incident light (source) angles in V-shape systems with a concave mirror at 40° mirror tilt angle is shown in Fig. 4.10. In contrast with the plane mirror, the V-shape concave mirror has slightly higher power production with incident light in +θ angle (TiO_2 side) and with a half-acceptance angle ~6°. The cause may be that the concave mirror reflection is concentrated light. As the incident light angle increased, the point contact of the reflected light and DSSC (receiver) decreased (movement of the mirror accumulation point), which led to a power production dominated by direct light to the DSSC.

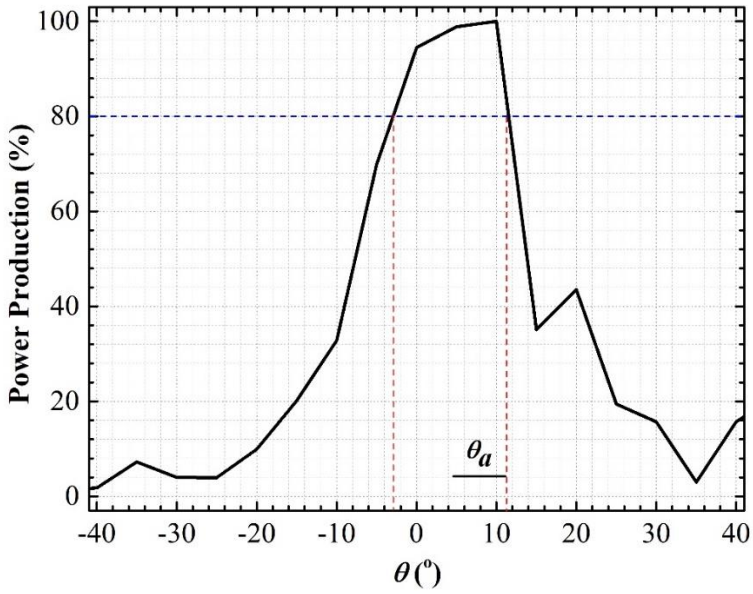

Figure 4.10 Power production with different incident light angles of the V-shape concave mirror.

The optical efficiency of the system with a V-shape concave mirror at different incident angles is shown in Fig. 4.11. The optical efficiency can reach 0.53 at the vertical incident light. The loss in optical efficiency may be caused by spillage loss, a substantial amount of the reflected light hitting outside of the receiver, and transparency of the DSSC. The transparent dye will influence the amount of light that arrived at the concentrator, as part of the light will hit the solar cell before the concentrator at $\theta \neq 0$ incident angle. The transmittance of Pt and TiO_2/dye is shown in Fig. 4.12.

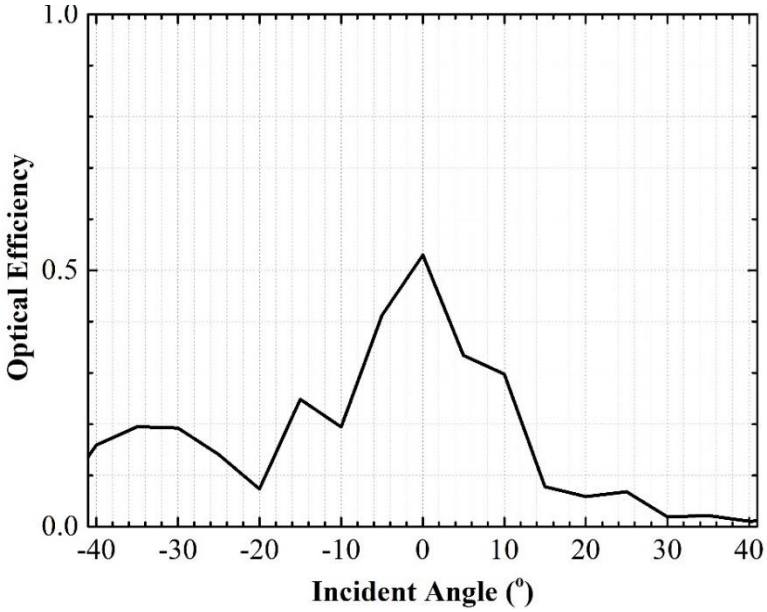

Figure 4.11 Optical efficiency of V-shape concave mirror with 0 cm mirror distance and 40° tilt angle.

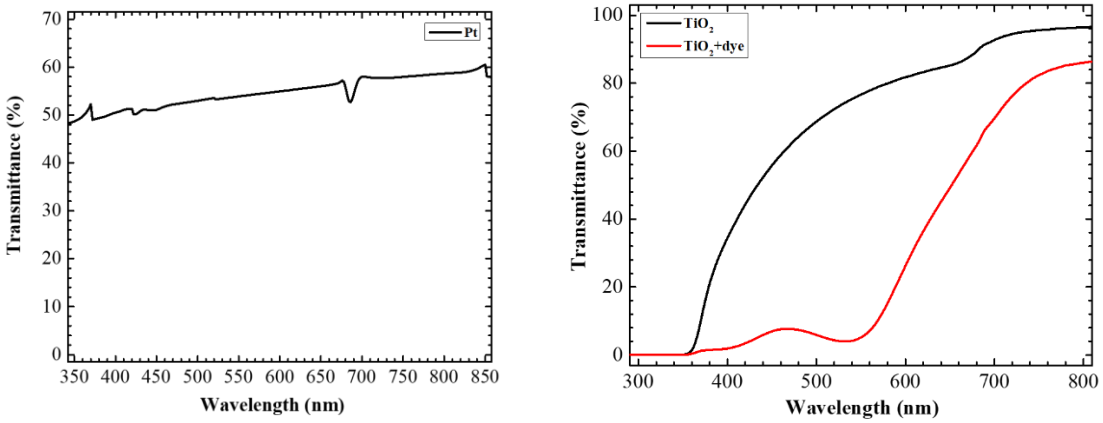

(a) (b)

Figure 4.12 Transmittance of (a) Pt and (b) TiO_2 and TiO_2/dye.

4.2.3 Effect of Time

The effect of operation time in bifacial DSSCs under V-shape concentrated light was examined to observe the phenomenon that occurs in these cells. The performance of bifacial DSSCs with V-shape plane and concave mirror concentrators was observed to

determine the possible effect of temperature in bifacial DSSCs during operation time. In this part, the operation time varied in the 150–180 min range with observations every 30 min.

The surface temperature changes in the 2.5 h operation of bifacial solar were measured for both bifacial DSSCs with the plane and concave mirror. The surface temperature of a bifacial DSSC with a V-shape plane mirror increased to approximately 57 °C from an initial 25 °C (room temperature) after light exposure with a 60° tilt angle for both the front and rear surfaces and became stable at approximately 57 °C for the rest of the measurement, as shown in Fig. 4.13 (a). The stability of the surface temperature was also followed by a stabilized performance of the solar cell, as shown in Fig. 4.13 (b), at P_{out} of approximately 6.4 mW/cm^2.

In comparison, the surface temperature increased rapidly in a bifacial DSSC with a concave mirror and decreased in P_{out}, as shown in Fig. 4.13. The decrease in P_{out} may be attributed to cell degeneration. The rise in temperature led to a reduction in V_{OC} (see Fig. 4.14 (a)). This is caused by the increased recombination in the solar cell, which is related to an increased dark current saturation.

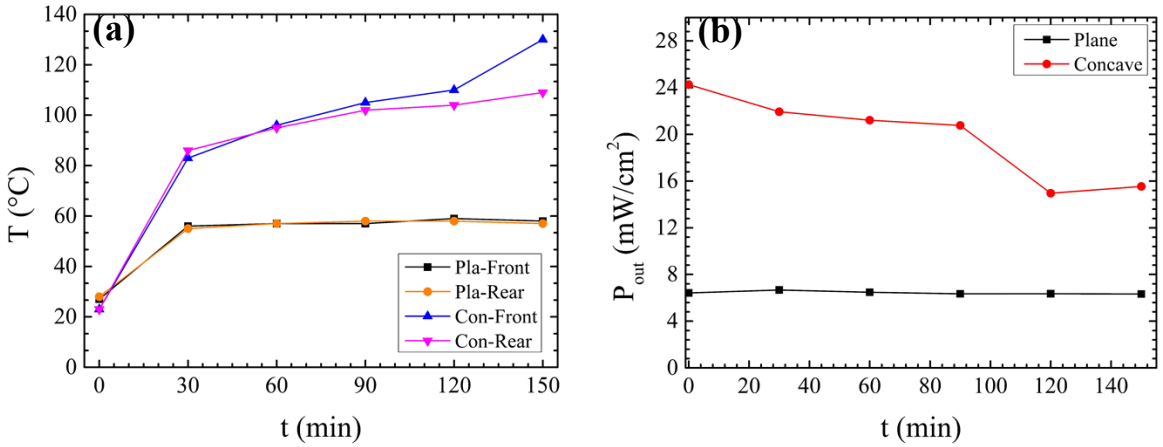

Figure 4.13 (a) Surface temperature and (b) output power of a bifacial solar cell with plane and concave mirrors as a function of time at an optimum tilt angle.

The decrease in J_{SC} is possibly caused by the reduced electrolyte volume. As the temperature increases, the charge transfer kinetic energy and the number of redox reactions increased, indicating a decrease in R_s, R_{CT1}, and R_{CT2} (see Fig. 4.14 (b)). As the surface temperature increases further, part of the electrolyte evaporated, which reduced the available I_3^- and I^- for the redox reaction, as shown by the increasing R_{CT2} and reducing J_{SC} (see Table 4.5).

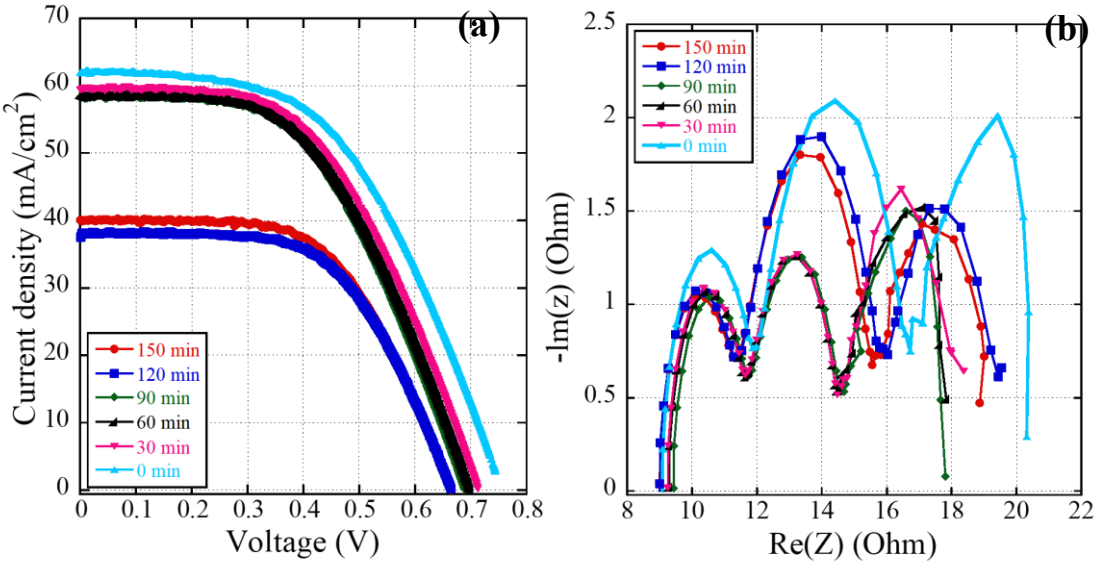

Figure 4.14 (a) $J-V$ curves and (b) EIS of bifacial solar cell with a concave mirror as a function of time.

Table 4.5 EIS parameter of V-shape concave mirror operational time dependent. Increase of surface temperature cause R_S and R_{CT1} decrease. In other hand evaporated electrolyte cause Rd increases.

t (minutes)	R_S (Ω)	Z1 R_{CT1} (Ω) C (μF)	Z2 R_{CT2} (Ω) C (μF)
0	10.61	3.21	5.04
		2.17	208
30	10.51	2.61	3.22
		1.82	221
60	10.56	2.62	3.11
		1.80	229
90	10.68	2.60	3.11
		1.82	229
120	10.29	2.69	4.65
		1.76	225
150	10.28	2.66	4.42
		1.78	161

The influence of temperature on electrolyte performance in solar cells with a 0 distance V-shape concave mirror was investigated using the Arrhenius plot in Fig. 15. Two different trends were observed with a breaking point at 100 °C, corresponding to the additional activation energy (E_A). The E_A extracted from the slope of ln FF shows 5.4×10^{-3} and 0.2 eV values below and above 100 °C of surface temperature, respectively. These small values of E_A below 100 °C indicate temperature independence in DSSCs. The increasing E_A above 100 °C corresponds to the dye degradation caused by temperature. The UV-VIS spectrum analysis of two TiO_2 samples soaked in N719 dye (see Fig. 16) revealed a change in absorbance and reflectance spectrum after 150 °C heat treatment for 30 min.

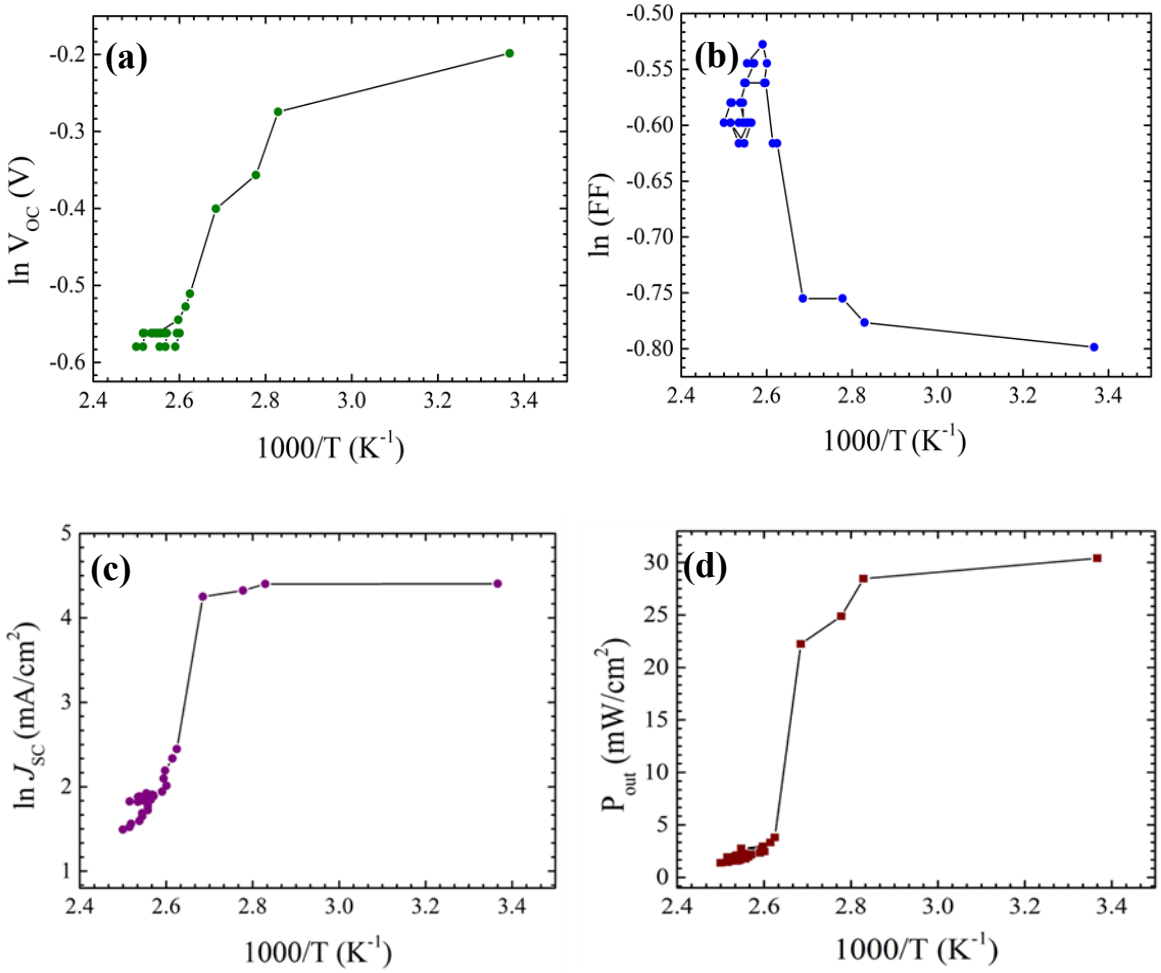

Figure 4.15 Arrhenius plot of T dependent $J-V$ performance in (a) V_{OC}, (b) FF, (c) J_{SC}, and (d) P_{OUT} for DSSCs with 0 cm distance V-shape concave mirrors.

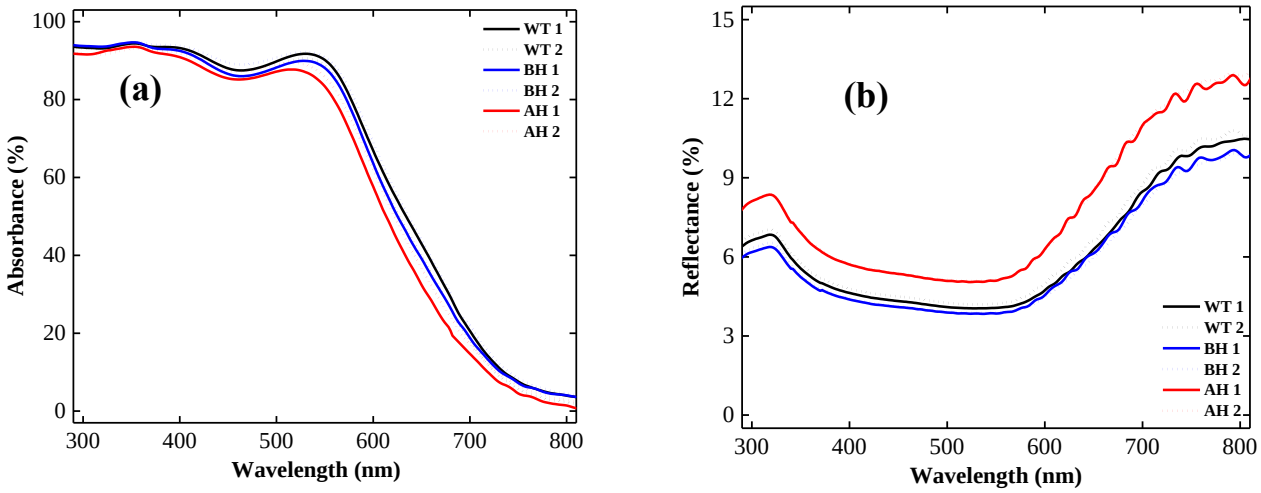

Figure 4.16. UV-VIS spectra of TiO_2 samples soaked with N719 dye for ~20 h, without heat treatment (WT1 and WT2), with 30 min heat treatment at 70 °C (BH1 and BH2), and with 30 min heat treatment at 150 °C (AH1 and AH2); a) absorbance, and b) reflectance.

4.2.4 Effect of Cell-Mirror Distance

The rapid rise in temperature caused by concave mirrors can be controlled with the distance between mirrors and solar cells. Bifaciality is defined as the ratio between the efficiency of the rear side to that of the front side [17]. As the irradiation light is the same for both sides, bifaciality can be expressed as

$$Bifaciality = \frac{\eta_{rear}}{\eta_{front}}$$

where η is the efficiency of the DSSC. The bifacialities of the DSSC are 0.26, 0.27, 0.19, 0.28, and 0.50 with distances of 0, 1, 2, 3, and 4 cm, respectively (see fig. 4.17).

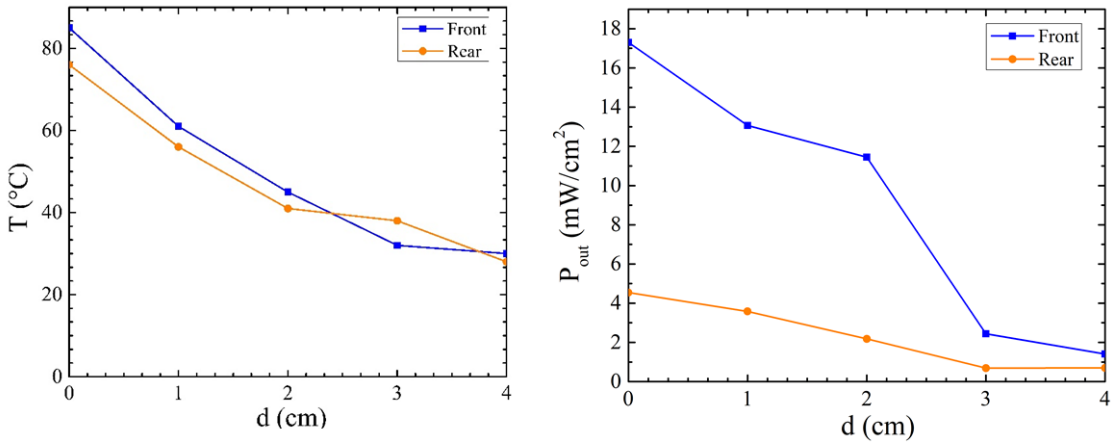

Figure 4.17 (a) Temperature and (b) PCE of bifacial DSSCs with a concave mirror as a function of distance.

The front side P_{out} decreases rapidly compared to that at the rear side because the P_{out} mainly contributes by the front side, which directly intersects with TiO_2 and dye. The front side temperature also increases faster than that at the rear side, which may cause added energy dissipation. This result suggests the use of a 1 cm distance to obtain a surface temperature similar to that of the plane mirror concentrator with higher P_{out}.

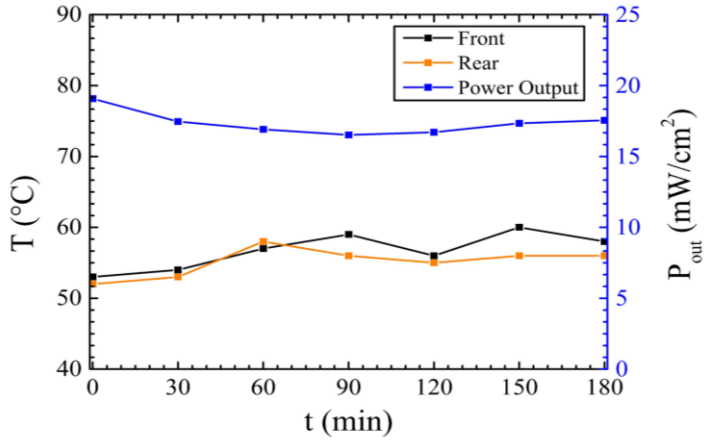

Figure 4.18 Measured surface temperature and output power as a function of time at 1 cm concave mirror distance.

The performance of bifacial DSSCs with a 1 cm distance of the concave mirror was examined in terms of operational time. Figure 4.18 shows a stable surface temperature at less than 60 °C and P_{out} of ~17 mW/cm^2 for 3 h of operation with 1 cm mirror distance. This system successfully obtains 4 and 2.6 times more P_{out} than that without mirrors and that with a V-shape plane mirror system in bifacial DSSCs, respectively. The deterioration in performance of the bifacial DSSC for 7 days measurement of the concave mirror with 1 cm distance showed a similar pattern to that of the cell without mirrors (see Fig. 4.19). This result confirmed the 1 cm distance as the optimum condition for the V-shape concave mirror concentrator system in bifacial DSSCs.

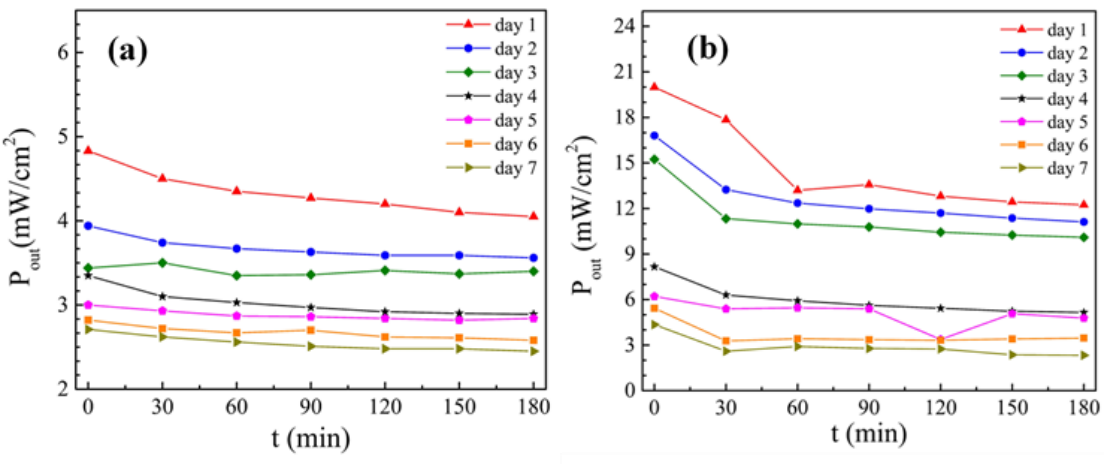

Experiment condition; Average temperature: 20 °C

Average pressure: 101.6 kPa

Average humidity: 50%

Figure 4.19 Deterioration in performance of cells with (a) no mirror and (b) 1 cm distance concave mirror.

4.3 Conclusions

In conclusion, V-shape concentrated irradiated light with plane and concave mirrors was successfully utilized to maximize the absorption in both sides of DSSC bifacial systems. The result shows that the concave concentrator is more effective than the plane concentrator to boost the power output (P_{out}) of bifacial DSSCs. The half-acceptance of V-shape concave systems is $\sim 6°$ with optical efficiency 0.53. The increase in temperature caused by the applied concave concentrator can be controlled by adjusting the distance between the mirrors and the solar cell. The V-shape plane mirror concentrator could produce 6.42 mW/cm^2 in P_{out} with optimum tilt angle of 60° and a stable temperature of 57 °C for 2.5 h measurement. The concentrated irradiation light with a V-shape concave mirror concentrator could produce 24.3 mW/cm^2 P_{out} with a rapid increase in temperature to no more than 80 °C after 30 min of operation. An adjustment in distance to 1 cm between the concave mirror and solar cell can reduce the temperature effect to 60 °C for a 3 h measurement with an average P_{out} of ~17 mW/cm^2. This condition successfully boosts the P_{out} absorption more than the condition without mirror. Hence, through the current method, we can achieve a high P_{out} value for solar cells. These results may encourage the utilization of concentrating systems for high-efficiency bifacial DSSCs.

REFERENCES

[1]. Regan, B. O. and Gratzel, M. (**1991**) 'A low-cost, high-efficiency solar cell based on dye-sensitized colloidal TiO_2 films', *Nature*, 353, 737–740.

[2]. Yum, J., Baranoff, E., Wenger, S., Nazeeruddin, M. K. and Gratzel, M. (**2011**) 'Panchromatic engineering for dye-sensitized solar cells', *Energy Environ. Sci.* 4, 842–857.

[3]. Chung, I., Lee, B., He, J., Chang, R. P. H., Kanatzidis, M. G. (**2012**) All-solid-state dye-sensitized solar cells with high efficiency, *Nature,* 485, 486–489.

[4]. Xue, G., Guo, Y., Yu, T., Guan, J., Zhang, J., Liu, J. and Zuo, Z. (**2012**) 'Degradation Mechanisms Investigation for Long-term Thermal Stability of Dye-Sensitized Solar Cells', *Int. J. Electrochem. Sci.,* **7**, 1496–1511.

[5]. Sharma, K., Sharma, V. and Sharma, S. S. (**2018**) 'Dye-Sensitized Solar Cells: Fundamentals and Current Status', *Nanoscale Res. Lett.* 13, 381.

[6]. Seo, H., Son, MK., Hashimoto, S., Takasaki, T., Itagaki, N., Koga, K. and Shiratani, M. (**2016**) 'Surface Modification of Polymer Counter Electrode for Low-Cost Dye-sensitized Solar Cells', *Electrochim. Acta*, 210, 880-887.

[7]. Saidi, N. M., Farhana, N. K., Ramesh, S. and Ramesh, K. (**2021**) 'Influence of different concentrations of 4-tert-butyl-pyridine in a gel polymer electrolyte towards improved performance of Dye-Sensitized Solar Cells (DSSC)'. *Sol. Energy*, 216, 111-119.

[8]. Omar, A. and Abdullah, H. (**2014**) 'Electron transport analysis in zinc oxide-based dye-sensitized solar cells: A review'. *Renewable Sustainable Energy Rev.,* 31, 149-157.

[9]. Seo, H., Nam, SH., Itagaki, N., Koga, K. and Shiratani, M. (**2016**) 'Effect of sulfur-doped TiO_2 on photovoltaic properties of dye-sensitized solar cells', *Electron. Mater. Lett.* 12, 530–536.

[10]. Seo, H., Son, MK., Itagaki, N. and Shiratani, M. (**2016**) 'Polymer counter electrode of poly(3,4-ethylenedioxythiophene): Poly(4-styrenesulfonate) containing TiO_2 nanoparticles for dye-sensitized solar cells', *J. Power Source*, 307, 25-30.

[11]. Wu, J., Li, Y., Tang, Q., Yue, G., Lin, J., Huang, M. and Meng, L. (**2014**) 'Bifacial dye-sensitized solar cells: A strategy to enhance overall efficiency based on transparent polyaniline electrode', *Sci. Rep.*, 4 (4028) 1–7.

[12]. Xu, T., Kong, D., Tang, H., Qin, X., Li, X., Gurung, A., Kou, K., Chen, L., Qiao, Q. and Huang, W. (**2020**) 'Transparent MoS 2 / PEDOT Composite Counter Electrodes for Bifacial Dye-Sensitized Solar Cells', *ACS Omega,* 5, 8687-8696.

[13]. Miranda-Munoz, J. M., Carretero-Palacios, S., Jimenez-Solano, A., Li, Y., Lozano, G., Miguez, H. (**2016**) 'Efficient bifacial dye-sensitized solar cells through disorder by design'*, J. Mater. Chem. A,* 4, 1953-1961.

[14]. Cai, H., Tang, Q., He, B., Li, R. and Yu, L. (**2014**) 'Bifacial dye-sensitized solar cells with enhance rear efficiency and power output', *Nanoscale*, 6, 15127-15133.

[15]. Ito, S., Zakeeruddin, S. M., Comte, P., Liska, P., Kuang, D. and Gratzel, M. (**2008**) 'Bifacial dye-sensitized solar cells based on an ionic liquid electrolyte', *Nat. Photonics*, 2, 693–698.

[16]. Lo, C. K., Lim, Y. S. and Rahman, F. A. (**2015**) 'New integrated simulation tool for the optimum design of bifacial solar panel with reflectors on a specific site', *Renew. Energy,* 81, 293–307.

[17]. Ooshaksaraei, P., Sopian, K., Zulkifli, R., Alghoul, M. A. and Zaidi, S. H. (**2013**) 'Characterization of a bifacial photovoltaic panel integrated with external diffuse and semimirror type reflectors', *Int. J. Photoenergy*, 2013, 465837.

[18]. Ustaoglu, A.; Kandilli, C.; Cakmak, M.; Torlaklı, H. (**2020**) 'Experimental and economical performance investigation of V-trough concentrator with different reflectance characteristic in photovoltaic applications', *J. Clean. Prod.,* 272, 123072.

[19]. Wang, N. Y., Chiang, S. Y., Chou, T. L., Lee, H. L. and Chiang, K. N. (**2010**) Life prediction of high concentration photovoltaic modules subjected to thermal cycling test', *2010 5th International Microsystems Packaging Assembly and Circuits Technology Conference,* 3–6.

[20]. Wang, P., Yang, L., Wu, H., Cao, Y., Zhang, J., Xu, N., Chen, S., Decoppet, J. D., Zakeeruddin, S. M. and Gratzel, M. (**2018**) 'Stable and Efficient Organic Dye-Sensitized Solar Cell Based on Ionic Liquid Electrolyte', *Joule*, 2, 2145–2153.

[21]. Raga, S. R. and Fabregat-Santiago (**2013**) 'Temperature effect in dye-sensitized solar cells', *Phys. Chem. Chem. Phys.* 15, 2328-2336.

[22]. J. Bisquert and F. Fabreagat-Santiago (**2010**) 'Impedance spectroscopy: a general introduction and application to dye-sensitized solar cells', in K. Kalyanasundaram (ed) *Dye-Sensitized Solar Cells* First Edition. p. 457. CRC; Taylor & Francis, Boca Raton, Fla, USA

[23]. Sarker, S., Ahammad, A. J. S., Seo, H. W. and Kim, D. M. (**2014**) 'Electrochemical Impedance Spectra of Dye-Sensitized Solar Cells: Fundamentals and Spreadsheet Calculation', *International Journal of Photoenergy,* Article ID 851705

[24]. Santiago, F. F., Bisquert, J., Palomares, E., Otero, L., Kuang, D., Zakeeruddin, M. and Gratzel, M. (**2007**) 'Correlation Between Photovoltaic performance and

Impedance Spectroscopy of Dye-Sensitized Solar cells based on Ionic Liquids', *J. Phys. Chem. C*, 111, 6550-6560.

[25]. Chawarambwa, F. L., Putri, T. E., Attri, P., Kamataki, K., Itagaki, N., Koga, K. and Shiratani, M. (**2021**) 'Highly Efficienct and Transparent Counter Electrode for Application in Bifacial Solar Cells', *Chem. Phys. Lett.,* 768, 138369

[26]. Wang, Q., Moser, J. E. and Gratzel, M. (**2005**) 'Electrochemical Impedance Spectroscopy Analysis of Dye-Sensitized Solar Cells', *J. Phys. Chem. B,* 109, 14945-14953.

[27]. Seo, H., Son, M. K., Kim, J. K., Choi, J., Choi, S., Kim, S.K. and Kim, H. J. (**2012**) 'Analysis of Current Loss from a Series-parallel Combination of Dye-Sensitized Sloar Cells Using Electrochemical Impedance Spectroscopy', *Photonic and nanostructures – Fundamentals and Application,* 10. 568-574

[28]. Chawarambwa, F. L., Putri, T. E., Attri, P., Kamataki, K., Itagaki, N., Koga, K. and Shiratani, M. (**2021**) 'Effect of Concentrated Light on the Performance and Stability of a Quasi-Solid Electrolyte in Dye-Sensitized Solar Cells', *Chem. Phys. Lett.*, 781, 138986.

[29]. Bagienski, W., Kinsey, G. S., liu, M., Nayak, A. and Garbousahian, V. (**2012**) 'Open Circuit Voltage Temperature Coefficiencts Vs Concentration: Theory, Indoor Measurements, and Outdoor Measurements', *8th International Conference on Concentrating Photovoltaic Systems, AIP. Conf. Proc.* 1447.

[30]. Nishioka, K., Takamoto, T., Agui, T., Kaneiwa, M., Uraoka, Y. and Fuyuki, T. (**2006**) 'Annual output estimation of concentrator photovoltaic systems using high-efficiency InGaP/InGaAs/Ge triple-junction solar cells based on experimental solar cell's characteristics and field-test meteorological data', *Solar Energy Materials & Solar Cells,* 90, 57-67.

[31]. Kinsey, G. S., Hebert, P., Barbour, K. E., Krut, D. D., Cotal, H. L. and Sherif, R. A. (**2008**) 'Concentrator Multijuction Solar Cell Characteristics Under Variable Intensity and temperature', *Prog. Photovolt: Res. Appl.,* 16: 503-508.

[32]. Wu, J., Lan, Z., Lin, J., Huang, M., Huang, Y., Fan, L. and Luo, G. (**2015**) 'Electrolyte in Dye-Sensitized Solar Cells', *J. Chem. Rev.,* 115, 2136-2173.

[33]. Hagfeldt, A., Boschloo, G., Sun, L., Kloo, L. and Pettersson, H. **(2010) '**Dye-Sensitized Solar Cells', *J. Chem. Rev.,* 110, 11, 6595-6663.

[34]. Gnanasekar, S., Kollu, P., Jeong, S. K. and Grace, A. N. (**2019**) 'Pt-Free, Efficient, and Low Cost Counter Electrode with Carbon Wrapped VO2(M) Nanofiber for Dye-Sensitized Solar Cells, *Sci. Rep*., 9, 5177.

Chapter 5

Low Concentrator Coupled with Flowing Electrolyte System in Bifacial Dye-Sensitized Solar Cells

DSSCs are promising for the future photovoltaics because of their good price to performance ratio, functioning at wider angles and in low light, long life, mechanical robustness, and low internal temperature operation [2,2]. The efficiency produced by DSSCs has reached approximately 14%, and it can be increased by approximately 67% using concentrated light [3-4]. Although a DSSCs coupled with a concentrator increases the efficiency [5], the device temperature is also increased. In conditions of one sun intensity (100 mW/cm^2), the solar cell temperature can reach 70 °C [6-7]. The solar cell temperature can attain 1200 °C without a cooling aid when the light intensity ratio increases 400x by using a concentrator [8]. This high temperature could cause instability and evaporation of the DSSC's liquid electrolyte, thus leading to limited operation lifetime. Even tough electrolyte evaporation can be lessened with solid or semi solid electrolytes, liquid electrolytes are still being used because of their advantages such as high ionic conductivity, relatively high viscosity, electrochemical potential window, and room-temperature long-term performance stability [10-12]. Based on the aforementioned several advantages of liquid electrolytes, an active cooling system is needed to support the performance of DSSCs using liquid electrolytes.

Active cooling systems generally work by flowing water at a speed of approximately 0.1–1 L/min under a block-mounted solar cell system. In contrast, passive cooling systems utilize a phase change material (PCM) as a coolant [16]. Various types of cooling systems have been introduced to overcome the thermal problems in solar cells, such as PCM- [17-22], thermoelectric- [23], air cooling- [24-28], heat pipe- [29], and liquid cooling-based systems [30-33]. More recently, the liquid electrolyte was used in a circulation system to improve the photovoltaic performance. In such a system, the electrolyte is used as the coolant, and it could also solve the electrolyte evaporation as the

new electrode always circulate. However, there is not yet a study regarding the DSSC electrolyte as a coolant especially coupled with low concentrated light. In this study, we applied an electrolyte-flowing cooling system in DSSCs and analyzed the effect to the cell performance.

5.1 Experimental Method

5.1.1 Cell Fabrication

Fabrication of TiO_2 photo-anode. FTO glass substrates (Sigma Aldrich 2.3 mm, ~13 Ω/sq) were cut to a size of 2 × 2 cm^2 and cleaned using acetone, ethanol, and purified water 20 min. TiO_2 (Solaronix Ti-Nanoxide T/SP) was printed on the FTO glass using the doctor blade method and sintered at 450 °C for 30 min in an electric furnace. After the substrate was cold, the dye solution (N719 Solaronix) was soaked on FTO/TiO_2 for 20–24 h.

Fabrication of counter electrode. FTO glass substrates (Sigma Aldrich 2.3 mm, ~13 Ω/sq) were cut to a size of 2 × 2 cm^2 and cleaned using acetone, ethanol, and purified water for 20 min. A hole was made on the FTO for iodine injection/flow. Platinum paste (Dyesol PT-1) was printed on the FTO glass using the doctor blade method and sintered at 450 °C for 30 min in an electric furnace.

For a normal cell. Two sealants (Solaronix Meltonix 1170-60) were cut to a size of 20 × 15 $mm^{2,}$ and the hole was put on one of it with size 15 × 10 mm^2. Afterwards, the FTO/Pt/sealant with a hole and the FTO/TiO_2/dye were overlapped into an FTO/Pt/Sealant/Dye/TiO_2/FTO sandwich structure. Subsequently, the cell was put on a hot plate and pressed until the sealant melted. After that, the iodide electrolyte was injected into the cell through the hole in the FTO/Pt side, closed using the second sealant, and then covered by a cover glass.

For flowing-electrolyte cell. The sealant (Solaronix Meltonix 1170-60) was cut to a size of 20 × 15 mm^2, and a hole was made in it with size of 15 × 10 mm^2. Afterwards, the FTO/Pt/sealant with the hole and FTO/TiO_2/dye were overlapped into a FTO/Pt/Sealant/Dye/TiO_2/FTO sandwich structure. Subsequently, the cell was put on a hot plate and pressed until the sealant melted. After that, a silicon pipe was installed in both holes of the Pt/FTO side as a medium to flow the electrolyte. A pump was installed in one of the pipes to pump the electrolyte into the cell. The pump was then connected to a timer to set the interval between flow and stop for 180 min.

5.1.2 Measurement

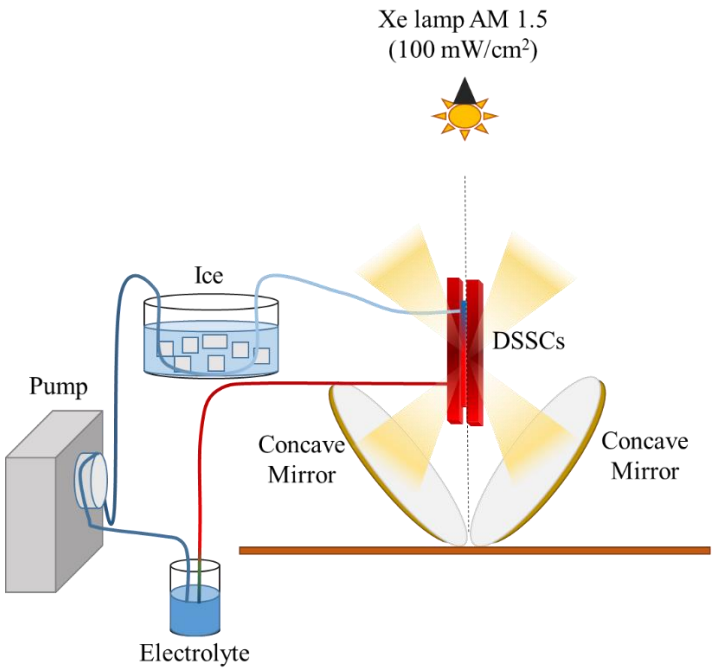

Figure 5.1 Schematic of the experiment.

The bifacial DSSC performance was measured under 1-sun illumination from a Xenon lamp equipped with an air mass (AM) 1.5 filter using a source meter (Keithley

2400). Plane and concave aluminum-coated mirrors (Edmund Optics, 43-469) as low concentrators were used during the measurement. A schematic of the experiment is shown in Fig. 5.1. The effect of the measurement time, mirror distance, and various types of electrolytes were investigated with the V-shape concentrator measurement, where *x* is the mirror distance to the cell and θ is the mirror tilt angle. The temperature was measured using an infrared thermometer gun (TIM-03, Asone 3-7406-01).

5.2 Experimental Results and Discussion

5.2.1 Flowing Electrolyte Systems

The V-shape concave mirror low concentrator can increase the P_{IN} of the DSSC from 100 mW/cm^2 to approximately 522 mW/cm^2 at 0 cm mirror-to-cell distance. Coupled with the flowing electrolyte system, the evaporation of the liquid electrolyte caused by the rise in temperature can be prevented. The DSSC with a flowing electrolyte system was similar in size and form to the standard normal cell. The additional hole in its back surface allows the electrolyte to flow in and out. To understand the effect of the applied electrolyte flowing system on the DSSC performance, we compared a normal cell (NC) DSSC with a continuously flowing electrolyte system cell (CF) DSSC for a 3 h measurement.

Photocurrent density–voltage (*J–V*)

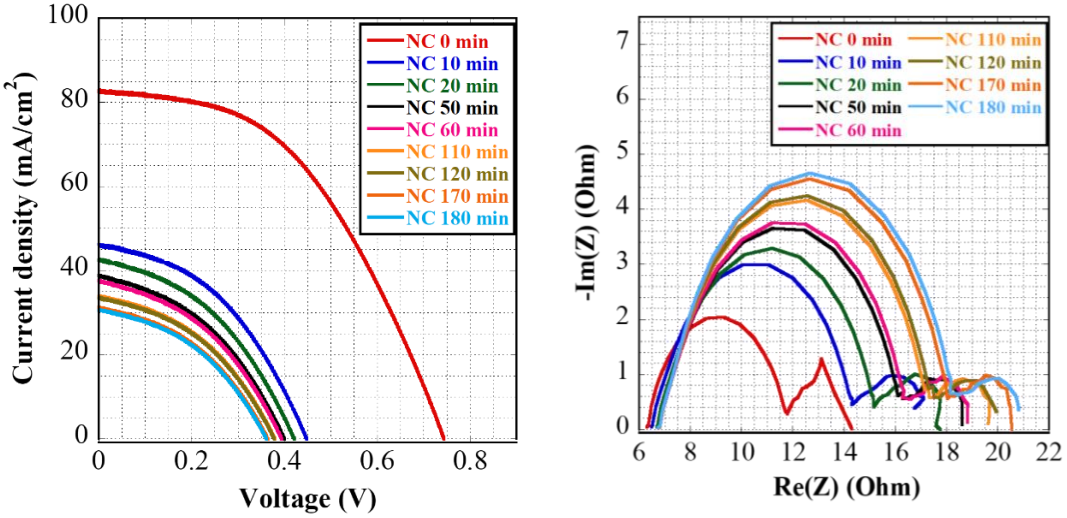

(a)

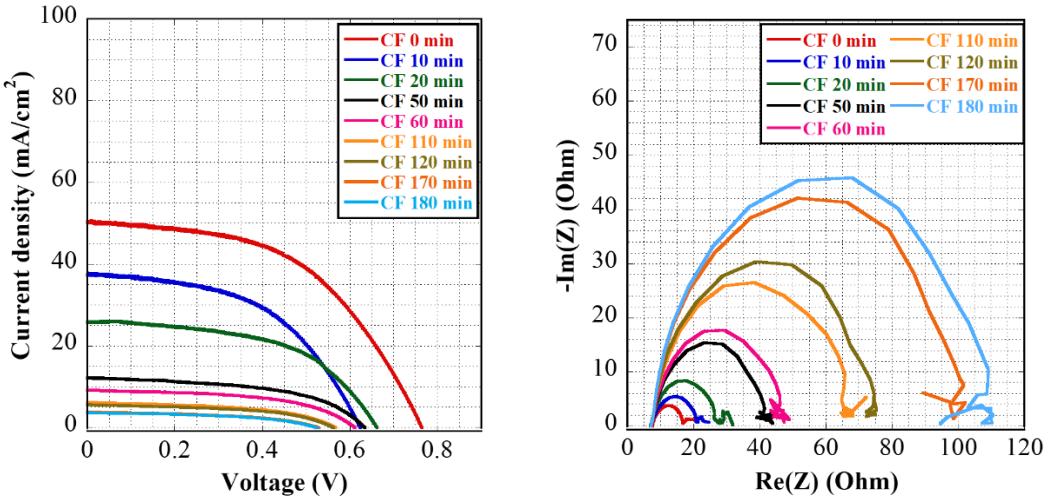

(b)

Figure 5.2 Photocurrent density–voltage (*J–V*) curves and electrochemical impedance spectroscopy (EIS) of (a) NC and (b) CF DSSCs under low concentrated light for 3 h measurement.

Figure 5.2 shows the photovoltaic performance of the cells under concentrated light as (a) NC and (b) CF. The I_{SC} in the NC condition decreased gradually, which can be caused by the dye desorption from the TiO_2 film occurring at high temperatures.

The open-circuit voltage (V_{OC}) on the NC condition decreased from approximately 0.75 to 0.36 V (see Tables 5.1 and 5.2), which indicates a relationship between the increasing temperature and decreasing Voc. This may be caused by the increased resistance in the circuit, which reduced the electron speed.

Table 5.1 Performance of normal cell (NC) DSSCs under V-shape concentrator for 3 hours measurement

t (min)	T (°C)	V_{OC} (V)	J_{SC} (mA/cm^2)	FF	P_{OUT} (mW/cm^2)	η (%)	Rs	Z1 R (Ω) C (μF)	Z2 R (Ω) C (mF)
0	66.2	0.74	82.62	0.47	28.73	5.5	6.32	5.49	1.38
								5.93	77
10	90.5	0.45	46.27	0.49	10.10	1.9	6.54	7.92	3.59
								6.04	29
20	104.5	0.42	42.40	0.54	9.62	1.8	6.75	8.57	2.65
								8.20	40
30	112.2	0.41	40.93	0.55	9.31	1.8	6.82	9.01	3.17
								7.80	33
40	118.1	0.40	39.97	0.57	9.18	1.8	6.85	9.26	2.58
								7.59	41
50	125.2	0.40	38.91	0.58	9.05	1.7	6.86	9.50	2.42
								7.42	30
60	132.7	0.39	37.79	0.59	8.75	1.7	6.87	9.68	2.68
								7.26	39
70	139.6	0.39	36.30	0.61	8.60	1.6	6.89	9.96	2.50
								10.38	62
80	144.7	0.38	35.57	0.61	8.40	1.6	6.89	10.14	2.99
								10.19	24
90	152.3	0.38	34.73	0.62	8.32	1.6	6.88	10.25	3.01
								10.09	35
100	164.5	0.38	34.56	0.62	8.25	1.6	6.88	10.37	2.48
								9.97	29

110	173.4	0.38	33.88	0.63	8.11	1.6	6.87	10.52	2.45
								9.82	43
120	186.3	0.38	33.48	0.62	7.89	1.5	6.87	10.69	2.88
								9.67	37
130	192.9	0.37	32.87	0.64	7.86	1.5	6.88	10.79	2.89
								9.58	36
140	200.0	0.37	32.15	0.65	7.85	1.5	6.88	11.05	2.90
								9.35	36
150	207.3	0.37	31.20	0.67	7.70	1.5	6.89	11.03	2.75
								9.15	38
160	213.5	0.37	31.47	0.66	7.67	1.5	6.89	11.23	2.78
								9.20	38
170	217.2	0.36	31.38	0.67	7.66	1.5	6.90	11.33	2.54
								9.12	41
180	221.8	0.36	30.51	0.69	7.57	1.5	6.89	11.57	3.05
								8.94	51

Table 5.2 Performance of continuous flowing electrolyte cell (CF) DSSCs under V-shape concentrator for 3 hours measurement

t (min)	**T (°C)**	**V_{OC} (V)**	**J_{SC} (mA/cm^2)**	**FF**	**P_{OUT} (mW/cm^2)**	**η (%)**	**Rs**	**Z1 R_{CT1} (Ω) C (μF)**	**Z2 R_{CT2} (Ω) C (mF)**
0	62.5	0.76	50.18	0.51	19.64	3.8	7.63	9.32	1.26
								7.54	57
10	69.7	0.62	37.03	0.51	11.91	2.3	7.30	14.17	-
								7.30	-
20	75.3	0.66	26.02	0.53	9.17	1.8	7.13	20.22	
								7.52	
30	84.3	0.67	20.10	0.54	7.32	1.4	7.21	22.62	-
								6.72	-
40	92.1	0.64	14.70	0.55	5.16	1.0	7.21	27.32	
								5.57	

50	95.2	0.63	12.18	0.52	4.04	0.8	7.47	33.99	
								6.58	
60	100.6	0.61	9.18	0.53	3.01	0.6	7.44	39.48	
								8.34	
70	105.0	0.61	8.07	0.51	2.51	0.5	7.37	45	
								7.32	
80	108.7	0.60	7.17	0.51	2.19	0.4	7.47	48.05	
								6.85	
90	112.5	0.58	6.43	0.52	1.94	0.4	7.41	57.92	-
								8.36	-
100	119.6	0.57	5.97	0.57	1.96	0.4	7.48	54.73	
								8.84	
110	125.5	0.57	6.23	0.50	1.77	0.3	7.34	60.66	
								7.98	
120	129.5	0.56	5.61	0.52	1.63	0.3	7.52	66.43	
								7.28	
130	133.7	0.55	5.05	0.51	1.43	0.3	7.55	74.45	
								9.58	
140	139.0	0.54	4.64	0.49	1.24	0.2	7.52	85	
								8.40	
150	145.4	0.54	4.26	0.50	1.15	0.2	6.32	106.1	-
								6.73	-
160	149.3	0.53	4.04	0.49	1.05	0.2	7.43	92.60	
								7.71	
170	154.8	0.53	3.90	0.47	0.98	0.2	7.50	92.93	
								7.68	
180	161.7	0.52	3.67	0.49	0.94	0.2	7.50	101.1	
								10.37	

When the flowing electrolyte system was applied, the V_{OC} could be reduced from approximately 0.75 to 0.6 V. This phenomenon indicated that the temperature could be reduced when an electrolyte-flowing system is applied. The J_{SC} in CF systems was

lowered compared to that in NC systems. At the end of the measurement, the J_{SC} of CF (3.67 mW/cm^2) was a tenth of that of the NC (30.51 mW/cm^2). This may be caused by the flowing motion of the electrolyte, which is perpendicular to the flow of electrons and prevents the electron from regeneration in the dye.

Electrochemical Impedance Spectroscopy

The first semicircle corresponds to the resistance associated with the electrochemical reaction of triiodide (I_3^-) to iodide (I^-) in the TiO_2/Pt and electrolyte interface. The second semicircle corresponds to the electrolyte diffusion in the liquid electrolyte. The first semicircle of the normal cell increased because of the decrease in current density, which reduced the number of ions at the TiO_2/dye or Pt interface. Similarly, the first semicircle of the FC system also shows a decrease in number of ions at the interface. The rise of the first semicircle in the FC system may be due to the flow motion of the electrolyte. The flow of the electrolyte also swaps the electrons from their path to the TiO_2/dye surface, causing improper electrolyte transfer. This leads to regeneration of a reduced number of electrons in the TiO_2/dye and a decrease in J_{sc}.

Flowing-stop electrolyte systems

To reduce the effect from electrolyte motion, a periodic 10 min stop was applied to the flowing system. The photovoltaic performance of flowing-stop systems (FS) is show in Fig. 5.3. The periodic stop could reduce the degeneration of current density as shown in the *J*–*V* curve in Fig. 5.3 (a) compared to FS systems. This result conforms the EIS data shown in Fig. 5.3 (b). At stopping periods such as 100, 120, 160, and 180 min, the impedance was reduced compared to the following flowing periods: 110 and 170 min. During this stopping period, the regeneration of electrons was better than that with the flowing period as it reduces the effect of flowing motion in the cooling system.

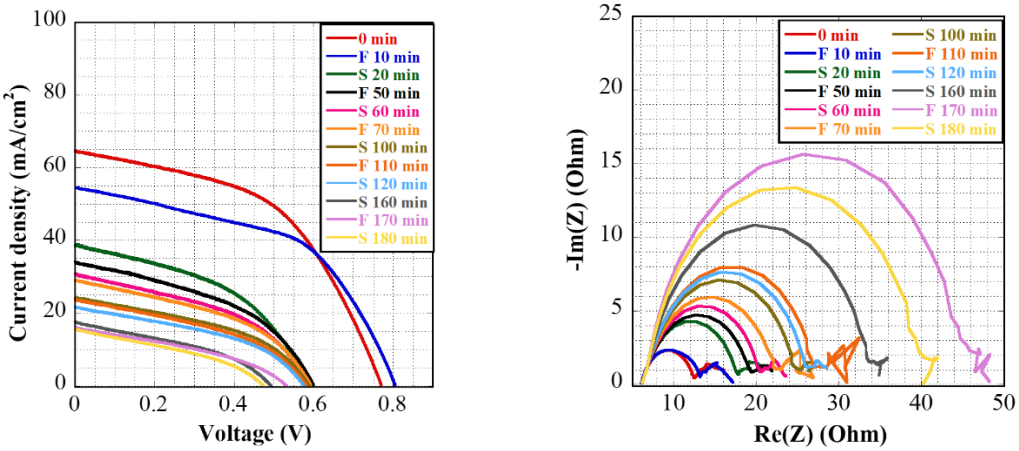

(a) **(b)**

Figure 5.3. (a) *J-V* curves and (b) EIS of flowing-stop system (FS) in flowing and stop condition under low concentrated light for 3 h measurement.

Temperature Comparison

By applying CF and FS electrolytes, the surface temperature of the cell was lower compared to NC, as shown in Fig. 5.4. The body temperature of the cell reduced from 221 °C (NC) to 161 °C (CF) and 167 °C (FS) for 3 h cell operation.

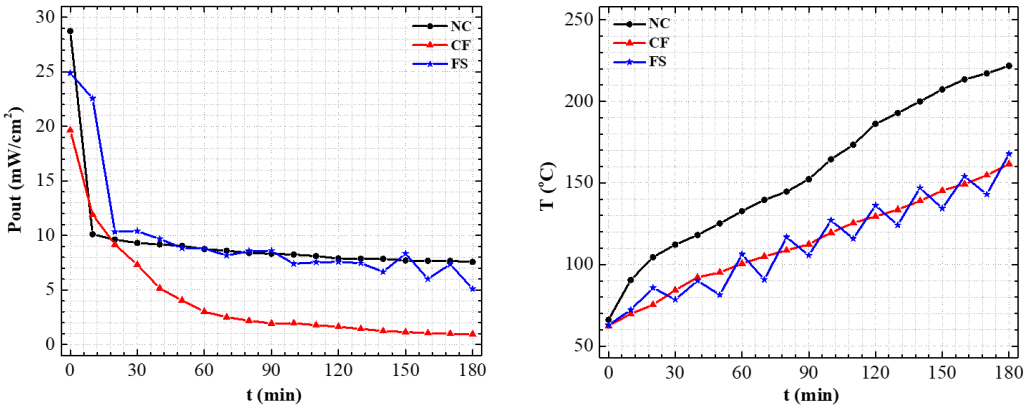

Figure 5.4. Comparison of temperature and P_{out} under 3 conditions of DSSCs.

5.2.2 Different Electrolytes

In contrast to Z-100, which has a high boiling point, the effect of applying electrolyte flowing systems could be observed by using the lower boiling point but higher performance acetonitrile-based electrolyte (AN-50). As shown in fig 5.5 (a) and (b), the flowing electrolyte with FS systems could maintain the performance of the cell during the stop condition for 3 h measurement. In contrast, the propionitrile-based electrolyte (PN-50) with lower performance compared to that of AN-50 but better than that of Z-100 and higher boiling point compared to that of AN-50 can maintain the performance with the FS system for 3 h measurement in both the flowing and stop conditions, as shown in Fig. 5.5 (c) and (d). This result shows that by lowering the temperature further, the AN-50 could be used in DSSCs coupled with low concentrated light.

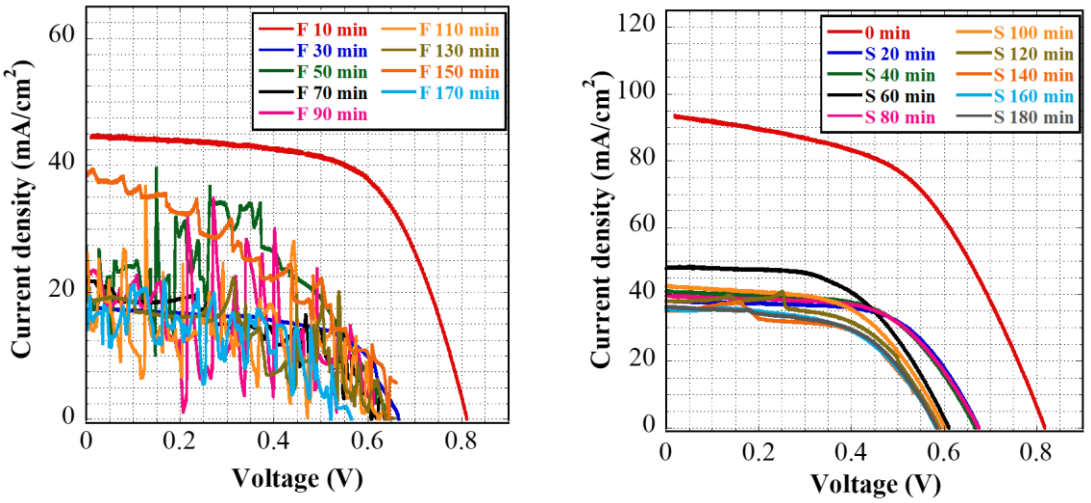

(a) **(b)**

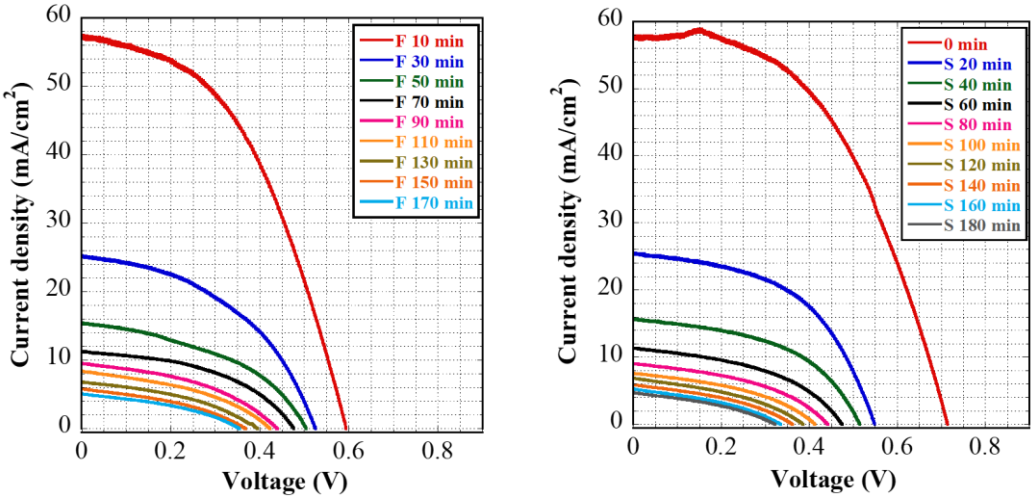

(c) **(d)**

Figure 5.5. *J–V* curves of the flowing-stop system (FS) in AN-50 and PN-50 in the (a), (c) flowing and (b), (d) stop condition, respectively.

5.2.3 Temperature Reduced FS Systems

By cooling the initial temperature of the electrolyte, it is possible to further increase the electrolyte flowing system cooling effect. An electrolyte cooled with ice was used before the electrolyte flowed to the CF and FS systems. The P_{out} of the cell was improved, as shown in Fig. 5.6. The ice can lower the overall temperature cell 20 °C compared to that of normal flowing electrolyte systems.

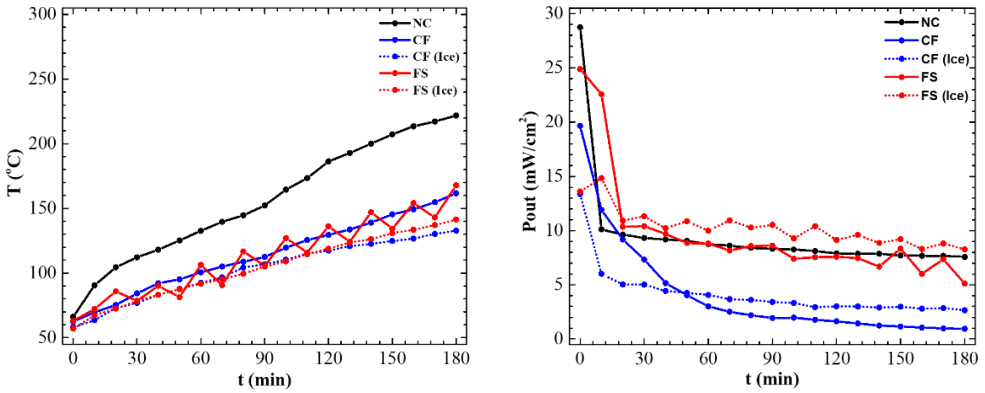

Figure 5.6 Temperature and P_{out} of DSSCs with lowered temperature compared to room-temperature electrolytes.

4.3 Conclusions

In conclusion, the DSSC using a flowing electrolyte system can decrease the temperature and prevent electrolyte evaporation in bifacial DSSCs with a low concentrator. The flowing electrolyte system successfully reduced by 60 °C the body temperature of the cell, from ~220 °C without the flowing system to ~160 °C with the flowing system. In contrast, the flowing system gradually reduced the P_{OUT} of cell until it reached 0.94 mW/cm^2 compared to 7.57 mW/cm^2 in a 3 h measurement. This occurs because the flowing motion of the electrolyte hinders the electron regeneration. This flowing motion effect could be possible reduced by introducing a periodic stop to the flowing electrolyte system. In that case, the cell P_{OUT} could be maintained at 5.10 mW/cm^2 after 3 h measurement.

REFERENCES

[1]. Regan, B. O. and Gratzel, M. (**1991**) 'A low-cost, high-efficiency solar cell based on dye-sensitized colloidal TiO_2 films', *Nature,* 353, 737–740.

[2]. Yum, J., Baranoff, E., Wenger, S., Nazeeruddin, M. K. and Gratzel, M. (**2011**) 'Panchromatic engineering for dye-sensitized solar cells', *Energy Environ. Sci.,* 4, 842–857.

[3]. Sharma, K., Sharma, V. and Sharma, S. S. (**2018**) 'Dye-Sensitized Solar Cells: Fundamentals and Current Status', *Nanoscale Res. Lett.,* 13, 381.

[4]. Selvaraj, P., Baig, H., Mallick, T. K., Siviter, J., Montecucco, A., Li, W., Paul, M., Sweet, T., Gao, M., Knox, A. R. and Sundaram, S. (**2018**) 'Enhancing the efficiency of transparent dye-sensitized solar cells using concentrated light', *Solar Energy Materials and Solar Cells*, *175*. DOI: https://doi.org/10.1016/j.solmat.2017.10.006

[5]. Hirst, L. C. and Ekins-Daukes, N. J. (**2011**) 'Fundamental losses in solar cells', *Progress in Photovoltaics: Research and Applications*, 19(3). DOI: https://doi.org/10.1002/pip.1024

[6]. Ceylan, İ., Gürel, A. E., Demircan, H. and Aksu, B. (**2014**) 'Cooling of a photovoltaic module with temperature controlled solar collector', *Energy and Buildings*, *72*. DOI: https://doi.org/10.1016/j.enbuild.2013.12.058

[7]. Dwivedi, P., Sudhakar, K., Soni, A., Solomin, E. and Kirpichnikova, I. (**2020**) 'Advanced cooling techniques of P.V. modules: A state of art', *Case Studies in Thermal Engineering*, *21*. DOI: https://doi.org/10.1016/j.csite.2020.100674

[8]. Min, C., Nuofu, C., Xiaoli, Y., Yu, W., Yiming, B. and Xingwang, Z. (**2009**) 'Thermal analysis and test for single concentrator solar cells', *Journal of Semiconductors*, *30*(4). DOI: https://doi.org/10.1088/1674-4926/30/4/044011.

[9]. Abu Talip, R. A., Yahya, W. Z. N. and Bustam, M. A. (**2020**) 'Ionic Liquids Roles and Perspectives in Electrolyte for Dye-Sensitized Solar Cells', *Sustainability*, *12*(18), 7598. DOI: https://doi.org/10.3390/su12187598.

[10]. Iftikhar, H., Sonai, G. G., Hashmi, S. G., Nogueira, A. F. and Lund, P. D. (**2019**) 'Progress on Electrolytes Development in Dye-Sensitized Solar Cells', *Materials*, *12*(12), 1998. DOI: https://doi.org/10.3390/ma12121998

[11]. Marszalek, M., Arendse, F. D., Decoppet, J.-D., Babkair, S. S., Ansari, A. A., Habib, S. S., Wang, M., Zakeeruddin, S. M. and Grätzel, M. (**2014**) 'Ionic Liquid-Sulfolane Composite Electrolytes for High-Performance and Stable Dye-Sensitized Solar Cells', *Advanced Energy Materials*, *4*(6), 1301235. DOI: https://doi.org/10.1002/aenm.201301235.

[12]. Lin, B., Shang, H., Chu, F., Ren, Y., Yuan, N., Jia, B., Zhang, S., Yu, X., Wei, Y. and Ding, J. (**2014**) 'Ionic liquid-tethered Graphene Oxide/Ionic Liquid Electrolytes for Highly Efficient Dye Sensitized Solar Cells', *Electrochim. Acta*, *134*, 209–214. DOI: https://doi.org/10.1016/j.electacta.2014.03.064

[13]. Guo, M., Fang, J., Xu, H., Li, W., Lu, X., Lan, C. and Li, K. (**2010**) 'Synthesis and characterization of novel anion exchange membranes based on imidazolium-type ionic liquid for alkaline fuel cells', *Journal of Membrane Science*, *362*(1–2), 97–104. DOI: https://doi.org/10.1016/j.memsci.2010.06.026

[14]. Yan, F., Yu, S., Zhang, X., Qiu, L., Chu, F., You, J. and Lu, J. (**2009**) 'Enhanced Proton Conduction in Polymer Electrolyte Membranes as Synthesized by Polymerization of Protic Ionic Liquid-Based Microemulsions', *Chemistry of Materials*, *21*(8), 1480–1484. DOI: https://doi.org/10.1021/cm900098r

[15]. Lin, B., Cheng, S., Qiu, L., Yan, F., Shang, S. and Lu, J. (**2010**) 'Protic Ionic Liquid-Based Hybrid Proton-Conducting Membranes for Anhydrous Proton Exchange Membrane Application', *Chemistry of Materials*, *22*(5), 1807–1813. DOI: https://doi.org/10.1021/cm9033758

[16]. Ahmadi, R., Monadinia, F. and Maleki, M. (**2021**) 'Passive/active photovoltaic-thermal (PVT) system implementing infiltrated phase change material (PCM) in PS-CNT foam', *Solar Energy Materials and Solar Cells*, *222*, 110942. DOI: https://doi.org/10.1016/j.solmat.2020.110942

[17]. AL-Musawi, A. I. A., Taheri, A., Farzanehnia, A., Sardarabadi, M., & Passandideh-Fard, M. (**2019**) 'Numerical study of the effects of nanofluids and phase-change materials in photovoltaic thermal (PVT) systems', *Journal of Thermal Analysis and Calorimetry*, *137*(2), 623–636. DOI: https://doi.org/10.1007/s10973-018-7972-6

[18]. Al-Waeli, A. H. A., Chaichan, M. T., Sopian, K., Kazem, H. A., Mahood, H. B. and Khadom, A. A. (**2019**) 'Modeling and experimental validation of a PVT system using nanofluid coolant and nano-PCM', *Solar Energy*, *177*, 178–191. DOI: https://doi.org/10.1016/j.solener.2018.11.016

[19]. Al-Waeli, A. H. A., Sopian, K., Chaichan, M. T., Kazem, H. A., Ibrahim, A., Mat, S. and Ruslan, M. H. (**2017**) 'Evaluation of the nanofluid and nano-PCM based photovoltaic thermal (PVT) system: An experimental study', *Energy Conversion and Management*, *151*, 693–708. DOI: https://doi.org/10.1016/j.enconman.2017.09.032

[20]. Atkin, P. and Farid, M. M. (**2015**) 'Improving the efficiency of photovoltaic cells using PCM infused graphite and aluminium fins', *Solar Energy*, *114*, 217–228. DOI: https://doi.org/10.1016/j.solener.2015.01.037

[21]. Biwole, P. H., Eclache, P. and Kuznik, F. (**2013**) 'Phase-change materials to improve solar panel's performance', *Energy and Buildings*, *62*, 59–67. DOI: https://doi.org/10.1016/j.enbuild.2013.02.059

[22]. Choubineh, N., Jannesari, H. and Kasaeian, A. (**2019**). Experimental study of the effect of using phase change materials on the performance of an air-cooled photovoltaic system. *Renewable and Sustainable Energy Reviews*, *101*, 103–111. DOI: https://doi.org/10.1016/j.rser.2018.11.001

[23]. He, W., Zhou, J., Chen, C. and Ji, J. (**2014**) 'Experimental study and performance analysis of a thermoelectric cooling and heating system driven by a photovoltaic/thermal system in summer and winter operation modes', *Energy Conversion and Management*, *84*, 41–49. DOI: https://doi.org/10.1016/j.enconman.2014.04.019

[24]. Tiwari, S., Agrawal, S. and Tiwari, G. N. (**2018**) 'PVT air collector integrated greenhouse dryers', *Renewable and Sustainable Energy Reviews*, *90*, 142–159. DOI: https://doi.org/10.1016/j.rser.2018.03.043

[25]. Bambrook, S. M. and Sproul, A. B. (**2012**) 'Maximising the energy output of a PVT air system', *Solar Energy*, *86*(6), 1857–1871. DOI: https://doi.org/10.1016/j.solener.2012.02.038

[26]. Boutina, L., Khelifa, A., Touafek, K., Lebbi, M. and Baissi, M. T. (**2018**) 'Improvement of PVT air-cooling by the integration of a chimney tower (CT/PVT)', *Applied Thermal Engineering*, *129*, 1181–1188. DOI: https://doi.org/10.1016/j.applthermaleng.2017.10.097

[27]. Sarhaddi, F., Farahat, S., Ajam, H., Behzadmehr, A. and Mahdavi Adeli, M. (**2010**) 'An improved thermal and electrical model for a solar photovoltaic thermal (PV/T) air collector', *Applied Energy*, *87*(7), 2328–2339. DOI: https://doi.org/10.1016/j.apenergy.2010.01.001

[28]. Franklin, J. C. and Chandrasekar, M. (**2019**) 'Performance enhancement of a single pass solar photovoltaic thermal system using staves in the trailing portion of the air channel', *Renewable Energy*, *135*, 248–258. DOI: https://doi.org/10.1016/j.renene.2018.12.004

[29]. Diallo, T. M. O., Yu, M., Zhou, J., Zhao, X., Shittu, S., Li, G., Ji, J. and Hardy, D. (**2019**) 'Energy performance analysis of a novel solar PVT loop heat pipe employing a microchannel heat pipe evaporator and a PCM triple heat exchanger', *Energy*, *167*, 866–888. DOI: https://doi.org/10.1016/j.energy.2018.10.192

[30]. Ebaid, M. S. Y., Ghrair, A. M. and Al-Busoul, M. (**2018**) 'Experimental investigation of cooling photovoltaic (PV) panels using (TiO_2) nanofluid in water -polyethylene

glycol mixture and (Al_2O_3) nanofluid in water- cetyltrimethylammonium bromide mixture', *Energy Conversion and Management*, *155*, 324–343. DOI: https://doi.org/10.1016/j.enconman.2017.10.074

[31]. Nasrin, R., Rahim, N. A., Fayaz, H. and Hasanuzzaman, M. (**2018**) 'Water/MWCNT nanofluid based cooling system of PVT: Experimental and numerical research', *Renewable Energy*, *121*, 286–300. DOI: https://doi.org/10.1016/j.renene.2018.01.014

[32]. Abdulgafar, S. A., Omar, O. S. and Yousif, K. M. (**2007**) 'Improving The Efficiency Of Polycrystalline Solar Panel Via Water Immersion Method, *International Journal of Innovative Research in Science, Engineering and Technology (An ISO Certified Organization)*, *3297*(1), 8127–8132. www.ijirset.com

[33]. Hazi, A., Hazi, G., Grigore, R. and Vernica, S. (**2014**) 'Opportunity to use PVT systems for water heating in industry', *Applied Thermal Engineering*, *63*(1), 151–157. DOI: https://doi.org/10.1016/j.applthermaleng.2013.11.010

[34]. Zhao, D., Peng, T., Lu, L., Cai, P., Jiang, P. and Bian, Z. (**2008**) 'Effect of Annealing Temperature on the Photoelectrochemical Properties of Dye-Sensitized Solar Cells Made with Mesoporous TiO_2 Nanoparticles', *J. Phys. Chem. C*, *112*(22), 8486–8494. DOI: https://doi.org/10.1021/jp800127x

[35]. Xu, J., Jin, J., Ying, Z., Shi, W. and Peng, T. (**2015**) 'Composite electrode of TiO 2 particles with different crystal phases and morphology to significantly improve the performance of dye-sensitized solar cells', *RSC Advances*, *5*(41), 32536–32545. DOI: https://doi.org/10.1039/C5RA01122A

[36]. Saidi, N. M., Farhana, N. K., Ramesh, S. and Ramesh, K. (**2021**) 'Influence of different concentrations of 4-tert-butyl-pyridine in a gel polymer electrolyte towards improved performance of Dye-Sensitized Solar Cells (DSSC)', *Solar Energy*, *216*, 111–119. DOI: https://doi.org/10.1016/j.solener.2020.12.058

Chapter 6
Summary and Future Prospect

6.1 Summary

In this Ph.D. thesis, we successfully enhanced the power output of DSSCs with a low concentrated light system using plane and concave mirror low concentrators. We also investigated and evaluated the performance of DSSCs coupled with plane and concave mirror concentrators. We considered two types of measurement for the low concentrated light system in order to find the more efficient system for DSSCs. For these two types of measurements, we found that the high temperature, as a side effect, occurs as consequence of using the concave mirror concentrator. This high temperature effect can decrease the performance of DSSCs because of the dye degradation and electrolyte evaporation. By combining the low concentrated light with a cooling system, we studied in detail the possible relation between the liquid electrolyte as a redox mediator and as an active cooling system. To investigate the performance of DSSCs with low concentrated light and active cooling systems, we compared the properties of these systems with a normal cell without such systems.

To increase the light harvesting in DSSCs, a plane mirror back reflector and concave mirror back concentrator have been applied to bifacial DSSCs. The plane and concave mirrors have been effective for increasing the current density J_{SC} from 8.78 $mA.cm^{-2}$ to 11.50 and ~82 $mA.cm^{-2}$, respectively. The power output P_{OUT} also increased from 4.25 $mW.cm^{-2}$ to 5.62 and 29.01 $mW.cm^{-2}$ with mirror distances of 2 and 2.5 cm, respectively. The EIS analysis showed an expansion in the second circle Z_2, R_{CT} with the increased light intensity produced by the reflector and concentrator. The

DSSC temperature increased slightly ~1 °C with the back plane mirror. In contrast, the temperature of the back concave mirror increased sharply because the liquid electrolyte evaporated before 30 min of operation. By using a 3-methoxypropionitrile (MPN-100)-based liquid electrolyte with high boiling point, the DSSC can operate for more than 4 days. In contrast, acetonitrile (AN-50) and propionitrile (PN-50)-based electrolytes with a lower boiling point but higher performance were degraded after the first day of measurement with 3x light power input (Chapter 3).

The V-shape concentrated mirror system was applied to increase the illumination power in bifacial DSSCs. The system successfully increased P_{OUT} to 24.01 $mW.cm^{-2}$ with 0 cm cell-to-mirror distance with 5x illumination power in each side of the bifacial DSSC. The temperature of the cell was increased more than 80 °C after 30 min of operation. By adjusting the cell-to-mirror distance in the V-shape system, the temperature was stable at 80 °C in 3 h of operation with P_{OUT} of approximately 17 $mW.cm^{-2}$ (Chapter 4).

The used of a liquid electrolyte is more common in DSSCs than the typical solid- and quasi-solid state electrolyte. A cooling systems using the flowing liquid electrolyte was employed to decrease the temperature resulting from the applied concentrated light. The flowing electrolyte successfully reduced by 60 °C the body temperature of the cell, from ~220 °C without the flowing system to ~160 °C with the flowing system. In contrast, the flowing system gradually reduced the P_{OUT} of the cell until it reached 0.94 mW/cm^2, compared to 7.57 mW/cm^2 in a 3 h measurement. This occurs because the flowing motion of the electrolyte hinders the electron regeneration. This flowing motion effect could be reduced by introducing a periodic stop to the flowing electrolyte system. In this case, the cell P_{OUT} could be maintained at 5.10 mW/cm^2 after 3 h measurement (Chapter 5).

6.2 Prospects for Future Research

In this Ph.D. thesis, we studied the effect of using a low concentrated light system. The increase in light harvesting allowed us to perform an in-depth study of the DSSC and, at the same time, to draw general conclusions about the improvement in power output as an important parameter of the DSSC. The power output is important because DSSCs essentially convert light into electricity. Clearly, a detailed study of the increase in PCE would provide better performance and strengthen the results presented here. Moreover, when we compared the photovoltaic and EIS performance of solar cells with concentrators, we considered only the silicon solar cell that is available in the literature for a limited number of objects. On-going and future studies of DSSCs with low concentrated light will provide further references and datasets, allowing us to make a more extensive comparison between the power output and power conversion efficiency. In particular, DSSCs with better structures are needed to investigate the high temperature effect and whether the fill factor, voltage, and resistance show any dependence on the light intensity. The problem of temperature could also be solved using other type of electrolyte, such as a semi-solid electrolyte. Regarding the concentrator itself, it could be built to be selective and reflect only a certain wavelength to match that of dye adsorption. The space for a V-shape concentrator could be minimized for a large area solar cell, making it possible to research on the efficiency of solar cell placement.

The flowing electrolyte as an active cooling system, as discussed in Chapter 5, is a candidate solution for decreasing the high temperature effect and electrolyte evaporation when applying a light concentrator. To further investigate the performances, it would be interesting to resolve the flowing motion/rate and derive the electron regeneration in the dye.

Acknowledgements

Alhamdulillah…

First, I wish to express my gratitude to my kind supervisor, Prof. M. Shiratani, to whom I am deeply indebted for his guidance, continuous support throughout the whole research, patience, motivation, enthusiasm, immense knowledge, and understanding. I will never forget his contagious enthusiasm or the many times we met to discuss this research.

I am also thankful to Prof. Yuji Oki, Prof. Kazunori Koga, and Prof. Naho Itagaki for their critical reading, useful suggestions, and comments during the development of this manuscript.

In our laboratory, a number of very stimulating discussions with Assoc. Prof. Pankaj Attri and research group mate, Lesley Chawarambwa, led to new insights, fresh motivation, and helped me in the progress of my research as well as in writing the manuscript. In addition, the warmth, kindness, and hospitality offered to me by all the lab members will always be remembered.

My studies at Kyushu University were financially supported by a scholarship granted by the Japan International Cooperation Agency (JICA).

The three years spent in a foreign country would not have been possible without the support of all the Indonesian, Japanese, and foreign friends, both inside and outside the university.

I also express my gratitude to my parents, husband, brothers, and sisters, and to those who endured the effort required for this research.

Finally, I would like to dedicate this dissertation to my beloved parents, *Bapak & Ibu*, who had always supported my dreams since I was young and always believed in me, and to my beloved husband, *Wahyu Waskito Aji,* for his understanding and encouragement when enthusiasm waned.

Fukuoka, August 2022

Tika Erna Putri

List of Publication

No.	Title	Year	Journal	Author
1.	Graphene-Si_3N_4 Nanocomposite Blended Polymer Counter Electrode for Low-Cost Dye-Sensitized Solar Cells	2020	Chemical Physic Letter	Fadzai Lesley Chawarambwa, **Tika Erna Putri**, Min-kyu Son, Kunihiro Kamataki, Naho Itagaki, Kazunori Koga, and Masaharu Shiratani
2.	Effects of Activated Carbon Counter Electrode on Bifacial Dye Sensitized Solar Cells (DSSCs)	2021	Material Science Forum, www.Scientific.net	**Tika Erna Putri**, Yuan Hao, Fadzai Lesley Chawarambwa, Hyunwoong Seo, Min-Kyu Son, Kunihiro Kamataki, Naho Itagaki, Kazunori Koga, and Masaharu Shiratani
3.	Performance Characteristic of Bifacial Dye Sensitized Solar Cells Under V-Shape Low Concentrated Light System	2021	American Chemistry Society (ACS) Applied Energy Material	**Tika E. Putri**, Fadzai Lesley Chawarambwa, Pankaj Attri, Minkyu Son, Kunihiro Kamataki, Naho Itagaki, Kazunori Koga, and Masaharu Shiratani
4.	Synthesis of Yb^{3+}/Ho^{3+} Co-doped Y_2O_3 Nanoparticles and Its Application to Dye Sensitized Solar Cells	2021	Journal of Molecular Structure	Fadzai Lesley Chawarambwa, **Tika Erna Putri**, Kunihiro Kamataki, Masaharu Shiratani, Kazuniro Koga, Naho Itagaki, and Daisuke Nakamura
5.	Highly Efficient and Transparent Counter Electrode for	2021	Chemical Physics Letters	Fadzai Lesley Chawarambwa, **Tika Erna Putri**, Pankaj Attri,

	Application in Bifacial Solar Cells			Kunihiro Kamataki, Naho Itagaki, Kazunori Koga, and Masaharu Shiratani
6.	Effects of Concentrated Light on the Performance and Stability of a Quasi-Solid Electrlyte in Dye Sensitized Solar Cells	2021	Chemical Physics Letters	Fadzai Lesley Chawarambwa, **Tika Erna Putri**, Pankaj Attri, Kunihiro Kamataki, Naho Itagaki, Kazunori Koga, and Masaharu Shiratani
7.	Performance Comparison of Nitrile-Based Liquid Electrolytes on Bifacial Dye-Sensitized Solar Cells Under Low-Concentrated light	2022	Material Research Society Advances (MRSA)	**Tika E. Putri**, Fadzai Lesley Chawarambwa, Pankaj Attri, Kunihiro Kamataki, Naho Itagaki, Kazunori Koga, and Masaharu Shiratani
8.	Improved Luminescence performance of Yb^{3+}-Er^{3+}-Zn^{2+}:Y_2O_3 Phosphor and Its Application to Solar Cells	2022	Optical Material	Fadzai Lesley Chawarambwa, **Tika Erna Putri**, Sung-Hwa Hwang, Pankaj Attri, Kunihiro Kamataki, Naho Itagaki, Kazunori Koga, and Masaharu Shiratani
9.	Performance of Carbon Black-Titanium Nitrate and Carbon Black-Titanium/Triton X-100 Composite Polymer Counter Electrodes for Dye Sensitized Solar Cells	2022	Advanced Material Research	Fadzai Lesley Chawarambwa, **Tika Erna Putri**, Pankaj Attri, Kunihiro kamataki, Naho Itagaki, Kazunori Koga, Masaharu Shiratani
10.	The Effect of Spin-Coating Rate on	2022	Advanced Engineering Forum	Fadzai Lesley Chawarambwa, **Tika**

	Surface Roughness, Thickness, and Electrochemical Properties of a Pt Polymer Counter Electrode			**Erna Putri**, Pankaj Attri, Kunihiro kamataki, Naho Itagaki, Kazunori Koga, Masaharu Shiratani